

**Solid-state transformations induced by pharmaceutical processes
during manufacturing**

Dissertation

zur Erlangung des akademische Grades eines Doktors der Naturwissenschaften

Der Fakultät für Mathematik, Informatik und Naturwissenschaften der Universität Hamburg

vorgelegt von

Sönke C. Rehder

aus Hamburg

Hamburg 2013

Reviewer of the dissertation: Prof. Dr. Claudia S. Leopold

Prof. Dr. Detlef Geffken

Date of the disputation: 05.04.2013

Danksagungen

An dieser Stelle möchte ich allen Personen danken, die mich während der Anfertigung der vorliegenden Dissertation begleitet und unterstützt haben.

Diese Dissertation wurde an der Universität Hamburg am Fachbereich Chemie in der Abteilung Pharmazeutische Technologie auf Anregung und unter der Leitung von Frau Prof. Dr. Claudia S. Leopold verfasst.

An erster Stelle möchte ich mich ganz herzlich bei Frau Prof. Leopold für die Überlassung des sehr interessanten, aktuellen Themas sowie für die mir gewährten wissenschaftlichen Freiräume und dem damit einhergehenden mir entgegengebrachten Vertrauen bedanken. Ich bedanke mich weiterhin für die vielen anregenden und konstruktiven fachlichen Diskussionen sowie natürlich auch für die freundliche Aufnahme in ihre Arbeitsgruppe.

Ich möchte mich auch bei Prof. Dr. Thomas Rades von der Universität Kopenhagen ganz herzlich für die inspirierenden Diskussionen und die engagierte Co-Betreuung während meiner Dissertation bedanken.

Auch danke ich Dr. Albrecht Sakmann für seine Unterstützung während meiner Arbeit und für das sehr angenehme kollegiale Miteinander.

Herrn Prof. Dr. Detlef Geffken gilt mein besonderer Dank für die freundliche Übernahme des Gutachtens der vorliegenden Dissertation. Herrn Prof. Hans-Ulrich Moritz und Frau Dr. Ilka Haase danke ich für ihre Bereitschaft, als Begutachtende in der Prüfungskommission mitzuwirken.

Ich möchte mich weiterhin bei meinen Kollegen aus der Pharmazeutischen Technologie und der Pharmazeutischen Chemie sowie der Technischen und Makromolekularen Chemie für die anregenden wissenschaftlichen Diskussionen sowie das angenehme Arbeitsklima, aber natürlich auch für die vielen schönen Momente im universitären Alltag bedanken, die meine Zeit an der Universität Hamburg unvergesslich machen. In besonderer Erinnerung werden mir in diesem Zusammenhang auch die gemeinsamen Weiterbildungs-, Kongress- und Forschungsreisen mit Herrn Dr. Sebastian

Kruggel, Herrn Marc Michaelis und Frau Ines Saniocki bleiben. Dank gilt an dieser Stelle auch Herrn Julian Laackmann für die gute Zusammenarbeit am akustischen Levitator an der Universität Kopenhagen. Herrn Marten Klukkert möchte ich für die angenehme und erfolgreiche Zusammenarbeit an der University of Otago, Dunedin, Neuseeland, sowie für das Korrekturlesen dieser Arbeit besonders danken. Für das Korrekturlesen dieser Dissertation danke ich außerdem Herrn Markus Kubczigk.

Des Weiteren bedanke ich mich bei Prof. Jukka Rantanen von der Universität Kopenhagen für die freundliche Aufnahme in seine Arbeitsgruppe während meiner dortigen Forschungsaufenthalte und für seine Unterstützung bei gemeinsamen Projekten. Herrn Jian X. Wu und Prof. Dr. Clare Strachan (University of Helsinki) möchte ich meinen Dank aussprechen für die begeisternden Diskussionen über multivariate Datenanalyse.

Außerdem möchte ich mich bei den Mitarbeitern verschiedener Arbeitsgruppen an der Universität Hamburg für ihre tatkräftige experimentelle Unterstützung bedanken. Frau Petra Borbe aus der Pharmazeutischen Technologie danke ich für ihre unermüdliche experimentelle Unterstützung, v. a. bei der DSC-Analytik, Herrn Joachim Ludwig vom Mineralogischen und Petrochemischen Institut sowie Frau Isabelle Nevoigt vom Institut für Anorganische Chemie für das Messen der Röntgenpulverdiffraktometrie, Herrn Manfred Preuße vom Institut für Organische Chemie für die massenspektroskopische Analyse einiger Proben und Frau Renate Walter vom Biozentrum Grindel + Zoologisches Museum für die rasterelektronenmikroskopischen Aufnahmen. Dank gebührt weiterhin vom Department of Geology der University of Otago Herrn Damian Walls für seine Unterstützung mit der Röntgenpulverdiffraktometrie sowie für seine Unterstützung mit der Raman-Spektroskopie Herrn Prof. Dr. Keith C. Gordon vom Department of Chemistry, ebenfalls University of Otago.

Mein besonderer Dank gilt natürlich Susanne, meinen Eltern und meinen Brüdern, sowie meinen Freunden. Ihr Interesse, Verständnis und Unterstützung hat mich in jeder Phase der Promotion sehr unterstützt, wofür ich von ganzem Herzen dankbar bin.

Zusammenfassung

Laut aktueller Literatur werden 60 bis 70 % der Wirkstoffe, die sich momentan in der pharmazeutischen Entwicklung befinden, in die Klasse II des Biopharmaceutical Classification System (BCS) eingestuft, da sie zwar eine ausreichende Membrangängigkeit, jedoch eine niedrige Wasserlöslichkeit aufweisen. Die Bioverfügbarkeit kann daher nach oraler Applikation auflösungslimitiert sein. Um ihre Wasserlöslichkeit und somit auch ihre Bioverfügbarkeit zu erhöhen, können andere feste Erscheinungsformen als das thermodynamisch stabilste Polymorph zur Herstellung von festen oralen Darreichungsformen verwendet werden, da diese Formen andere physikochemische Eigenschaften aufweisen, die zu verbesserter Wasserlöslichkeit, aber auch zu unterschiedlich guten Verarbeitungseigenschaften führen. Die Erscheinungsform des Arzneistoffs kann sich jedoch während der Verarbeitung aufgrund der unter Umständen rauen Prozessbedingungen ändern, was wiederum einen signifikanten Einfluss auf die Wirkung des Arzneimittels haben kann.

Im Frühstadium der Arzneimittelentwicklung stehen den Herstellern nur geringe Wirkstoffmengen für die Untersuchung der Eigenschaften der unterschiedlichen Erscheinungsformen zur Verfügung. Deshalb wurde im ersten Kapitel dieser Arbeit die akustische Levitation verwendet, um die Transformationskinetik dieser festen Erscheinungsformen, in diesem Falle von amorph zu kristallin, in kleinen, hochviskosen amorphen Arzneistoffproben zu bestimmen.

Während der sogenannten Präformulierungsphase folgt nach der gründlichen Charakterisierung des Wirkstoffs die Formulierung in eine feste Darreichungsform, häufig als Tablette.

Der erste Schritt bei der Tablettierung besteht meist in der Optimierung der Partikelgrößenverteilung, um die anschließenden Produktionsschritte zu erleichtern. Dies geschieht in der Regel durch Vermahlen. Wird der Arzneistoff jedoch mit einem geeigneten

anderen Stoff vermahlen, kann sich ein sogenannter Cokristall bilden. Im zweiten Kapitel dieser Arbeit wurde daher der Mechanismus der Cokristallbildung während des Vermahlens untersucht: Während stöchiometrische Mischungen von Piracetam und Zitronensäure teilmorph wurden, konnte für Piracetam und Weinsäure nur ein sehr geringer Verlust an Kristallinität beobachtet werden. Zudem konnte gezeigt werden, dass Flüssigkeitsunterstütztes Vermahlen die effektivste Mahlmethode zur Herstellung der untersuchten Cokristalle ist.

Um das Fließverhalten und die Kompressibilität von Pulvern vor der Tablettierung zu optimieren, wird der Arzneistoff häufig mit unterschiedlichen Hilfsstoffen granuliert. Im dritten Kapitel der vorliegenden Arbeit wurde deshalb die In-Prozess-Herstellung von Piracetam-Weinsäure-Cokristalle während der Feuchtgranulierung untersucht. Cokristall-Granulate konnten mit der High Shear-Feuchtgranulierung in Anwesenheit verschiedener Hilfsstoffe in großem Maßstab hergestellt werden.

Um die Löslichkeit und damit die Bioverfügbarkeit von Arzneistoffen aus der BCS-Klasse II zu erhöhen, kann deren amorphe Form zu Tabletten verarbeitet werden. Im vierten Kapitel dieser Promotionsarbeit wird gezeigt, dass die physikalische wie auch die chemische Stabilität von tablettierte amorphes Glibenclamid von der Herstellungsmethode der amorphen Form abhängt, jedoch erwartungsgemäß auch von den Lagerbedingungen. Interessanterweise zeigte sich bei erhöhtem Pressdruck eine reduzierte Rekristallisation.

Eine weitere interessante Beobachtung wurde während der physikochemischen Charakterisierung von Glibenclamid gemacht: Bei der Substanz, die durch Sublimation von amorphem Glibenclamid entsteht, handelt es sich nicht, wie in der Literatur beschrieben, um eine weitere, stabilere polymorphe Form des Glibenclamids, sondern um das thermische Abbauprodukt 1,3-Dicyclohexylharnstoff. Im letzten Kapitel der vorliegenden Dissertation wird dieses Degradationsprodukt beschrieben.

Summary

According to the literature, between 60 and 70 % of the active pharmaceutical ingredients (API) in the pipeline show a sufficient membrane permeability but a low water solubility and thus belong to BCS class II. Therefore, their bioavailability may be dissolution rate-limited after oral administration. To increase their water solubility and thus their bioavailability, other solid-state forms than the most thermodynamically stable polymorph, which may differ in their physico-chemical properties as well as in their processibility, may be used for formulation. However, the solid-state of the API can alter during manufacturing, as the applied conditions in the various processing steps may be relatively harsh. This alteration in the solid-state of the API may have a significant impact on drug performance.

In the very early phase of drug development only small amounts of the API are available for solid-state analysis. Therefore, in the first chapter of the present work acoustic levitation was applied to estimate the kinetics of solid-state phase transformations such as amorphous-to-crystalline transformation of small, highly viscous amorphous samples.

During preformulation and after a thorough characterization the API may be formulated as solid oral dosage form such as tablets. The tablet manufacturing process usually includes particle size reduction, granulation with excipients, drying, and compacting. These manufacturing processes may induce solid-state phase transformations.

Usually, the first step of the manufacturing process of a tablet is to reduce the particle size of the API into a practical range for down-stream processing, often performed by milling. Co-milling of an API with suitable compounds may lead to cocrystal formation. In the second chapter of this work the cocrystal formation mechanism during dry-milling was investigated: With stoichiometric piracetam/citric acid blends a partial amorphization of the substances was observed, while with piracetam/tartaric acid there was only a slight loss of crystallinity.

Furthermore, liquid-assisted milling was shown to be the most efficient cocrystal preparation method among milling techniques.

To improve the bulk properties of fine particles such as flowability and compressibility, the API may be granulated with various excipients. Therefore, the third chapter of the present work deals with the in-process formation of the piracetam/tartaric acid cocrystal in presence of different excipients during high-shear wet granulation. Cocrystal granules could be produced by high-shear wet granulation on a large scale with different excipients in the formulation.

To improve water solubility and thus bioavailability of BCS class II drugs the API may also be formulated in its amorphous form. In the fourth chapter of this dissertation the influence of different manufacturing parameters on the physical and chemical stability of amorphous glibenclamide was examined. The physical as well as the chemical stability of amorphous glibenclamide was shown to depend on the preparation method of the amorphous drug and, as expected, on the storage conditions such as temperature and relative humidity. Interestingly, at a higher compaction pressure during tableting, a lower degree of recrystallization was observed, most likely due to a reduction of the molecular mobility of the amorphous glibenclamide, induced by the microcrystalline cellulose present in the compact. In this chapter it is shown that the physical as well as the chemical stability of an amorphous drug is a multi-factorial process and needs to be evaluated thoroughly, as it may strongly affect drug performance and possibly even drug toxicity.

An interesting observation during the characterization of glibenclamide was that the substance obtained by sublimation of the amorphous form is the thermal degradation product 1,3-dicyclohexylurea and not, as previously published, a further, more stable polymorphic form of glibenclamide. In the last chapter of this thesis the characterization of this degradation product is presented.

Contents

| | |
|--|----|
| 1. Solid-state transformations induced by pharmaceutical processes during manufacturing | 4 |
| <i>Abstract</i> | 5 |
| 1.1 Introduction | 6 |
| 1.2 Solid-state forms of drugs | 9 |
| 1.2.1 <i>Definitions</i> | 9 |
| 1.2.2 <i>Influence of the solid-state form of an API on its properties</i> | 11 |
| 1.2.3 <i>Mechanisms of phase transformations</i> | 13 |
| 1.3 Process-induced solid-state transformations | 14 |
| 1.3.1 <i>Solid-state transformations during particle size reduction</i> | 14 |
| 1.3.2 <i>Solid-state transformations during high-shear wet granulation</i> | 21 |
| 1.3.3 <i>Solid-state transformations during drying</i> | 27 |
| 1.3.4 <i>Solid-state transformations during tableting</i> | 30 |
| 1.4 Conclusion | 33 |
| | |
| 2. A case study of real-time monitoring of solid-state phase transformations in acoustically levitated particles using near infrared and Raman spectroscopy | 36 |
| <i>Abstract</i> | 37 |
| 2.1 Introduction | 38 |
| 2.2 Experimental methods | 41 |
| 2.2.1 <i>Materials</i> | 41 |
| 2.2.2 <i>Methods</i> | 41 |
| 2.3 Results and discussion | 45 |
| 2.3.1 <i>High speed imaging of ibuprofen recrystallisation</i> | 45 |
| 2.3.2 <i>Ibuprofen recrystallisation monitored with NIRS</i> | 46 |
| 2.3.3 <i>Ibuprofen recrystallisation monitored with Raman spectroscopy</i> | 49 |
| 2.3.4 <i>Recrystallisation kinetic parameters estimated from NIR and Raman spectroscopy</i> | 52 |
| 2.4 Conclusion | 53 |
| | |
| 3. Investigation of the formation process of two piracetam cocrystals during grinding | 54 |
| <i>Abstract</i> | 55 |
| 3.1 Introduction | 55 |
| 3.2 Experimental section | 59 |
| 3.2.1 <i>Materials</i> | 59 |
| 3.2.2 <i>Methods</i> | 59 |
| 3.3 Results and discussion | 62 |
| 3.4 Conclusion | 75 |

| | |
|---|---|
| 4. High-shear granulation as a manufacturing method for cocrystal granules..... | 76 |
| <i>Abstract</i> | 77 |
| 4.1 Introduction | 78 |
| 4.2 Materials and methods | 81 |
| 4.2.1 <i>Materials</i> | 81 |
| 4.2.2 <i>Methods</i> | 81 |
| 4.3 Results and discussion | 87 |
| 4.3.1 <i>Cocrystal formation during high-shear granulation</i> | 87 |
| 4.3.2 <i>Storage stability the granules</i> | 96 |
| 4.3.3 <i>Technological characterization of the cocrystal granules</i> | 99 |
| 4.4 Conclusion | 107 |
| | |
| 5. Recrystallization of amorphous glibenclamide in tablets – a multi-factorial investigation | 108 |
| <i>Abstract</i> | 109 |
| 5.1 Introduction | 110 |
| 5.2 Materials and methods | 112 |
| 5.2.1 <i>Materials</i> | 112 |
| 5.2.2 <i>Methods</i> | 112 |
| 5.3 Results and discussion | 115 |
| 5.3.1 <i>Characterization of the investigated solid-state forms of glibenclamide</i> | 115 |
| 5.3.2 <i>Tableting of amorphous glibenclamide</i> | 116 |
| 5.3.3 <i>Storage of the prepared glibenclamide tablets</i> | 117 |
| 5.3.4 <i>Quantification model and prediction of crystalline glibenclamide in the stored tablets</i> | 119 |
| 5.4 Conclusion | 124 |
| | |
| 6. Thermal degradation of amorphous glibenclamide | 126 |
| <i>Abstract</i> | 127 |
| 6.1 Introduction | 127 |
| 6.2 Materials and methods | 130 |
| 6.2.1 <i>Materials</i> | 130 |
| 6.2.2 <i>Methods</i> | 130 |
| 6.3 Results and discussion | 132 |
| 6.4 Conclusion | 140 |
| | |
| Curriculum vitae | Fehler! Textmarke nicht definiert. |
| Publication list | 143 |
| Eidesstattliche Versicherung | 149 |
| References | 150 |

**1. Solid-state transformations induced by pharmaceutical processes
during manufacturing**

Solid-state transformations induced by pharmaceutical processes during manufacturing

Abstract

The most common orally applied drug formulations are solid dosage forms such as tablets and capsules. Thus, the active pharmaceutical ingredient is usually processed in one of its solid-state forms, i. e. crystalline polymorphs, solvates/hydrates, salts, or its amorphous form, which may all differ in their processibility as well as in their physico-chemical properties.

The tablet manufacturing process usually includes particle size reduction, granulation with excipients, drying, and compaction. As the conditions applied during these processing steps may be relatively harsh, process-induced solid-state phase transformations may be observed, which may not only influence down-stream processing of the formulation significantly, but also drug performance and safety.

Particle size reduction is often performed by milling. Milling-induced solid-state transformations can be influenced by the energy input into the system in terms of the type of the milling device, the milling frequency, and the milling time. Furthermore, the experimental temperature as well as the powder bed temperature play an important role regarding the resulting solid-state form of the milled product. To improve flowability and avoid segregation, the components of the powder blend are often granulated for instance by high-shear wet granulation. High-shear wet granulation is a complex process with the risk of solid state phase transformations depending on the drug content in the formulation, the amount and composition of the granulation liquid, the shear rate of the impeller, and the granulation period. Furthermore, the excipients used in the formulation strongly affect the degree of phase transformations of the drug. The subsequent drying step may influence phase transformation by the selected method, the drying temperature, and the drying time. Tableting also may

induce solid-state phase transformations, depending on the applied compaction pressure, the environmental temperature, and by the excipients used in the formulation. Drug manufacturing thus includes complex processing steps, which may all induce solid-state phase transformations. Therefore, an identification of process-induced phase transformations and a detailed understanding of the transformation mechanisms are of great relevance for the pharmaceutical industry.

This review follows the down-stream processing pipeline from particle size reduction, to granulation and drying and finally to tableting, highlighting the relevance of the different process parameters on solid-state phase transformations during manufacturing.

1.1 Introduction

Although the manufacture of most solid drug formulations is routine in the pharmaceutical industry, the product quality may be affected by many different parameters during processing, which must be considered already in the early stages of drug development. Thus, the Food and Drug Administration (FDA) as well as the International Conference on Harmonization (ICH) demand an increased process understanding in terms of identification and control of process parameters with a significant influence on product quality [1, 2].

As the most common orally administered drug formulations are solid dosage forms such as tablets and capsules, the active pharmaceutical ingredients (API) are usually processed in their solid-state forms, namely their amorphous or their crystalline forms, i. e. polymorphs, salts, and hydrates. In recent years, another crystalline form has attracted interest – cocrystals.

In the very early phase of drug development, it is necessary that the API is screened for its solid-state forms, because they may differ in their physico-chemical properties such as

water solubility and dissolution rate, which may consequently influence drug performance and safety, as the withdrawal of the protease inhibitor ritonavir [3] in 1998 and its costly reformulation has shown [4, 5]. Furthermore, the material properties and thus the processibility of an API may also depend on its solid form [6]. Another important aspect regarding the screening for solid-state forms of an API is the protection of intellectual property, illustrated for example by the patent legal case of ranitidine hydrochloride [7-9].

Usually, in this early phase of drug formulation only a very small amount of the API is available, thus various methods have been developed to perform solid-state screening and characterization in a small scale, which was demonstrated with well-plates [10]. Acoustic levitation in combination with non-contact real-time analytical techniques such as NIR or Raman spectroscopy was also found to be a valuable technique for solid-state characterization of small-scaled samples [11-13], as could be shown by the estimation of the recrystallization kinetics of small levitated amorphous ibuprofen samples with NIR spectroscopy combined with a Multivariate Curve Resolution approach [12].

Various analytical methods are available for solid-state characterization and are described in the literature in several reviews and book chapters [14-17]. As there is no single superior method for each analytical task, a combination of different techniques is necessary providing a comprehensive understanding of the solid-state form of interest. In most studies one particulate level technique (properties related to an individual solid particle), for example X-ray diffractometry or thermal methods, is combined with one molecular level technique (properties associated with individual molecules) such as spectroscopic methods [15].

Process analytical technology (PAT) allows monitoring of the solid-state form of an API during processing. Especially spectroscopic techniques such as Raman [18, 19] and NIR spectroscopy [20, 21] meet these requirements, as they provide real-time information without sample preparation. Another analytical challenge is the analysis of solid-state forms within

intact formulations such as tablets or capsules. Raman spectroscopy [22] and parallel-beam XRPD [23] have been shown to be promising methods for these demanding applications.

Interpretation of the data sets using multivariate data analysis approaches such as Principal Component Analysis (PCA) [24, 25], Partial Least Squares regression (PLS) [18, 26], and Multivariate Curve Resolution (MCR) [27, 28] may increase the information extracted from the obtained data set.

The identified solid-state forms of an API are characterized with regards to their stability, manufacturability, and dissolution rate [29]. Furthermore, already during this pre-formulation phase it is crucial to identify manufacturing parameters which could possibly induce changes in the solid-state of the API, as these so-called processing-induced transformations (PIT) cannot only affect drug performance and safety, but may also influence material workability and process efficiency [5].

This review presents an overview over PITs occurring during drug manufacturing, focussing on the relevant process parameters, and follows the API down-stream from particle size reduction to granulation and drying to tableting (Fig. 1, modified from [30]).



Fig. 1: Simplified presentation of the most important processing steps during the manufacturing of a tablet formulation (modified from [30]).

1.2 Solid-state forms of drugs

1.2.1 Definitions

In most cases, the API is processed in a solid form, which can either be crystalline or amorphous. The molecular structures of the different solid-state forms of an API are schematically presented in Fig. 2.

In crystalline drugs the molecules are arranged in a three-dimensional lattice and can be sub-classified as single- and multi-component compounds. Different single-component crystalline structures of one substance are named polymorphs, while multi-component compounds can be crystalline salts, hydrates/solvates, and cocrystals.

Polymorphism is the ability of a substance to exist in more than one crystalline form with different unit cell parameters with the identical chemical composition [31]. Polymorphs can be classified into two groups with respect to their interconversion to different forms, namely enantiotropes and monotropes [32]. Enantiotropy implies that one form is the most stable form at some conditions, while at other conditions another form is the most stable one. Polymorphs are monotropic if one form is the most stable form at all conditions below the melting point of the API. In this case, the polymorph with the lowest solubility is the most stable form [31].

In the past, the term pseudopolymorphism was used to describe a crystal structure in which solvent molecules are integrated into the crystal lattice. Today, this term has been replaced by solvatomorphism and includes solvates and hydrates [31]. As hydrates are the most relevant solvatomorphs from the pharmaceutical point of view, this review focuses on hydrates. The water molecules can either occupy isolated positions in the crystal lattice (discrete position hydrates), be included in a molecular channel (channel-type hydrates), or be metal-ion coordinated (ion-associated hydrates) [33].

Cocrystals are defined as stoichiometric multiple component crystals formed by an API and a cocrystal former, which both are solid under ambient conditions. API and cocrystal former interact via π - π electrostatic forces, van der Waals forces, or hydrogen bondings [34].

Salts are multi-component materials in which the compounds interact via ionic forces. All three groups, solvates/hydrates [35], cocrystals [36], and salts [7, 9], can show polymorphism.

In contrast to crystalline APIs, amorphous forms of a drug are disordered on the molecular level. To circumvent the debate, if drugs (especially milled) are amorphous or nano-crystalline, in this review a drug system is defined as “amorphous” if two constraints are fulfilled: (1) the X-ray diffraction pattern does not show any reflexes, and (2) upon heating, a calorimetric glass transition can be observed [37]. The absence of a long-range order of the molecules of an amorphous drug [38] results in a high Gibbs energy and thus a higher reactivity compared to the crystalline counterparts. Furthermore, amorphous materials show a higher apparent solubility and may therefore exhibit an increased bioavailability, making amorphization interesting for formulation of poorly water-soluble drugs. Thus, it is not surprising that some drug formulations have reached the market containing an amorphous API, for example itraconazole (Sporanox[®]) and indomethacin (Indocin[®]) [39]. However, due to the high thermodynamic energy, amorphous substances tend to recrystallize. In addition, amorphous substances are more hygroscopic than crystals, and the absorbed moisture may function as a plasticizer, reducing the glass transition temperature. This may lead to an increase in the molecular mobility, and therefore to a further increase in the risk of recrystallization. Furthermore, the stability of the amorphous API may depend on its manufacturing method: The stability of amorphous indomethacin regarding recrystallization for example, decreases from quench-cooling over cryo-milling and spray-drying towards ball-milling [40]. Different approaches have been undertaken to stabilize amorphous drugs, for

example by processing a mixture of the API with a polymer to form a glass solution [41-43], or by forming coamorphous systems of two drugs [44-48].

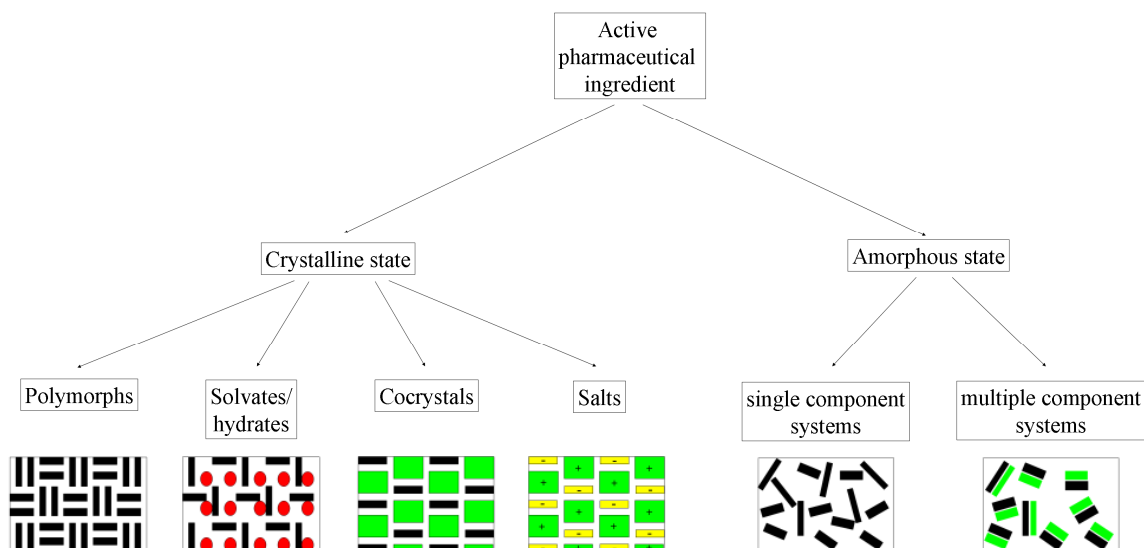


Fig. 2: Overview of the possible solid-state forms of an API.

1.2.2 Influence of the solid-state form of an API on its properties

The different structures of the various solid-state forms presented in section 1.2 may result in different physico-chemical properties, which may affect processing as well as drug performance and safety. For example, amorphous substances show a higher free surface energy compared to their crystalline counterparts, which may lead to unfavourable bulk properties such as poor flowability and cohesiveness and thus reduced miscibility [49]. Additionally, amorphous substances may be more hygroscopic, which may not only increase the thermodynamic driving force of recrystallization by plasticizing effects, but may also affect the bulk properties of the API negatively. Furthermore, the mechanical properties of the drug solid-state forms may differ and thus affect processibility of an API. Differences in the crystal habit may have an impact on miscibility and on the reproducibility of the API content in single dosage forms such as capsules or tablets. Interestingly, polymorphs and cocrystals

may vary in their tableting behaviour, which in many cases results from a different quantity of slip planes in the crystal lattice [6].

Not only processibility may depend on the solid-state form of an API. It is known that also drug performance and safety may be affected, as differences in solubility and dissolution rate between the different solid forms may occur. Often the amorphous form has a higher apparent solubility compared to the stable crystalline form [50], which may potentially result in an increased bioavailability of the drug if the gastro-intestinal absorption is dissolution rate-limited. Thus, an unintended amorphization might lead to a toxic blood level of the drug. However, a higher bioavailability cannot be observed in all cases of a decreased crystallinity of the drug, as recrystallization upon dissolution may occur, as soon as supersaturation with respect to the stable crystalline form is achieved. For many stable crystalline forms, hydrate formation may occur in the aqueous environment after oral administration or in dissolution tests, which may again decrease the solubility of the drug. This may also antagonize the advantage gained by the improved solubility of the amorphous form [51].

Many processing steps include drastic manufacturing conditions, which can be divided into three groups: (1) exposure of the API to mechanical stress, (2) exposure to solvents (including water), and (3) exposure to heat [5], enabling phase transformations of the solid-state forms of the API.

Due to the above-mentioned differences in mechanical as well as in physico-chemical properties of the different solid-state forms it becomes evident that solid-state characterization of the API in the final product is not sufficient. An extensive understanding of the process parameters influencing these phase transformations and the detailed knowledge of their mechanisms is crucial to guarantee a trouble-free processing and product performance.

1.2.3 Mechanisms of phase transformations

The mechanisms of solid-state phase transformations are described in detail by Zhang et al. [32] and are briefly summarized in the following sub-chapters.

1.2.3.1 Transformations in the solid-state

Transformations in the solid-state proceed without passing a liquid or vapour intermediate state. The kinetics of these phase transitions depend on factors such as temperature, humidity, pressure, and the presence of crystalline defects and impurities. Transformations in the solid-state have been observed for polymorphic transitions, hydration/dehydration, cocrystal formation, crystallization of the amorphous form, and vitrification [32].

1.2.3.2 Transformations via the melt

Cooling of the melt of an API may lead to a different solid-state form than the original form. Factors determining the final solid-state form include for example the cooling rate, nucleation rate, and crystal growth rate, as well as the presence of impurities and excipients. Phase transitions via a melting step include polymorphic transitions, cocrystal formation, and vitrification [32].

1.2.3.3 Transformations in solution

Dissolution of the API and subsequent removal of the solvent may also lead to changes in the solid-state form of the drug. The transformation may proceed from the meta-stable to the stable form and vice versa. However, only the dissolved drug can be transformed. The

final solid form is determined by nucleation and crystal growth, the solvent-removal rate, and also by the presence of excipients and insoluble impurities, which can function as nucleation seeds. Phase transitions in solution may include polymorphic transitions, hydration/dehydration, cocrystal formation, crystallization of amorphous substance, and vitrification [32].

1.2.3.4 Solution-mediated transformations

Solution-mediated solid-state transformations occur while the API is in intimate contact with the solvent and proceed via three steps: first, dissolution of the meta-stable form; second, nucleation of the stable form; and third, crystal growth of the stable form. The second and third step can be transformation rate-determining. If nucleation is the rate-determining step, the transition depends on solubility differences between the meta-stable and the stable form, presence of soluble excipients, contact surfaces, temperature, and agitation. If crystal growth is rate-determining, the conversion rate correlates with the solubility differences of the solid forms, the solid/solvent ratio, particle size of the original form, agitation, temperature, and soluble excipients. Polymorphic transitions, hydration/dehydration, crystallization of the amorphous form, and the transition of the meta-stable to the stable polymorph as well as cocrystal formation have been observed to proceed via a solution-mediated mechanism [32].

1.3 Process-induced solid-state transformations

1.3.1 Solid-state transformations during particle size reduction

The first step of the manufacturing process of a solid dosage form is usually to transfer the particle size and particle size distribution of the API into a practical range for down-

stream processing by milling. The input of a significant amount of mechanical energy to an API during the milling process may result in different solid-state changes. Milling of the plain API may either lead to amorphization or polymorphic changes, while with hydrates dehydration may be observed, resulting in the anhydrate or the amorphous form. The risk of these resulting solid-state forms is their high thermodynamic energy, increasing the likelihood to change to a thermodynamically more stable solid-state form. Co-milling of an API with some compounds may result in cocrystals or co-amorphous systems.

In a milling operation, the applied stress is sufficient to dislocate weak crystal lattice planes, leading to a decrease in the collective molecular interactions and thus to a loss in the long-range order. This may cause a regional formation of amorphous material, which, in the case of sufficient mechanical shear energy, can result in complete amorphization of the API [5, 52].

According to the theoretical considerations presented above, the degree of amorphization of an API during milling depends on the energy input into the system. Furthermore, the glass transition temperature (T_g) of the amorphous API in relation to the environmental temperature [53] and the substance temperature during milling play an important role: If the processing temperature is approximately 50 °C lower than the T_g of the amorphous API, formation of the amorphous form may be expected, because the molecular mobility is not sufficient for molecular reassembly and thus recrystallization [54]. Moreover, the influence of the original solid-state form also has an impact on the resulting form after milling [53].

In this review, amorphization of an organic API prepared by ball-milling of the crystalline phases is discussed using the example of indomethacin, as the amorphization ability of this drug is thoroughly investigated. Amorphous indomethacin has a glass transition temperature of approximately 45 °C and crystalline indomethacin has been shown to be

sensitive to milling with respect to solid-state transformations. Furthermore, the polymorphism of the crystalline forms of indomethacin is well investigated.

The mechanical energy input into the system is determined by the milling time and the milling frequency. Crowley and Zografis reported that the intensity of the XRPD reflections of milled crystalline indomethacin decreases as a function of milling time due to a loss of crystallinity, until after 60 min of milling the crystalline-to-amorphous phase transition is completed and only the amorphous halo is observable in the XRPD pattern [55]. However, Chieng et al. reported that ball-milling of crystalline indomethacin does not yield in complete amorphization within 60 min of milling [45], which is consistent with Planinšek et al. [56] and Patterson et al. [57], who observed complete amorphization only after 120 min of milling. This putative inconsistency of the data results from different experimental conditions such as milling frequency and environmental temperature, emphasizing the relevance of a detailed knowledge of the experimental conditions and their impact on the solid-state form of the product. Chieng et al. used a milling frequency of 30 Hz [45], while Crowley and Zografis performed milling at only 10 Hz [55]. On first sight, this observation seems unexpected, as the higher mechanical energy applied in the process described by Chieng et al. did not result in complete amorphization of crystalline indomethacin. The essential influencing factor to explain this observation is the environmental temperature: While Chieng et al. milled at 4 °C, Crowley and Zografis performed milling in liquid nitrogen and thus at a significantly lower temperature, therefore increasing the amorphization tendency during milling. Otsuka et al. compared different environmental temperatures on the degree of amorphous indomethacin formed during milling. At 30 °C only approximately 50 % of the crystalline substance converted into the amorphous material and another polymorph. Milling at 4 °C resulted in complete amorphization after 2-4 h [53], which is consistent with the results presented by Chieng et al. [45] and Patterson et al. [57]. The effect of T_g of the amorphous API and the

experimental milling temperature on solid state conversions of APIs as well as of pharmaceutically relevant excipients was demonstrated by Descamps et al. [58]. These authors could show that a decrease of the milling temperature yields a higher content of amorphous material, while milling above the T_g favours crystalline-to-crystalline, i. e. polymorphic transformations.

Crowley et al. reported complete amorphization of all three different indomethacin polymorphs by cryo-milling for 20 min with consistent T_g values of 45 °C [55]. However, significant differences in the stability of the cryo-milled samples were observed. This was explained by residual crystalline structures in the amorphous samples and the increased specific surface area [55]. Karmwar et al. compared the stability and differences in the molecular structure of differently prepared amorphous indomethacin. It was observed that the recrystallization rate of amorphous indomethacin prepared by ball-milling was higher compared with that of the quench-cooled substance. This observation was explained by the differences in relaxation time values and not by structural differences, as it could be anticipated [40].

Conversion from one to a different crystalline phase, i. e. polymorphic transformation, can also occur during milling and may structurally be explained by the introduction of defects in the crystalline lattice, providing mobility to lattice elements to collectively reassemble forming another polymorph [59]. As with the amorphization of an API during milling, the resulting solid-state phase transformations depend on the mechanical energy input, influenced by the type of mill and the milling frequency. Furthermore, the environmental temperature and the original solid-state form of the API may affect the solid-state form of the product.

Chieng et al. investigated the influence of the parameters of a milling process performed with an oscillatory ball mill with respect to the solid-state phase transformation of ranitidine hydrochloride form I. A complete transformation from form I to form II via an amorphous

intermediate form within 2-4 h was shown [60]. This transformation was also reported by Dunkel et al., who described the transformation in a rolling ball mill taking several days [61]. The faster transformation rate observed with the oscillatory ball mill may be explained by the higher mechanical energy input of this mill type [60]. It was suggested that ranitidine hydrochloride form II exists in a disordered crystalline state, while form I is arranged in an ordered crystal state. Milling generates large amounts of heat and vibrational energy [55], leading to milling-induced crystal disorder. Thus, formation of form II crystals was initiated by the disruption of the ordered form I crystals as a result of the energy introduced by the milling process. In addition, the environmental temperature was found to influence the conversion rate of form I, which was faster at 35 °C compared to that observed at 12 °C. While conversion from form I to form II was observed at 12 °C and at 35 °C, milling of form I at 4 °C only resulted in the amorphous form [60].

The solid-state of the milled product may further be influenced by the original solid-state form, as discussed by Zhang et al., who showed that milling of form II of sulfamerazine only leads to peak-broadening of the XRPD reflections due to particle size reduction and loss of crystallinity, while the stable form I completely converts into form II within 2 h of milling [62].

Milling of API hydrates may result in the dehydrated or the amorphous form, depending on the process of the release of water molecules as well as on the reassembly of the dehydrated material [63, 64]. Furthermore, the milling period plays an important role regarding the solid-state form of the product: Prolonged milling periods may lead to a complete formation of the amorphous or an anhydrous form.

Co-milling of an API with some substances, so-called cocrystal formers, may lead to the formation of cocrystals depending on the milling intensity, milling time, and on the solid-state form of the API [65]. Three formation mechanisms for cocrystal formation via milling are

discussed in the literature: molecular diffusion [66], intermediate formation of eutectic mixtures [67], and intermediate formation of an amorphous phase [25]. In some cases the loss of crystallinity is clearly detectable as a broadening of the reflections in the XRPD patterns, as displayed in Fig. 3 [25]: The XRPD reflections broadened as a function of milling time of piracetam and citric acid, until after 5 min a maximum of crystalline disorder could be observed. Prolonged co-milling periods led to a higher crystallinity of the milling product, i. e. the cocrystal [25].

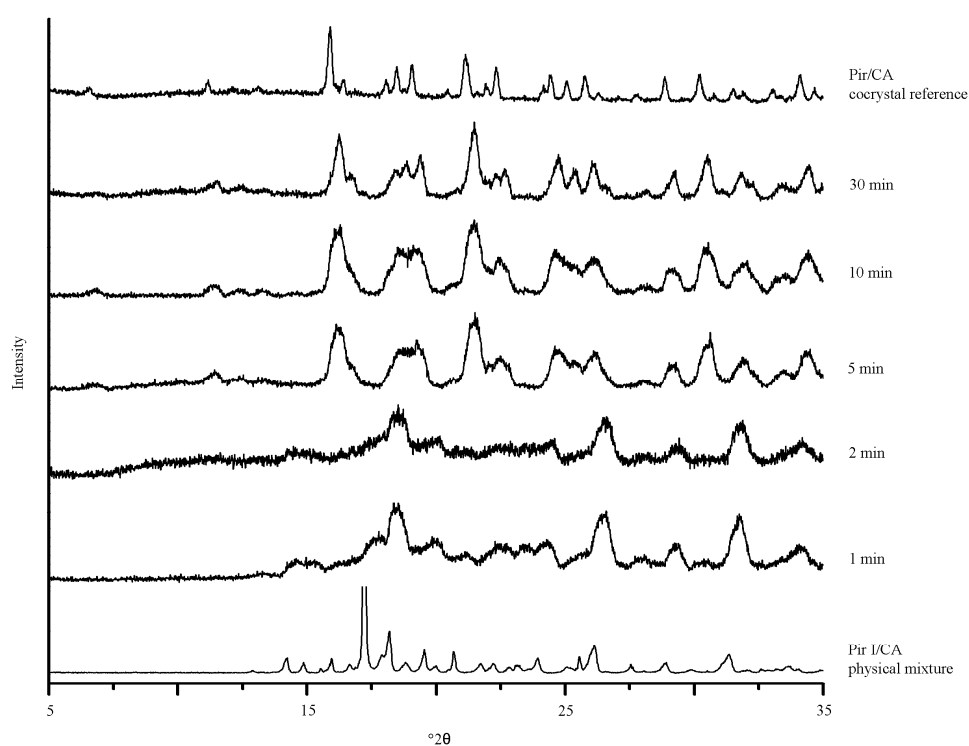


Fig. 3: XRPD diffractograms obtained after co-milling of piracetam form I (Pir I) and citric acid (CA) at predefined milling periods [25].

In other cases the lattice disorder during co-milling only subtly changes and can only be followed as a function of milling time by the combination of Raman spectroscopy and PCA (Fig. 4), detectable by the ‘arch’ of the cocrystal formation path of piracetam and tartaric

acid in the PCA 2D scores plot, which might be the result of peak shifts due to a loss of crystallinity [25].

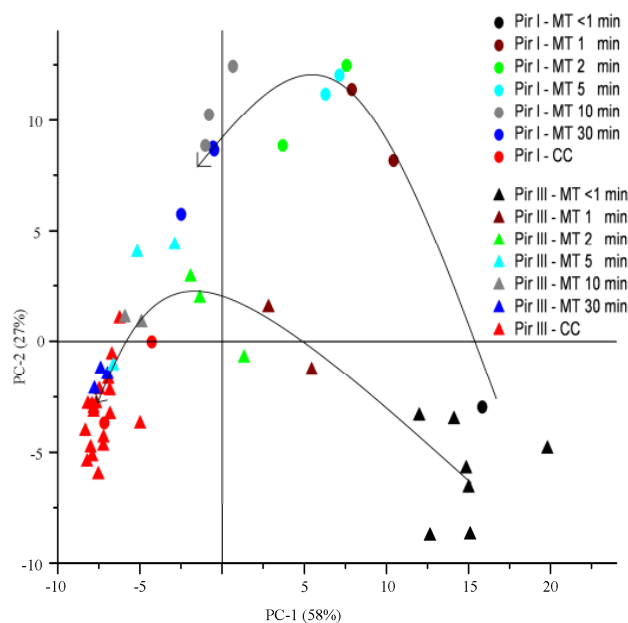


Fig. 4: PCA 2D scores plot of piracetam form I / form III co-milled with tartaric acid (TA), based on the Standard Normal Variate-corrected Raman spectra [25].

Co-milling of the dihydrate of carbamazepine with nicotinamide resulted in the fastest cocrystal formation rate compared with the metastable and the stable polymorphs of carbamazepine, with the stable polymorph converting at the slowest transformation rate. The reason for the fast cocrystal formation with carbamazepine dihydrate was suggested to be the release of the hydrate water, following a mechanism as observed with so-called liquid-assisted grinding. Here, a small amount of liquid is added before the milling process, increasing the cocrystal formation rate by acting as a catalyser. The differences in the cocrystal formation rate of the polymorphs of carbamazepine were discussed to be the free energy differences due to packing differences. Thus, a higher amount of mechanical activation energy was required to cause lattice defects in the stable carbamazepine anhydrous crystals [68].

Interestingly, in some cases co-milling of stoichiometric mixtures of two low molecular weight APIs produces stable amorphous systems [47, 48]. These so-called co-amorphous systems are stabilized by intermolecular interactions [69] and may show a significantly increased dissolution rate compared to the crystalline APIs [44]. Chieng et al. prepared a co-amorphous system containing indomethacin and ranitidine hydrochloride by ball-milling over 60 min in a cold room at 4 °C [45]. Interestingly, milling of the single substances did not lead to complete amorphization under the applied conditions.

1.3.2 Solid-state transformations during high-shear wet granulation

Usually APIs cannot be directly compressed into tablets, as flowability and compressibility of the powder often are insufficient for unproblematic down-stream processing[70]. To solve these problems, excipients are used to allow a trouble-free compaction process. Granulation is a well-established operation in the tablet manufacturing process and can be performed as dry, wet, and melt granulation. All granulation methods include the risk of PITs [5]. However, this review will focus on the process of high-shear wet granulation. Different approaches have been undertaken to model PITs during high-shear wet granulation [71, 72], but a detailed survey during the pre-formulation phase is important, as this process is very complex and therefore PITs in this process are hard to predict.

The high-shear wet granulation process can be divided into three steps: The first step is the addition of a liquid (in most cases water or hydroethanolic binder solutions) to a dynamic powder bed, leading to the agglomeration of the particles. The second step is a wet-massing step, where a rotating impeller (rotation speed between 100 and 500 rpm) homogenizes the mixture in the granulation jar, distributes the granulation liquid, and forms agglomerates. A fast-rotating chopper (rotation speed between 1000 and 3000 rpm) disintegrates the large

agglomerates and therefore supports granule formation. The third step is the drying of the granules [73].

The solid-state transformations observed during the wetting and the wet-massing steps either follow a solution or a solution-mediated mechanism, depending on the drug content in the formulation and the volume of the solvent, the solubility of the respective solid-state forms in the granulation liquid, and their dissolution rates [32]. The transformation rate of the conversion determines if the conversion will proceed completely during the processing time period [72].

Hydrate formation is the best-documented PIT during high-shear wet granulation and also proceeds via a solution or a solution-mediated mechanism [32]. In the wet environment the hydrated form of an API (if it exists) is the thermodynamically most stable form and will most likely be formed [72]. However, the unintended formation of the hydrate may decrease the dissolution rate of the API [74] and thus might negatively affect the bioavailability.

The PITs occurring during high-shear wet granulation are multi-factorial and depend on the physico-chemical properties of the processed API, on the granulation conditions such as granulation liquid, impeller speed, and processing time, as well as on the excipients used in the granule formula. Furthermore, the parameters applied in the subsequent drying step have a significant impact on the solid-state form of the API in the final product [32]. Various analytical methods were used including Raman spectroscopy [18, 75, 76], NIR spectroscopy [77, 78], and XRPD [79] combined with different multivariate data analysis approaches, i. e. PCA [20], PLS regression [75], and interval Partial Least Squares regression (iPLS) [18, 80] to monitor the observed PITs and to quantify the solid-state form of the API in the product.

The most obvious physico-chemical properties which are affected by API solid-state transformations are solubility and dissolution rate. Otsuka et al. observed a dependence of the

solvent on the polymorphic transformation rate of mefenamic acid form II into form I, being higher if ethanol was used as granulation liquid compared to distilled water. This observation was explained by the higher solubility of mefenamic acid form II in ethanol. Furthermore, it was shown that the transformation rate was also enhanced by increasing the processing temperature [81].

Interestingly, the polymorphic form of the API itself also has a significant impact on the transformation process. Otsuka et al. reported that the hydrate formation of three carbamazepine polymorphs resulted in significant differences in granule yield, with anhydrous carbamazepine leading to the lowest amount of granules. Anhydrous carbamazepine absorbed water, which consequently was not available for granule formation [82].

Not only the physico-chemical properties of the API play an important role regarding solid-state transformations induced by high-shear wet granulation: The amount of the granulation liquid as well as that of the API and the contact time with the API are also of interest. This was observed with the transformation of anhydrous baclofen to the monohydrate via a solution-mediated mechanism: A large volume of granulation liquid led to a complete conversion to the hydrate form, while a small amount only yielded incomplete hydrate formation. As expected, with a prolonged contact time between API and granulation liquid, a smaller volume of granulation liquid was required to achieve complete hydrate formation [83]. Furthermore, the amount of API needs to be taken into account to estimate the degree of transformation: A high drug content in the formulation usually requires a larger volume of granulation liquid to lead to complete conversion [84].

The dependence of the composition of the granulation liquid on the transformation process was also observed in a study performed by Otsuka et al.: Hydration of carbamazepine anhydrate to the dihydrate was found to depend on the character of the granulation liquid.

With distilled water or ethanol, formation of the dihydrate was not observed, while a mixture of ethanol and water (50%/50%) led to the formation of carbamazepine dihydrate. This observation was suggested to be a result of the higher solubility of carbamazepine in ethanol, leading to precipitation of carbamazepine dihydrate in the presence of water [82]. In contrast, Christensen et al. observed that a reduced water activity by the use of a water/ethanol mixture as granulation liquid delayed the formation onset of piroxicam monohydrate compared to plain water by reducing the reaction rates involving water molecules [18]. These studies show that process-induced transformations do not only depend on the physico-chemical properties of the API, but also of those of the granulation liquid.

The other possible parameter influencing PITs during high-shear wet granulation is the shear force provided by the impeller. Wikström et al. reported that an increase of the impeller speed shortens the onset time and increases the formation rate of theophylline monohydrate [76]. However, the influence of the impeller speed compared to that of the granulation liquid and the exposition time of the API to the liquid are suggested to be relatively small, as the largest portion of the shear strain is expected to dissipate by translational movement of the particles [32, 73].

The influence of excipients used in granule formulations on the solid-state PITs during high-shear wet granulation is thoroughly examined and well-described in the literature. Amorphous or semi-amorphous excipients such as the fillers microcrystalline cellulose or silicified microcrystalline cellulose were found to decrease the amount of anhydrate transformed into the hydrate [18, 75, 84-86]. However, hydrate formation was only reduced, but in none of the described cases it could be fully prevented, yielding a mixture of API hydrate and anhydrate in the granules, which might lead to unpredictable properties of the product. To completely inhibit unwanted hydrate formation, Gift et al. investigated various polymers. Caffeine hydrate formation was completely inhibited by polyacrylic acid, while

carbamazepine hydration was prevented by both polyacrylic acid and hydroxypropyl methylcellulose (HPMC) [75]. Hydrate formation was further completely prevented by addition of small amounts of HPMC to the granule formulation when granulating theophylline anhydrate; however, the granule properties remained unchanged [87]. This effect of HPMC was also observed with ciprofloxacin [88].

Crystalline excipients such as α -lactose monohydrate or mannitol did not always have an influence on the transformation, as they were not able to absorb the granulation liquid [18, 85, 87]. In other cases however, α -lactose monohydrate slightly increased the hydrate formation compared to processing without excipients. The suggested mechanism is the dissolution of the α -lactose monohydrate, which improved the wetting of examined theophylline particles [86]. The alkalizing excipient sodium bicarbonate decreased the onset time of piroxicam monohydrate formation by deprotonating the molecule, which increased its water solubility. This led to a faster dissolution and thus an increased hydrate formation [18].

Cocrystal formation during high-shear wet granulation has only rarely been observed. Jayasankar et al. established Raman spectroscopy as a real-time monitoring method to determine the formation rate of carbamazepine-nicotinamide cocrystals [89]. Recently, formation of a known cocrystal consisting of piracetam and tartaric acid (CSD reference code RUCDUP) [90] during high-shear wet granulation was investigated [91]. At-line Raman spectroscopy in combination with PLS revealed that the degree of cocrystal formation depended on the excipients used in the granulation formulation (Fig. 5). While calcium hydrogen phosphate did not affect cocrystal formation, microcrystalline cellulose significantly hindered a complete conversion, most likely by absorbing the granulation liquid, which was required for the solution-mediated cocrystal formation process [92-94]. This example shows that during high-shear granulation not only polymorphic transformations and hydrate formation can occur, but also cocrystallization may take place. On the one hand, this can be

advantageous for formulators, if the cocrystal is the solid-state form of choice, because the cocrystal can be formed during the granulation process, which saves a separate cocrystallization step. On the other hand, one has to be aware of accidental cocrystal formation during high-shear wet granulation, as the API properties may be altered.

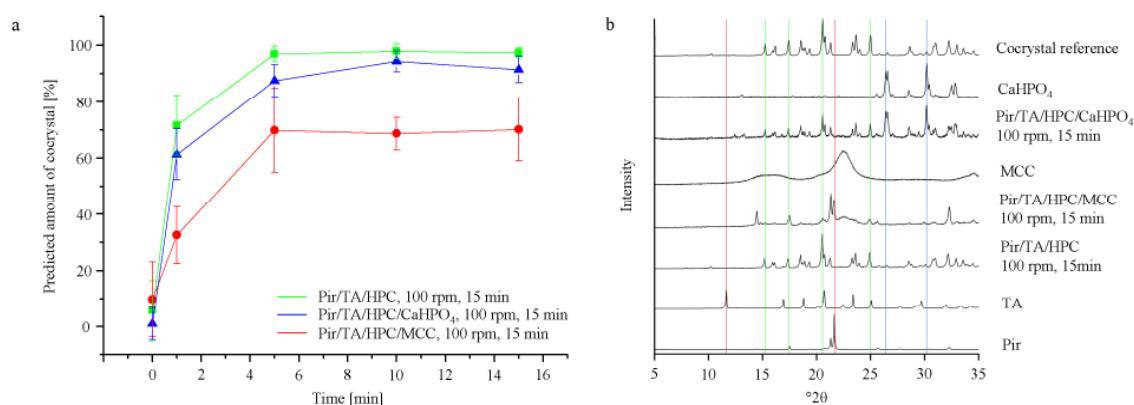


Fig. 5: (a) Predicted amount of cocrystal as a function of granulation time. Granulation was performed in duplicate; each time point represents the mean predicted amount of cocrystal \pm standard deviation at three representative sampling spots. Green curve: Pir/TA/HPC. Red curve: Pir/TA/HPC/MCC. Blue curve: Pir/TA/HPC/CaHPO₄. (b) XRPD patterns of the neat compounds and the granules at an impeller speed of 100 rpm over 15 min, immediately after preparation. Coloured lines highlight relevant reflections. (Pir: piracetam; TA: tartaric acid) HPC: hydroxypropyl cellulose; MCC: microcrystalline cellulose; CaHPO₄: calcium hydrogenphosphate) [91].

As discussed above, solid-state PITs during high-shear wet granulation are multifactorial, very complex, and thus hard to predict. As the product performance is significantly influenced by the solid-state form of the API, formulators need quantitative or even real-time [18, 76, 77, 79] methods to detect unwanted PITs or to follow desired PITs during the granulation process. For example, Koradia et al. established PLS models based on Raman and NIR spectroscopy to estimate the transformation kinetics of amlodipine besylate monohydrate during wet granulation [80]. In the presence of excipients it can be challenging to establish a universal PLS model and different models need to be created. To circumvent the spectral influence of the excipients, Christensen et al. have successfully applied iPLS to establish a

prediction model by selecting only the spectral windows relevant for the PIT. This approach reduces experimental workload and saves time in the manufacturing process [18].

1.3.3 Solid-state transformations during drying

The last step of the high-shear wet granulation process is the drying of the granules [73], where PITs can also be expected [5, 32]. PITs have further been observed during spray-drying and lyophilisation. However, this review will focus on the conventional tray-drying procedure as well as on fluidized-bed drying.

The highest risk of inducing solid-state transformations during drying is the modification of the drying parameters to make the process faster and more effective, because this may be accompanied by either an increase in temperature or in rapid solvent removal. If the drying temperature exceeds the transformation temperature of an enantiotropic pair of polymorphs, a polymorphic transformation of the API may be observed. Fast solvent removal might lead to a kinetic trapping of meta-stable solid-state forms of the API and/or the excipients [5].

Tray-drying is a traditional drying method, where the granule bed is placed on trays and kept in a constant temperature-controlled airflow. As the granule bed is static, drying only takes place at the upper surface of the particle bulk, which results in a moisture gradient within the granule bed. Thus, higher temperatures and longer drying periods are required, increasing the possibility of PITs [5, 95]. The risk of phase transformations during tray-drying may be reduced by fluidized-bed drying, a common operation in the pharmaceutical industry, as less harsh drying conditions can be applied. The granule bed is agitated by a warm air stream, allowing lower temperatures and shorter drying periods compared to tray-drying. Fluidized-bed drying can be divided into two drying stages, namely the heat-transfer controlled phase and the mass-transfer controlled phase, which are discussed in detail by

Wildfong et al. [5]. During the heat-transfer controlled phase, the particle temperature is lower compared to the inlet temperature, as most of the energy is dissipated by evaporation of the solvent, thus temperature-dependent PITs are unlikely to occur. During the mass-transfer controlled phase, the temperature of the granule bed increases significantly, resulting in temperature-dependent PITs [5]. An optimal fluidized-bed drying process may be real-time temperature-monitored and -controlled, with an inlet temperature above the phase transition temperature of the API and a subsequent down-regulation of the temperature below the transformation temperature as soon as the mass-transfer drying phase is reached and the granule bed temperature increases [5, 96].

Although the temperatures applied during fluidized-bed drying are relatively mild compared to tray-drying, the fast evaporation of the solvent may again result in kinetic trapping of meta-stable forms of APIs. This may be explained by the significantly higher drying rate compared to that observed during the solution-mediated transformation mechanism during tray-drying [71].

It is expected that drying procedures may have a high impact especially on the structure of hydrates due to dehydration of the hydrated crystalline lattices, which can lead to the formation of the dehydrated structure, the anhydrate, the amorphous form or a mixture of these forms. The processing stress leading to the before-mentioned phase transformations may be high temperature on the one hand and low relative humidity on the other hand [71]. Furthermore, the resulting solid form of the API is affected by excipients used in the granule formulation. The drying behaviour of a particle further depends on its structural properties such as the presence and size of pores as well as on the packing of the molecules. It is also strongly influenced by the orientation of the solvent molecules in relation to the orientation of the host molecules and the number and strength of hydrogen bonds between solvent and host [97, 98].

The drying of theophylline monohydrate with respect to solid-state changes is well-examined [99, 100]. Theophylline monohydrate granules were dried by fluidized-bed drying and tray-drying and both methods were compared with regard to the theophylline forms present in the granules [97]. Dehydration of theophylline monohydrate (form II) can either lead to the metastable anhydrate (form I*) or the stable anhydrate (form I). Form I* can convert into form I over time. It could be shown that theophylline monohydrate granules dried between 40 and 50 °C consisted mostly of form I*, independent of the drying method applied. Tantry et al. observed a conversion from form I* to form I during drying depending on the drying temperature: An increase of the drying temperature from 45 °C to 55 °C enhanced the transformation rate significantly [101]. Tray-drying at 60 °C, simulated by Airaksinen et al. using variable-temperature XRPD, led to complete transformation into form I within 15 min, while with fluidized-bed drying even at 90 °C still approximately 20 % of form I* remained unchanged over the complete drying process [97].

The solid-state transformation upon drying may furthermore be influenced by excipients present in the granule formulation. The transformation from theophylline form I* to form I during tray-drying was slowed down by polyvinyl pyrrolidone (PVP) solution as granulation liquid [101]. A higher molecular weight of the PVP resulted in an increased stabilisation of form I*.

The transformation of erythromycin dihydrate to the stable anhydrate or to the amorphous form requires relatively high activation energy, while the formation of the isomorphic dehydrate needs less energy and already occurs during storage at low relative humidity [102, 103]. If the water is removed completely from the channels in the crystalline lattice including bound water a molecular vacuum is generated, and polar excipients such as magnesium hydroxide may be incorporated, leading to a significant decrease in dissolution rate [104]. However, Römer et al. observed formation of the erythromycin dehydrate only at

drying temperatures above 60 °C and suggested that formation of the erythromycin dehydrate during processing is only relevant at harsh conditions such as high drying temperatures [95].

For a deeper understanding of the transformation mechanism or if the solid-state transformations are desired to occur during drying, in-line real-time quantification methods are required. Zeitler et al. used terahertz pulsed spectroscopy to gain a mechanistic in-situ insight into the dehydration of theophylline monohydrate upon drying. Two phases could be distinguished during the temperature-dependent drying, namely the phase transition itself and the evaporation of the hydrate water, making this technique valuable to gain a deeper insight into dehydration processes [105].

Kogermann et al. established a PLS model based on Raman spectroscopy to simultaneously quantify multiple solid-state transformations of carbamazepine dihydrate during fluidized-bed drying. Although model performance was lower compared to the calibration set resulting from differences in recording the spectra such as moving of the sample or distance from the probe to the sample, it could be shown that during water removal large amounts of the carbamazepine dihydrate were transformed into the amorphous form, which subsequently crystallized to a mixture of the two polymorphs with a small amount of remaining amorphous substance. It was concluded that real-time process monitoring allows an improvement in process-understanding, which may help to control the process [106].

Aaltonen et al. successfully combined either NIR or Raman spectroscopy with PLS regression to determine the dehydration of theophylline monohydrate during fluidized-bed drying [107].

1.3.4 Solid-state transformations during tableting

Tablets are the most often administered drug formulations. Their administration is convenient and their manufacture is simple, as powder or granules are compressed by an

upper and a lower punch in a die. While the punches apply axial stress to the powder/granules, radial stress occurs by particle deformation at the die wall [5]. Generally it is assumed that the solid-state form of a drug remains unchanged under the compaction stress applied during tableting, as the softer excipients are expected to deform preferentially compared to the hard crystalline drug [108]. However, as a result of the compaction stress, with some substances solid-state transformations may be observed after tableting [5, 32, 51], depending on the amount and the type of stress (hydrostatic or shear-based), the environmental temperature as well as on the solid-state forms of the API, their particle size, and the excipients in the tablet formulation.

Compaction of chlorpropamide polymorphic forms A or C by an eccentric press at compaction pressures of 196 MPa resulted in a partial transformation into the respective other polymorphic form [109], showing that solid-state phase transformations may occur already at routine compaction pressures. The reason for this transformation is the structural similarity in terms of one common slip plane in the crystal lattices of both chlorpropamide polymorphs. Thus, polymorphic transformation can take place easily by distortion and minimal translation. Hydrostatic pressure does not lead to polymorphic transformation, as lattice distortion does not occur, resulting from the uniform pressure applied on the crystal [110].

Matsumoto et al. investigated the influence of the tableting temperature on the polymorphic transformation of the chlorpropamide polymorphs A and C and observed that the amount of form A that transformed into form C at 45 °C was approximately twice as large compared to that transformed at 0 °C. However, the compression-induced transformation of form C into form A was temperature-independent [111].

Otsuka further described that the degree of transformation of the chlorpropamide polymorphs increases with increased compression energy up to a certain level [109]. Another study dealing with the influence of the compaction pressure on the degree of solid-state

transformation was published by Chan and Doelker, who examined transformation of meta-stable polymorphs of drugs as a function of compaction pressure with an eccentric press. It was observed that the transformation of sulfabenzamide form B to form A increased with increasing tableting pressure [112]. Furthermore, the transformation of the API depending on the position of the drug in the tablet was investigated. As a result of the highest tableting energy being applied onto the upper tablet surface polymorphic transformation was highest, decreasing over the thickness of the tablet with the lowest transformation on the lower surface due to the loss of tableting energy by rearrangement and deformation of the particles [112]. Interestingly, with maprotiline hydrochloride a dependence of the particle size on the degree of transformation was observed, which was explained by differences in the surface area of the particles and thus differences in the pressure at the points of particle contact, as well as by differences in friction at the die wall [112].

It was found that the recrystallization of amorphous indomethacin may also be induced by compaction [113]. The recrystallization behaviour of amorphous melt-quenched indomethacin induced by compression as a function of the cooling rate of the melt was investigated [114]. Interestingly, it was observed that the rapidly cooled melt of indomethacin was more susceptible to compression-induced crystallization compared to the slowly cooled melt, which was surprising, as Karmwar et al. showed that the stability regarding recrystallization upon storage increased with increasing cooling rate [115]. It was concluded that the stability with regard to recrystallization after compression might not be directly correlated with the physical stability during storage of glassy APIs and thus needs to be evaluated separately [114].

For an optimized tableting process the solid-state form of the API needs to be carefully evaluated, as for example Lefebvre et al. showed for the compaction of carbamazepine polymorphs and the dihydrate. Although the dihydrate showed the best compaction

properties, it could not be used for tablet formulation because it was not stable under compression and was partially transformed into the β form. The most stable α form could not be used either, as it induced sticking to the punches. Thus, the commercially used β form was found to be a good compromise regarding stability and processibility [116].

Tableting-induced phase transformations may also be affected by excipients used in the tablet formulation, resulting from their different mechanical properties. Schmidt et al. investigated the potential of different excipients to protect amorphous indomethacin from recrystallization and theophylline monohydrate from dehydration, as both transformations may be induced mechanically. Carrageenans showed the best protection because most of the compaction energy of the tableting process is taken up by elastic deformation of the carrageenans. However, a complete protection could not be achieved. Chitosans were slightly less protective than the carrageenans, but were significantly better protectors than HPMC, which again was better compared to MCC (carrageenans > chitosans > HPMC > MCC). Dicalcium phosphate dihydrate did not show any protective behaviour [113, 117]. In a subsequent study polyethylene oxides were also found to decrease tableting-induced recrystallization of amorphous indomethacin because of interactions between drug and excipient [118].

1.4 Conclusion

This review dealt with solid-state transformations induced by pharmaceutical processes. Although manufacturing of solid dosage forms is a routine operation in pharmaceutical industry, solid-state transformations of an API may be induced by all processing steps from particle size reduction to granulation and drying to tableting. The mechanisms and thus the parameters influencing these transformations are complex and need to be thoroughly

investigated in drug development. This includes identification and monitoring of process-induced solid-state transformations during manufacturing with modern real-time analytical techniques to circumvent problems in down-stream manufacturing as well as a decrease in drug performance and safety.



**2. A case study of real-time monitoring of solid-state phase transformations
in acoustically levitated particles
using near infrared and Raman spectroscopy**

A case study of real-time monitoring of solid-state phase transformations in acoustically levitated particles using near infrared and Raman spectroscopy

Abstract

The objective of this study was to monitor the amorphous-to-crystalline solid-state phase transformation kinetics of the model drug ibuprofen with spectroscopic methods during acoustic levitation. Chemical and physical information was obtained by real-time near infrared (NIRS) and Raman spectroscopy measurements. The recrystallization kinetic parameters (overall recrystallization rate constant β and the time needed to reach 50 % of the equilibrated level t_{50}), were determined using a multivariate curve resolution approach.

The acoustic levitation device coupled with non-invasive spectroscopy enabled monitoring of the recrystallization process of the difficult-to-handle (adhesive) amorphous sample. The application of multivariate curve resolution enabled isolation of the underlying pure spectra, which corresponded well with the reference spectra of amorphous and crystalline ibuprofen. The recrystallization kinetic parameters were estimated from the recrystallization profiles. While the empirical recrystallization rate constant determined by NIR and Raman spectroscopy were comparable, the lag time for recrystallization was significantly lower with Raman spectroscopy as compared to NIRS. This observation was explained by the high energy density of the Raman laser beam, which might have led to local heating effects of the sample and thus reduced the recrystallization onset time.

It was concluded that acoustic levitation with NIR and Raman spectroscopy combined with multivariate curve resolution allowed direct determination of the recrystallization kinetics of amorphous drugs and thus is a promising technique for monitoring solid-state phase transformations of adhesive small-sized samples during the early phase of drug development.

2.1 Introduction

Many new chemical entities are poorly water soluble but show sufficient membrane permeability. Thus, they are solubility- or dissolution rate-limited in their bioavailability after oral administration. To increase their solubility and dissolution rate, the amorphous form may be used for formulation and manufacturing instead of the stable crystalline drug form [119]. However, the physical stability of the amorphous form remains an issue of concern [40]. Therefore, it is essential to understand the recrystallization kinetics of an amorphous active pharmaceutical ingredient (API) and the factors influencing crystallisation. Some amorphous APIs show a glass transition temperature below room temperature. At room temperature, these APIs become highly viscous and adhesive, making them difficult to handle and examine [120, 121]. Furthermore, in the early phase of drug development the availability of sufficient amounts of API is limited [122]. Therefore, characterisation techniques, which allow a non-destructive analysis of small amounts of the compound, are required [123]. Lab-on-a-chip approaches might be undertaken to examine small amounts of compounds, however these have the potential drawbacks of sample-container wall interactions [13] and optical interference at the container walls complicating detection [124]. To circumvent these drawbacks, acoustic levitation may be applied, which in the past has been established for a range of experiments such as containerless crystallization from solutions [125, 126] and supercooled melts [127]. An interesting study was recently published by Benmore and Weber, who described the preparation of amorphous APIs by melting the crystalline drug in the acoustic field of an acoustic levitator using a laser beam followed by a subsequent cooling step [11]. This method prevents seeding during the preparation of the amorphous sample. The operating mode and the theoretical background of acoustic levitation are thoroughly described in the literature [128]. Briefly, acoustic levitation deploys an ultrasonic wave, which originates at the transducer and is reflected by the reflector. Interference occurs because of the

same wavelength of the original and the reflected waves, leading to a standing acoustic wave which is characterised by the sound pressure and the sound velocity. The resulting pressure distribution in the acoustic field allows the levitation of small particles. Critical factors of acoustic levitation are sample size and weight. Whereas the weight of the sample only rarely represents a problem, the limitation by the size of the sample is usually more relevant. However, Xie et al. demonstrated stable levitation of tungsten spheres with a much higher density (18.92 g cm⁻³) than an aqueous samples (~1 g cm⁻³) [129]. The theoretical maximum sample diameter of a stably levitated particle can be estimated according to Eq. (1) [128]

$$d_{s,max} = \frac{1}{3} * \frac{c_0}{f_1} * \frac{4}{3} \quad \text{Eq. (1)}$$

where $d_{s,max}$ is the maximum sample diameter, c_0 is the sound velocity, and f_1 is the operating frequency of the sonotrode. However, levitation is most stable for smaller samples with a diameter below 1 mm if droplet deformation is undesired [128].

Although acoustic levitation represents a promising technique to study solid-state phase transformations in levitated samples, currently the challenge of this technique is to establish non-invasive analytical methods, which allow fast real-time monitoring of very small samples, i.e. single particles. Optical analysis with a camera [130], X-ray diffractometry [125], and Fourier transform infrared spectroscopy [131] have been successfully applied for analysis of levitated samples. Furthermore, Raman spectroscopy has been extensively used for *in situ* characterisation of levitated samples, allowing fast chemical and structural analysis [126, 127, 130, 132].

Near infrared spectroscopy is gaining increasing interest in preformulation because of the fast, non-destructive, non-invasive, and flexible analysis of the sample offered by this technique [133]. However, in contrast to mid infrared spectroscopy, NIR spectra are less specific with only subtle differences between different solid-state forms of the same

compound. Overlapping of bands often occurs in the NIR spectra if a multi-component system is investigated, complicating the interpretation of the spectra [133, 134]. If a calibration data set is not available, common multivariate data analysis approaches in analysing NIR spectra include various pre-processing methods together with Principal Component Analysis (PCA) [135]. Although PCA has proven to be a robust analysis method on multivariate data sets, the main limitation of PCA in analysing NIR spectra is the difficulty in the interpretation of the loadings from a chemical perspective. For quantitative analysis of multi-component systems Partial Least Squares regression (PLS) is a well-established method if a calibration data set is available [26, 136]. Multivariate Curve Resolution (MCR) offers an alternative approach to PCA and PLS when building a multivariate model [27, 28, 137]. The main advantage of MCR as compared to PCA and PLS is that the MCR model is easier to interpret and a calibration data set is not strictly required. This method is also known as soft modelling or mathematical resolution, which assumes that each spectrum can be described as the sum of N pure underlying chemical spectra (Eq. (2)):

$$\mathbf{D} = \mathbf{c}_1 \mathbf{s}_1^T + \mathbf{c}_2 \mathbf{s}_2^T + \dots + \mathbf{c}_N \mathbf{s}_N^T + \mathbf{E} \quad \text{Eq. (2)}$$

where \mathbf{D} is the obtained spectral matrix with each spectrum arranged row-wise, \mathbf{s} is the pure underlying chemical spectrum, \mathbf{c} is a vector containing the weight of the pure underlying chemical spectrum, T is the vector transpose, and \mathbf{E} is the residual matrix. The purpose of MCR modelling is for each spectrum to estimate the pure underlying chemical spectra, and their respective weights. This approach is useful when calibration samples are either impossible, or extremely difficult to prepare because of the dynamic nature of the investigated process.

The aim of the present study was to investigate the use of NIR and Raman spectroscopy combined with MCR to determine the recrystallization kinetic parameters of millimetre-sized levitated amorphous ibuprofen used as a highly viscous model API.

2.2 Experimental methods

2.2.1 Materials

Ibuprofen (pharmaceutical grade) was supplied by BASF, Germany.

2.2.2 Methods

2.2.2.1 Preparation of amorphous ibuprofen

Crystalline ibuprofen was transformed into the amorphous state by quench-cooling. First, the drug was heated in an oven at 85 °C until it was completely molten. Then the melt was poured into liquid nitrogen. The particles were kept in liquid nitrogen until further analysis.

2.2.2.2 Acoustic levitation of amorphous ibuprofen

A single amorphous ibuprofen particle in the glassy state was trapped in an acoustic field at 42 kHz (Fig. 6a, levitated coloured water droplet as an example). At a frequency of 42 kHz the theoretical maximum sample diameter is 3.6 mm (Eq. (1)). However, levitation is most stable with smaller samples (diameter <1 mm) and is recommended if droplet deformation is undesired [128]. The particle transformed into the rubbery state and recrystallized within minutes. The experiment was performed in triplicate at ambient conditions each for four minutes. To obtain spectroscopic data from the levitated sample, NIR or Raman spectroscopy probes were placed at a distance of approximately 5 mm to the particle without disturbing the acoustic field (Fig. 6b).

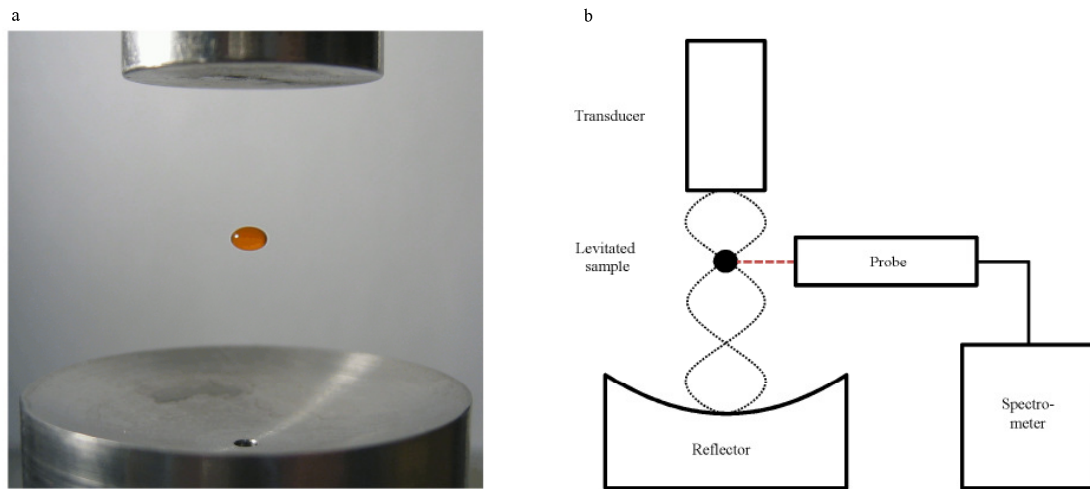


Fig. 6: (a) Levitated sample (coloured water). (b) Schematic experimental setup.

2.2.2.3 High speed camera

High speed camera images were obtained with a MotionPro Y4 Speed 2 camera (Imaging Solutions, Germany). Shutter speed was 5 ms and frequency was 30 frames per second.

Particle size was determined from the high speed camera images at the end of each experiment using an in-house written Matlab script (ver. 7.10, Mathworks, USA). The obtained 8 bit resolution gray scaled image array with size 1024×1024 was pre-processed using binarization by applying a 50 % threshold. In order to fill the holes within the particle in the binary image, a closing operation was performed with a 200 pixel diameter disc morphological structuring element [28]. The pixels belonging to the particle were counted and transformed into area.

2.2.2.4 Near infrared spectroscopy (NIRS)

Solid-state phase transformation of the levitated ibuprofen particle was monitored by NIRS using a NIR-256L-2.2T2 spectrometer (Control Development, UK) with a tungsten light source and a fibre optic probe. The detector used in this setup was a thermoelectrically cooled 256 element InGaAs array detector. Spectra were collected for four minutes in a continuous scanning mode with an integration time of 0.01 s. Each spectrum was the average of 32 spectra and had an 8 cm^{-1} resolution.

2.2.2.5 Raman spectroscopy

The levitated samples were investigated using a Raman spectrometer (Control Development, USA), equipped with a thermostatically cooled CCD detector and a fibre optic sampling probe (RamanProbeTM, InPhotonics, USA). Samples were excited using a laser with a wavelength of $\lambda = 785 \text{ nm}$ and a laser power of 300 mW (Starbright 785S, Torsana Laser Technologies, Denmark). The focal length of the laser beam was 5 mm. The Raman laser spot size was approximately 200 μm . The depth of field D_f was calculated according to Eq. (3) [138], the numerical aperture (NA) of the lens of the Raman probe was 0.22:

$$D_f = \frac{\lambda(1 - NA^2)^{1/2}}{NA^2} \quad \text{Eq. (3)}$$

Spectra were recorded between 543 and 1674 cm^{-1} in a continuous scanning mode with a resolution of 8 cm^{-1} and 1 s integration time. Each spectrum was the average of 8 spectra. Careful attention was paid to minimise the exposure of the sample to the laser.

2.2.2.6 Multivariate data analysis

Spectra were analysed using an in-house written Matlab script (ver. 7.10, Mathworks, USA) together with the Multivariate Curve Resolution Alternating Least Squares (MCR-

ALS) toolbox developed by Jaumot et al. [139]. NIRS is sensitive to adsorbed water, thus the water bands were excluded from further analysis, and the regions included in the MCR model were from 4731 to 5075 cm^{-1} , from 5263 to 6600 cm^{-1} , and from 7600 to 8944 cm^{-1} . Both NIR and Raman spectra were pre-processed using Standard Normal Variate (SNV) correction [140]. The negative intensity values after SNV correction were corrected by adding a constant offset to all spectra.

Evolving factor analysis was performed for each experiment in order to identify the number of evolving chemical components [141]. Initial estimations for the alternating least squares algorithm contained the first and the last experimental spectra corresponding to amorphous and crystalline ibuprofen, respectively. Non-negativity in spectral mode, unimodality in concentration mode, and closure constraint were applied to the MCR model. Furthermore, NIRS experiments were analysed with the use of column-wise matrix augmentation. After MCR, each estimated pure underlying spectrum was compared to the reference spectrum and Pearson's correlation coefficient P was calculated according to Eq. (4) [142]:

$$P = \frac{\sum_{i=1}^I (s_i - \bar{s})(s_{ref,i} - \bar{s}_{ref})}{\sqrt{\sum_{i=1}^I (s_i - \bar{s})^2 \sum_{i=1}^I (s_{ref,i} - \bar{s}_{ref})^2}} \quad \text{Eq. (4)}$$

where $s_i, s_{ref,i}, \bar{s}, \bar{s}_{ref}$ and I are the spectral element at index i of the pure spectrum, spectral element at index i of the reference spectrum, average of pure spectrum, average of reference spectrum, and the total vector length of the spectrum, respectively.

To estimate the recrystallization kinetics, the weights (c) of the underlying crystalline ibuprofen pure spectrum were plotted as a function of time and fitted to a logarithmic growth function (Eq. (5)) previously used to describe recrystallization phenomena [28, 143, 144]:

$$X = X_0 + \frac{\alpha}{1 + e^{-\beta(t-t_{50})}} \quad \text{Eq. (5)}$$

where X , X_0 , α , β , and t_{50} are the fraction of recrystallized ibuprofen at time t , the initial fraction of recrystallized ibuprofen, the equilibrated crystalline ibuprofen fraction, an empirical constant related to the amorphous-to-crystalline transformation rate, and the time needed to reach 50% of the equilibrated level, respectively.

2.3 Results and discussion

2.3.1 High speed imaging of ibuprofen recrystallization

Due to the low glass transition temperature of ibuprofen (-45 °C) [145], the ibuprofen particle gradually transformed from the glassy state into the rubbery viscous state upon levitation. The process of levitation of the particle prevented interactions with container walls, and hence eliminated a possible influence of the heat transfer from the container to the levitated sample. The droplet rotated around its vertical axis and moved three-dimensionally. The particle movement was estimated using the high speed camera images and was determined to be approximately $\pm 250 \mu\text{m}$ in horizontal (extreme values $\sim 600 \mu\text{m}$) and about $\pm 50 \mu\text{m}$ in vertical direction (extreme values $\sim 50 \mu\text{m}$). As a result of its high Gibbs free energy, recrystallization of the amorphous ibuprofen occurred fast and was observed with a high speed camera (Fig. 7). The crystal nuclei were arranged at the equator of the rotating droplet as a result of centrifugal forces. According to the high speed camera images, recrystallization as a function of time was completed within approximately one minute. With increasing crystalline material however, the optical density of the particle increased and thus observation of the recrystallization process became more difficult over time. Therefore, the images presented in Fig. 7, also illustrate the need for the use of a non-invasive spectroscopic

method in order to gain quantitative information and an increased understanding of ibuprofen recrystallization on a molecular level, as real-time monitoring is necessary to determine the recrystallization kinetic parameters β and t_{50} . Hence, NIR and Raman spectroscopy, in combination with MCR data analysis were applied.

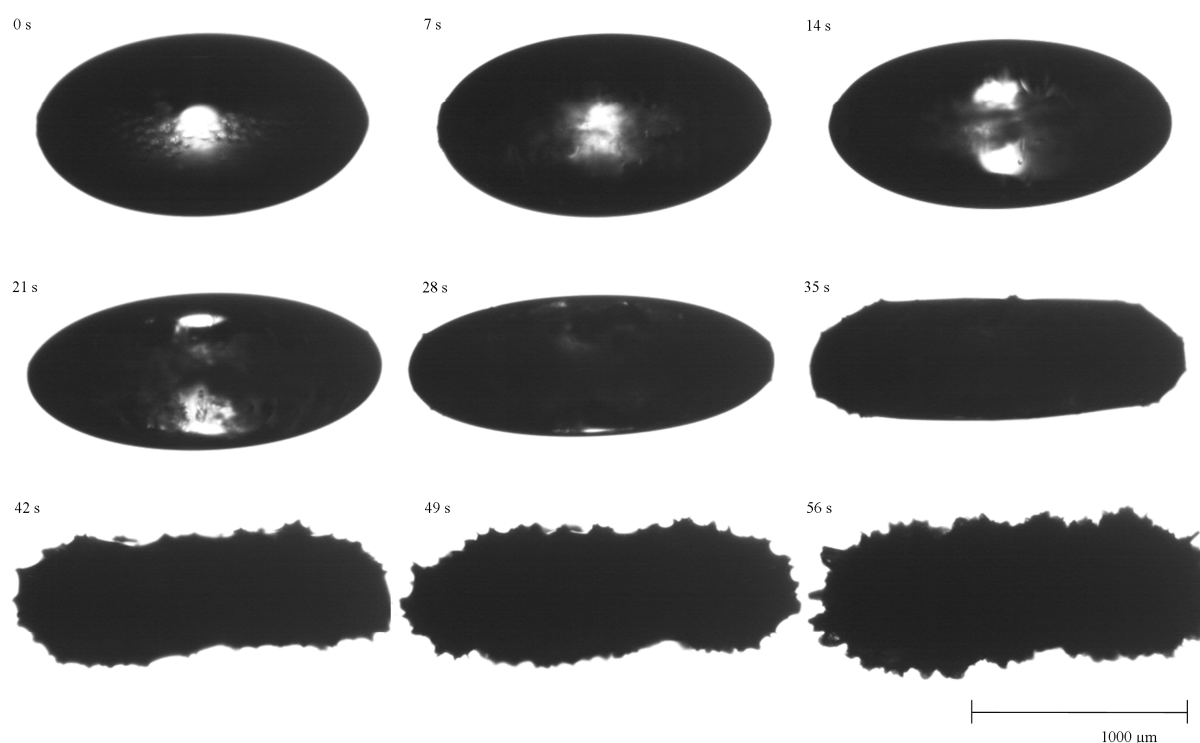


Fig. 7: High speed camera images of the recrystallization process of an amorphous ibuprofen particle with an approximate diameter of 2 mm. Transformation of fully amorphous to fully crystalline ibuprofen.

2.3.2 Ibuprofen recrystallization monitored with NIRS

In Fig. 8a the SNV-corrected NIR spectra are presented. They were in good agreement with the literature [146]. The colour gradient of the bar indicates the recrystallization process with the blue spectrum representing amorphous ibuprofen and the red spectrum crystalline ibuprofen. The most significant changes in the NIR spectra during recrystallization were found in the regions between 5660 and 5950 cm^{-1} , where the first overtone of the CH stretch

vibration bands is observed, and between 8000 and 8700 cm^{-1} , where the second overtone of the CH stretch vibrations appear [147].

Univariate data analysis of NIR spectra can be difficult due to the broad and overlapping absorption bands, and differences between amorphous and crystalline API spectra may be indistinct [148, 149], illustrating the need for multivariate data analysis. With MCR, chemical meaningful pure component spectra can be extracted from the data set. However, prior to MCR model building, it is important to know the number of evolving chemical components (pure chemical spectra N in Eq. (2)) underlying the data set. Evolving factor analysis [27] was performed to determine the number of components in the spectral data set and resulted in two significant evolving components. This finding matched well with the expectation, since the first component can be attributed to the decrease of amorphous ibuprofen and the second component can be attributed to the evolution of crystalline ibuprofen (data not shown).

To identify these two components, MCR was performed. In Fig. 8b the MCR pure spectra corresponding to the two evolving components (black spectra) are presented together with the uncorrected amorphous (blue spectrum) and crystalline ibuprofen reference spectra (red spectrum), respectively, for comparison. Visually, the MCR pure spectra are very close to their respective reference spectra (Fig. 8b). The Pearson's correlation coefficient of the MCR pure spectrum and the reference spectrum of amorphous ibuprofen was 0.990, the Pearson's correlation coefficient of the MCR pure spectrum and the reference spectrum of crystalline ibuprofen was 0.999, respectively. This indicates that MCR selectively modelled the evolution of amorphous and crystalline ibuprofen in the levitated particle from the NIR spectra.

The fitting of the amorphous-to-crystalline transformation profiles to Eq. (5) was considered satisfactory (average $R^2 = 0.992$) and is presented for each replicate experiment in

Fig. 8c. The overall transformation rate constant β was determined to be $2.57 \pm 0.53 \text{ min}^{-1}$ and t_{50} was $2.01 \pm 0.08 \text{ min}$.

It can be summarised that NIRS in combination with MCR is a valuable technique to estimate the recrystallization kinetic parameters of a levitated amorphous ibuprofen sample. However, extracting structural information of the recrystallization process on a molecular level from the NIR spectra was complicated because of overlapping bands, as also observed in other studies [148].

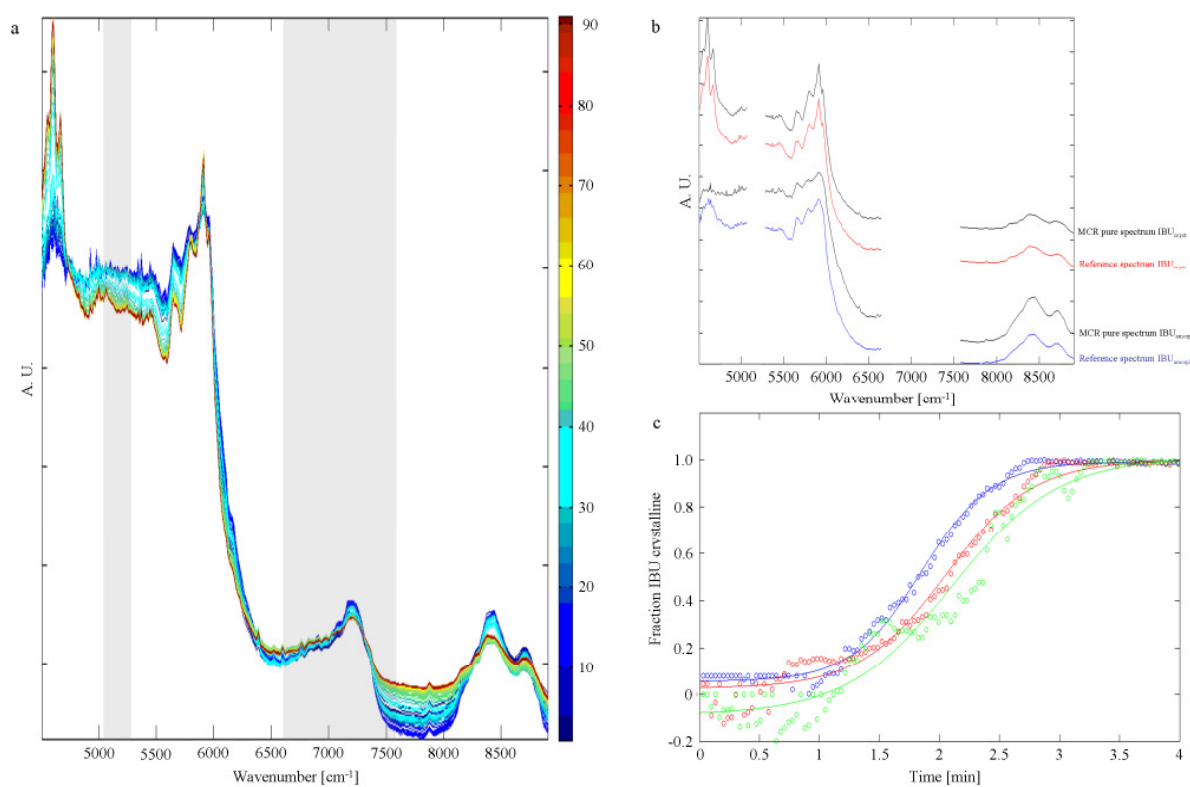


Fig. 8: (a) Time-dependent, SNV-corrected NIR spectra recorded during the recrystallization process (blue spectrum – amorphous ibuprofen, red spectrum – crystalline ibuprofen, colours on the bar are referring to the number of the spectrum, water bands greyed-out). (b) Comparison of the MCR pure spectra (black) with the amorphous (blue) and crystalline (red) reference spectrum. (c) MCR-ALS-predicted kinetic profiles of the amorphous-to-crystalline ibuprofen solid-state phase transformation (the solid curves represent the fitting to the data points according to Eq. (5)).

2.3.3 *Ibuprofen recrystallization monitored with Raman spectroscopy*

Structural interpretation of Raman spectra is more straightforward as compared to NIR spectra, but the disadvantages of Raman spectroscopy are a low signal intensity and an often inappropriate signal to noise ratio with levitated particles [132]. Wu et al. successfully applied Raman spectroscopy in combination with MCR for online-monitoring of nitrendipine antisolvent crystallization [28]. Thus, in this study Raman spectroscopy was combined with the MCR approach to determine the recrystallization kinetics of levitated amorphous ibuprofen.

The Raman peak positions of the amorphous and crystalline ibuprofen were in good agreement with the literature (Fig. 9a) [150]. As crystallization proceeded, the peaks became sharper and more intense, which is a well-known observation with amorphous-to-crystalline transformations [26, 151]. A frequency shift was observed for the aryl C=C Raman band at 1616 cm^{-1} in the spectrum of amorphous ibuprofen towards 1611 cm^{-1} in the spectrum of the crystalline form (Fig. 9b). This band shift was interpreted as a different molecular association in the crystalline and the amorphous form [150, 152].

The Raman signal intensity was low compared to offline measurements, because the particle shifted out of the laser focus, as a result of the previously described particle movement during acoustic levitation. This is a known problem with acoustically levitated samples. In a previous study by Santesson et al., the authors showed that surface enhanced Raman spectroscopy (SERS) can be useful to increase the signal to noise ratio by addition of a silver colloid solution into the levitated droplet [132], however this approach was not pursued in this study, as the effect of nanostructures on the recrystallization kinetics of the amorphous ibuprofen is unknown.

Evolving factor analysis revealed two chemical components as observed with the NIR spectra, probably attributed to the change in amorphous to crystalline ibuprofen (data not

shown). In Fig. 9c the pure MCR spectra corresponding to the two evolving components (black spectra) are presented together with the uncorrected amorphous and crystalline spectra (blue and red spectra, respectively). The MCR pure spectra were nearly noise-free and appeared visually almost identical to the reference spectra of amorphous and crystalline ibuprofen, respectively. The Pearson's correlation coefficient of the MCR pure spectrum and the reference spectrum of amorphous ibuprofen was 0.993, the Pearson's correlation coefficient of the MCR pure spectrum and the reference spectrum of crystalline ibuprofen was 0.984, respectively. In Table 1 an overview of the Pearson's correlation coefficients of the MCR pure spectra and the reference spectra of amorphous and crystalline ibuprofen, respectively, for NIRS as well as for Raman spectroscopy is presented. It can be stated that MCR selectively modelled the evolution of amorphous and crystalline ibuprofen in the levitated particle.

Table 1: Pearson's correlation coefficient (P) of the MCR pure spectra and the reference spectra of crystalline and amorphous IBU.

| | P <i>MCR pure spectrum - reference</i> Crystalline (n=3) | P <i>MCR pure spectrum - reference</i> Amorphous (n=3) |
|----------------------------|--|--|
| Near infrared spectroscopy | 0.999 | 0.990 |
| Raman spectroscopy | 0.984 | 0.993 |

The recrystallization kinetic parameters β and t_{50} were estimated for the Raman data, as the fit of the amorphous-to-crystalline transformation profiles to Eq. (5) was considered sufficient (average $R^2 = 0.991$). The solid lines in Fig. 9d represent the fitted transformation

profiles of each replicate experiment. In Table 2 the fitted parameters are summarised.

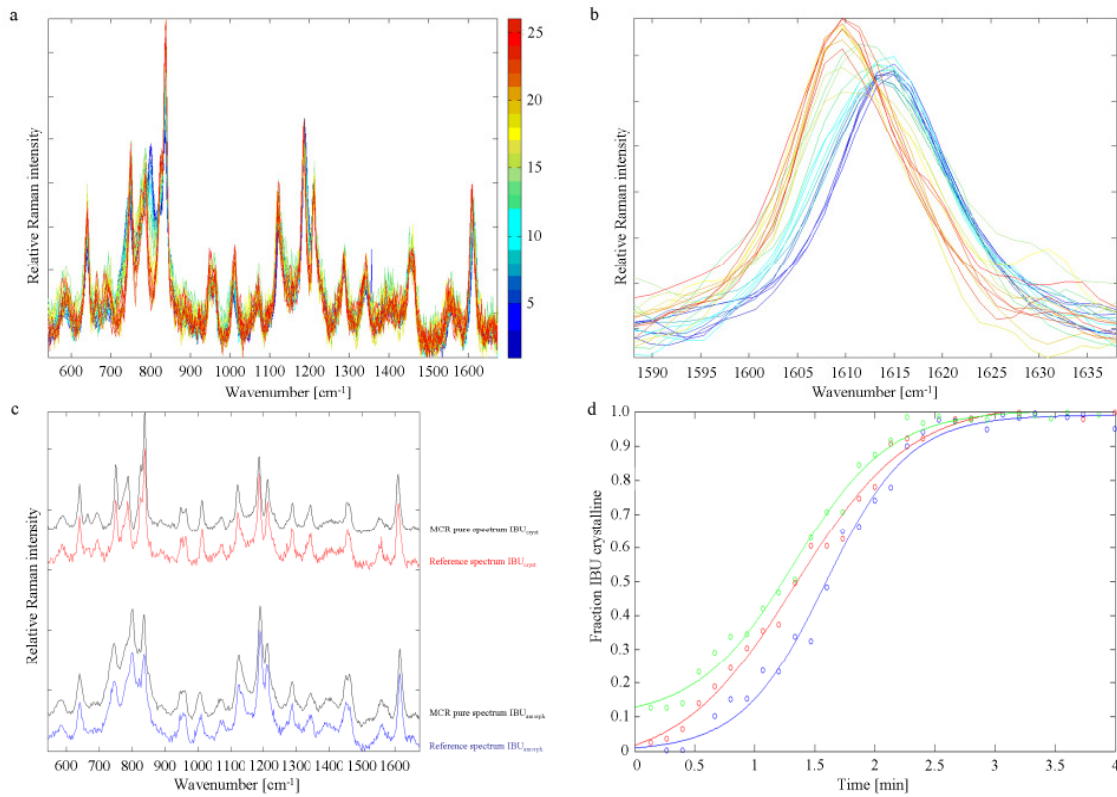


Fig. 9: (a) SNV-corrected Raman spectra recorded during the recrystallization process (blue spectrum – amorphous ibuprofen, red spectrum – crystalline ibuprofen). (b) Time-dependent shift of the aryl C=C Raman band during recrystallization. (c) Comparison of the MCR pure spectra (black), including amorphous (blue) and crystalline (red) reference spectra. (d) MCR-predicted kinetic profiles of the amorphous-to-crystalline ibuprofen solid-state phase transformation (the solid curves represent the fitting of the data points according to Eq. (5)).

Table 2: Comparison of the recrystallization kinetic parameters of NIRS and Raman spectroscopy.

| | R^2 (n=3) | β [min ⁻¹] (n=3) | t_{50} [min] (n=3) |
|----------------------------|----------------|--|----------------------------|
| Near infrared spectroscopy | 0.992 | 2.57 ± 0.53 | 2.01 ± 0.08 |
| Raman spectroscopy | 0.991 | 2.50 ± 0.40 | 1.42 ± 0.15 |

R^2 is the average coefficient of determination of the fit of the amorphous-to-crystalline transformation profile to Eq. (3), β overall recrystallization rate constant, and t_{50} the time needed to reach 50% of the equilibrated level.

2.3.4 Recrystallization kinetic parameters estimated from NIR and Raman spectroscopy

The empirical recrystallization rate constant β estimated from the two spectroscopic techniques were comparable, while t_{50} was lower for Raman spectroscopy than for NIRS (Table 2). The uncertainty in the determination of the empirical recrystallization rate constant β was rather large. The main reason could be the large variation in particle size of approximately $4.3 \pm 0.7 \text{ mm}^2$ (relative standard deviation (n = 3): 17 %). With increasing particle size the heat transfer into the centre of the particle also increases, resulting in a slower recrystallization. Controlling the particle size would most likely lead to a reduction of the uncertainty in determination of the β value.

It is hypothesised that the reason for the differences in the t_{50} values determined by Raman and NIR spectroscopy could be due to the Raman laser beam influencing nucleation [153, 154]. The levitated particle absorbs a certain amount of energy provided by the Raman laser, leading to a local heating of the sample. This local heating effect could have increased nuclei formation and therefore reduced the recrystallization onset time [155-157]. As the sample size was rather small (approximately 4 mm^2) a large amount of energy was dissipated on a rather small sample compared to bulk analysis using Raman spectroscopy.

However, in order to minimise the Raman laser influence on the recrystallization kinetics, careful attention was paid to minimize the exposure of the sample to the laser. With NIRS the excitation energy is provided by a wolfram light source which is less focussed than the Raman laser used in the study, hence its power density is lower. Therefore, the influence of the NIR light source on the actual recrystallization kinetics is less pronounced. Further, NIRS has a shorter collection time per spectrum than Raman spectroscopy. In this study, the time needed to collect one NIR spectrum was 0.32 s, while 8 s were required to obtain one Raman spectrum. Thus, even very fast solid-state transformations may be investigated using NIRS. However, Raman spectroscopy can provide a deeper insight into the solid-state phase transformation on a molecular level than NIRS because of the clearly resolved sharp peaks [134].

2.4 Conclusion

Acoustic levitation with NIR and Raman spectroscopy, combined with MCR, provides a valuable technique for monitoring solid-state phase transformations of small amorphous, highly viscous and adhesive materials and can therefore be an important tool in early formulation development. While NIRS allows the detection of fast solid-state phase transformations and gives an estimation of the actual recrystallization kinetics, Raman spectroscopy offers a detailed insight into the recrystallization process on a molecular level. The MCR data analysis approach was found to be useful in estimating the underlying pure spectra despite the small amount of sample and poor spectral signal to noise ratio, allowing chemically meaningful interpretation of the obtained spectral data sets.

3. Investigation of the formation process of two piracetam cocrystals during grinding

Investigation of the formation process of two piracetam cocrystals during grinding

Abstract

Cocrystal formation rates during dry grinding and liquid-assisted grinding were investigated by X-ray powder diffractometry and Raman spectroscopy. Two polymorphic forms of piracetam were used to prepare known piracetam cocrystals as model substances, i.e. piracetam-citric acid and piracetam-tartaric acid cocrystals. Raman spectroscopy in combination with principal component analysis was used to visualize the cocrystal formation pathways. During dry grinding, cocrystal formation appeared to progress via an amorphous intermediate stage, which was more evident for the piracetam-citric acid than for the piracetam-tartaric acid cocrystal. It was shown that liquid-assisted grinding led to faster cocrystal formation than dry grinding, which may be explained by the higher transformation rate due to the presence of liquid. The cocrystal formation rate did not depend on the polymorphic form of the applied piracetam and no polymorphic cocrystals were obtained.

3.1 Introduction

Pharmaceutical cocrystals can be defined as stoichiometric multiple component substances formed by active pharmaceutical ingredients (API) and cocrystal formers. At least two components of a cocrystal must be solid under ambient conditions [34].

Cocrystals are gaining increasing interest in the pharmaceutical community, because they differ in their physicochemical properties from single-component crystals, e.g. melting point [158], hydration stability [159], UV light stability [160], hygroscopic properties [90], dissolution behaviour [50], and bioavailability [161].

Although most cocrystals have been found by chance, an increased understanding of the cocrystal formation process during the last few decades has led to more systematic cocrystal design. Two approaches are common practice: one is based on a structural fit of the compounds, i.e. similarities in molecule packing, and the other is based on specific pair wise interactions, so-called supramolecular synthons [162]. The API and cocrystal former interact via non-ionic and non-covalent intermolecular interactions, such as van der Waals forces, π - π -interactions, and most importantly, hydrogen bonding. Hence, the presence of free hydrogen bond donors and acceptors is usually a prerequisite for cocrystal formation [158]. Supramolecular assemblies of cocrystals may be based on homosynthons, such as acid-acid interactions, and heterosynthons, for example acid-amide interactions [34].

Piracetam (2-oxo-1-pyrrolidineacetamide, shown in Fig. 10) is a nootropic substance, used for the treatment of memory and balance problems. Piracetam is a neutral molecule, containing two different amide moieties, which could form heterosynthons with carboxylic acid or hydroxyl groups. Five anhydrous polymorphic forms (forms I-V) and two hydrates of this drug have been reported [163, 164]. Form III was found to be the thermodynamically stable polymorph at ambient conditions [165]. The presence of different polymorphic forms increases the chance for cocrystal formation because polymorphism is based on molecular flexibility. Hence, it may be easier to pack such a molecule in a different crystal lattice arrangement with another substance than it is the case for structurally more rigid molecules [166].

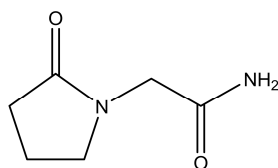


Fig. 10: Chemical structure of piracetam

As a result of the ability to form heterosynthons on the one hand and structural flexibility on the other hand, piracetam is a suitable model substance for the investigation of cocrystal formation. It is thus not surprising that several piracetam cocrystals are described in the literature. In 2005, Vishweshwar et al. characterised piracetam cocrystals formed with 2,5-dihydroxybenzoic acid (Cambridge Structural Database (CSD) reference code: DAVPAS) and 4-hydroxybenzoic acid (CSD reference code: DAVPEW) by slow evaporation of acetonitrile, slurring in water, and dry-grinding using Fourier transformation infrared spectroscopy (FTIR), differential scanning calorimetry (DSC), X-ray powder diffractometry (XRPD), and single-crystal X-ray diffractometry (SC-XRD) [167]. Liao et al. examined the formation of piracetam cocrystals with different isomers of dihydroxybenzoic acid by crystallisation from acetonitrile and characterised the cocrystals by DSC, FTIR, and XRPD [168]. Recently, Viertelhaus et al. described a screening experiment for piracetam cocrystals, using Raman microscopy, FT-Raman spectroscopy, XRPD, SC-XRD, dynamic vapour sorption, thermogravimetry coupled with FTIR, and DSC as characterisation techniques. Piracetam cocrystals with L-(+) tartaric acid (L-(+)-2,3-dihydroxybutanedioic acid) (CSD reference code: RUCDUP), racemic 2-hydroxy-2-phenylacetic acid (CSD reference code: RUCFIF), L-2-hydroxy-2-phenylacetic acid (CSD reference code: XOZSOV), and citric acid (2-hydroxypropane-1,2,3-tricarboxylic acid) at molar ratios of 1:1 (CSD reference code: RUCFAX) and 3:2 (CSD reference code: RUCFEB) as well as an ethanol solvate of the piracetam-2-hydroxypropane-1,2,3-tricarboxylic acid cocrystal (not published in the CSD) were detected. These cocrystals were prepared by solvent evaporation, solution crystallisation, and liquid-assisted grinding [90].

Cogrinding of an API and a cocrystal former is an important technique for cocrystal preparation and especially for cocrystal screening [65, 68, 90, 169]. Three mechanisms are discussed for cocrystal formation by dry-grinding: molecular diffusion, intermediate

formation of eutectic mixtures, and intermediate formation of an amorphous phase. Usually a more effective grinding method is liquid-assisted grinding [90, 170], although the mechanism, and especially the role of the liquid, is not yet fully understood. Some authors suggest that a small amount of liquid may act as a lubricant for the reaction, while others state that the liquid provides a medium to enhance molecular diffusion [171]. While many research articles have been published regarding cocrystal characterisation [90], screening [172], design [173], and storage stability [168], little work has been done to understand the kinetics of cocrystal formation during grinding. Chieng et al. followed the cocrystallization process of different solid-state forms of carbamazepine during dry-grinding with nicotine amide by combining XRPD with a multivariate data analysis approach [68], concluding that cocrystal formation using carbamazepine hydrate is faster than using the meta-stable polymorphic form I of the drug, which in turn was faster than using the stable polymorphic form III. Principal component analysis (PCA) provided a valuable tool to visualize the cocrystal formation process.

The aim of this study was to gain a deeper insight into the formation of two known piracetam cocrystals, i. e. piracetam-citric acid and piracetam-tartaric acid, during grinding. In the first part of the study cocrystal formation was investigated as a function of the grinding technique and the polymorphic form of the API, using XRPD, DSC, and Raman spectroscopy. In the second part PCA of the Raman spectra was performed to provide a more detailed insight into the cocrystallization mechanism.

3.2 Experimental section

3.2.1 Materials

Piracetam (M_w : 142.16 g/mol) was purchased from Hangzhou Dayangchem, China. Purity was confirmed by high performance liquid chromatography. The polymorphic form was determined to be form III by XRPD and DSC. However, to exclude impurities of other piracetam polymorphs, form III was used after recrystallization from methanol at ambient conditions. Piracetam form I was obtained by heating form III at 160 °C for 5 min and subsequent cooling to room temperature. Citric acid (M_w : 192.13 g/mol) was purchased from AppliChem, Germany, and L-(+)-tartaric acid (M_w : 150.09 g/mol) was purchased from Ajax Chemicals, Australia; both compounds were of pharmaceutical grade and were used as received.

3.2.2 Methods

3.2.2.1 Physical mixing

The cocrystal formers were ground before mixing to achieve the same particle size as the API. Physical mixtures were obtained by gently mixing API and cocrystal formers at a 1:1 molar ratio in a glass mortar with a glass pestle for 1 min.

3.2.2.2 Grinding

3.2.2.2.1 Dry-grinding

Dry-grinding was performed by co-milling piracetam with citric acid and tartaric acid, respectively, at a 1:1 molar ratio in 25 mL stainless steel milling jars using an oscillatory ball mill (Retsch MM301, Germany). Each jar contained three 9 mm stainless steel balls. Milling was carried out for predefined time periods from 1 min to 30 min at a frequency of 30 Hz.

3.2.2.2.2 *Liquid-assisted grinding*

For liquid-assisted grinding, the same process parameters as for dry-grinding were used. Additionally, 16.6 μL of water and 166 μL of ethyl acetate were added to prepare the piracetam-citric acid cocrystal before the milling process was started. For piracetam-tartaric acid cocrystal preparation, 16.6 μL of water were added [90].

3.2.2.3 Characterization methods

3.2.2.3.1 *X-ray powder diffraction (XRPD)*

Differences in crystal lattice configuration were examined using a PANalytical X'Pert PROMD diffractometer (PW3040/60, Philips, The Netherlands), with $\text{CuK}\alpha$ radiation at a wavelength of 1.54 \AA in continuous scanning mode. The step size was $0.0084^\circ 2\theta$ and the scanning rate was $0.1285^\circ 2\theta/\text{min}$. Powder samples were analysed in aluminium sample holders and scanned at 40 KV and 30 mA from 5 to $35^\circ 2\theta$. The powder diffraction patterns were analysed with X'Pert Highscore software (version 2.2.0) and plotted with OriginPro 7.5. The theoretical cocrystal patterns were calculated on the basis of the Cambridge Structural Data base (CSD 5.32, November 2010) [174] using ConQuest 1.13 [175] by Mercury software CSD 2.4 [176] (Cambridge Crystallographic Data Centre, UK).

3.2.2.3.2. *Differential scanning calorimetry (DSC)*

To confirm the XRPD results, DSC was performed. Each sample was analysed in triplicate. The material was weighed (1-5 mg) into a TA instruments standard aluminium pan using a micro balance and tweezers. The pan was covered with a lid and crimped using a TA crimper. The reference pan was crimped similarly to the sample pans but without any substance.

Thermograms were recorded on a Q100 V8.2 Build 268, (TA Instruments, USA) under a constant nitrogen gas flow of 50 mL/min. The DSC apparatus was calibrated with regard to temperature and enthalpy using indium as a standard. The heating rate was set to 10 K/min in a range from 20 to 180 °C. To determine any thermal events the TA Universal Analysis 2000 software (version 4.0c) was used.

3.2.2.3.3 *FT-Raman spectroscopy*

FT-Raman spectra were recorded using a Bruker FRA 106/S FT-Raman spectrometer (Bruker, Germany), equipped with a Coherent Compass 1064-500N laser (Coherent, USA), attached to a Bruker IFS 55 FT-IR interferometer, and a D 425 Ge diode detector. The laser wavelength was 1064 nm and laser power 120 mW. To monitor the wave number accuracy sulphur was used as a reference standard. Measurements were performed in triplicate (each spectrum was averaged over 64 scans) at a resolution of 4 cm⁻¹. Spectra were displayed using the OPUS 5.0 software.

3.2.2.3.4 *Chemometrics*

Spectral changes due to cocrystal formation were visualised by performing principal component analysis (PCA) of the Raman spectra. The data were pre-treated with a standard normal variate algorithm and scaled by mean centring. Multivariate data analysis was performed with The Unscrambler X (version 10, Camo, Norway). The spectral regions between 1800 cm⁻¹ and 2700 cm⁻¹ and above 3100 cm⁻¹ were excluded.

3.3 Results and discussion

The substances investigated in this study were characterised by XRPD, DSC, and Raman spectroscopy. The piracetam-citric acid and piracetam-tartaric acid cocrystal structure was thoroughly described by Viertelhaus et al. [90], a schematic overview over the interactions within the unit cells is presented in Fig. 11 (Cambridge Structural Database 2011) [174, 175].

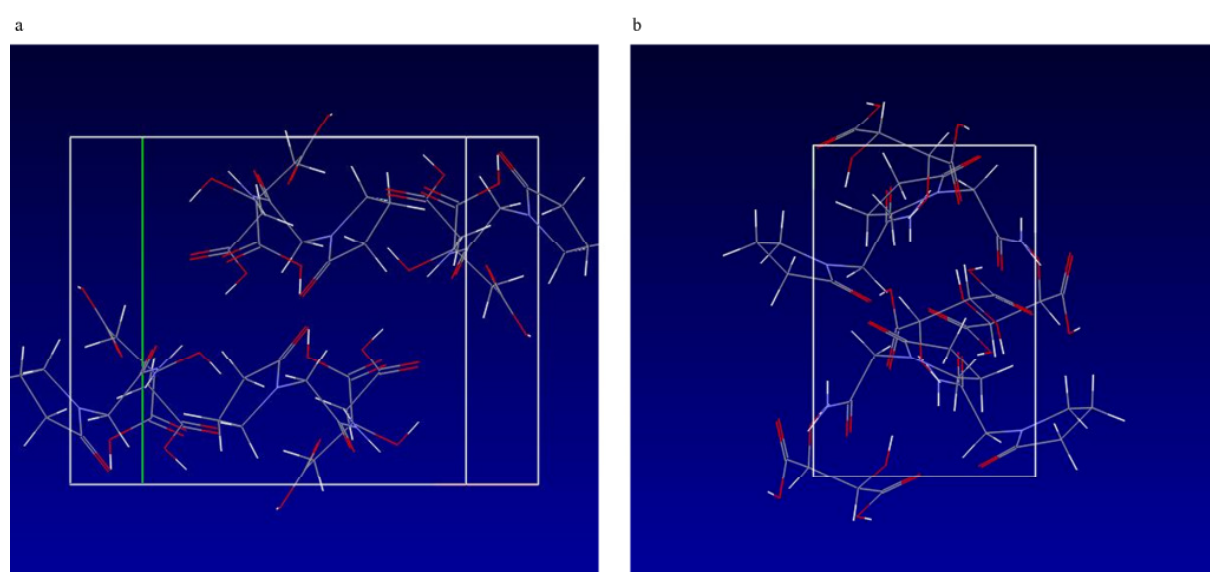


Fig. 11: (a) 3D structure of the piracetam-citric acid unit cell. (b) 3D structure of the piracetam-tartaric acid unit cell (Cambridge Structural Database 2011) [174, 175].

The XRPD patterns, DSC thermograms, and the Raman spectra of the model API piracetam (polymorphic forms I and III), the cocrystal formers citric acid and tartaric acid, and the cocrystals are displayed in Figs. 12-14. For clarity, only the data of the physical mixtures of piracetam form III and the cocrystal formers, rather than the individual components alone, are displayed. The calculated cocrystal XRPD patterns based on the single crystal data in the CSD are included in Fig. 12. The characteristic peaks of the physical mixtures are highlighted by red dotted lines. The patterns of the physical mixtures of piracetam form III and citric acid or tartaric acid, respectively, show combinations of the

diffractograms of both compounds expressing API as well as cocrystal former peaks. In contrast, the cocrystal patterns are completely different to those of the physical mixtures, showing peaks which are not observable in the physical mixture patterns, because the crystal configuration differs significantly from the crystal lattices of the single components. The measured cocrystal patterns are in good agreement with the patterns calculated on the basis of the CSD (green dotted lines).

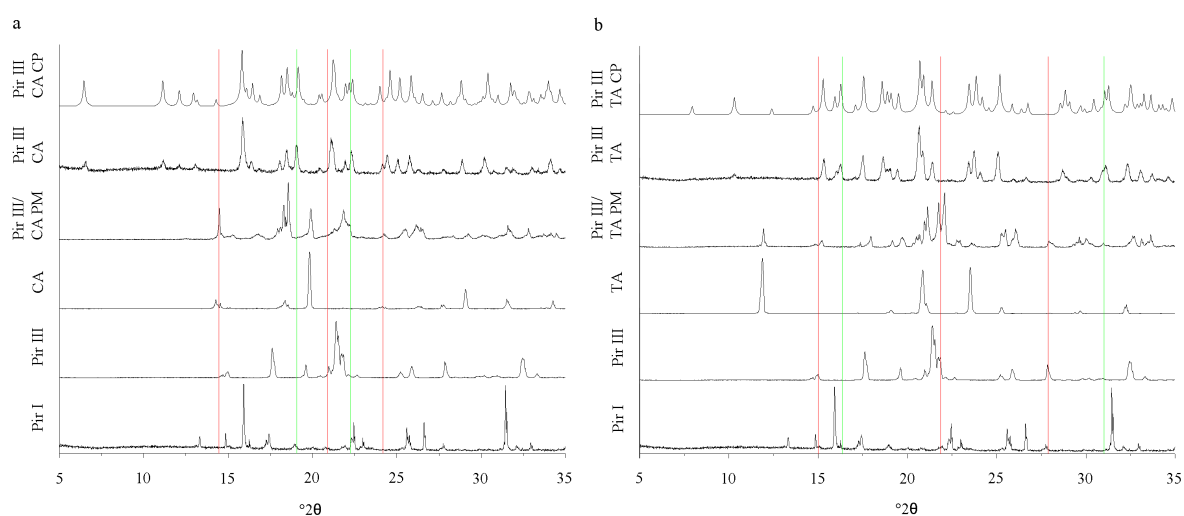


Fig. 12: (a) XRPD patterns of piracetam form I (Pir I) and form III (Pir III), citric acid (CA), physical mixture of piracetam form III and citric acid (Pir III/ CA PM), piracetam-citric acid cocrystal (Pir III CA), and calculated piracetam-citric acid cocrystal pattern (Pir III CA CP). (b) XRPD patterns of piracetam form I (Pir I) and form III (Pir III), tartaric acid (TA), physical mixture of piracetam form III and tartaric acid (Pir III/ TA PM), piracetam-tartaric acid cocrystal (Pir III TA), and calculated piracetam-tartaric acid cocrystal pattern (Pir III TA CP).

To confirm the XRPD results, DSC was performed. In Fig. 13 the various DSC thermograms are displayed. Piracetam form III shows three endothermic events at onset temperatures of 125 °C, 140 °C, and 150 °C. According to Maher et al. [177], the first endothermic event at 125 °C is the result of a partial transformation of form III into form I, which melts at 150 °C, while form III melts at 140 °C. Citric acid melts at 154 °C and L-tartaric acid at 170 °C. The melting onset temperature of the piracetam-citric acid cocrystal is 105 °C, while the piracetam-tartaric acid cocrystal melts at 160 °C. The melting points of the

pure substances and the cocrystals are in good agreement with the values published in the literature [90, 163, 165, 177].

Raman spectroscopy, which provides molecular level information, is a valuable technique for solid-state and cocrystal investigation [68, 172].

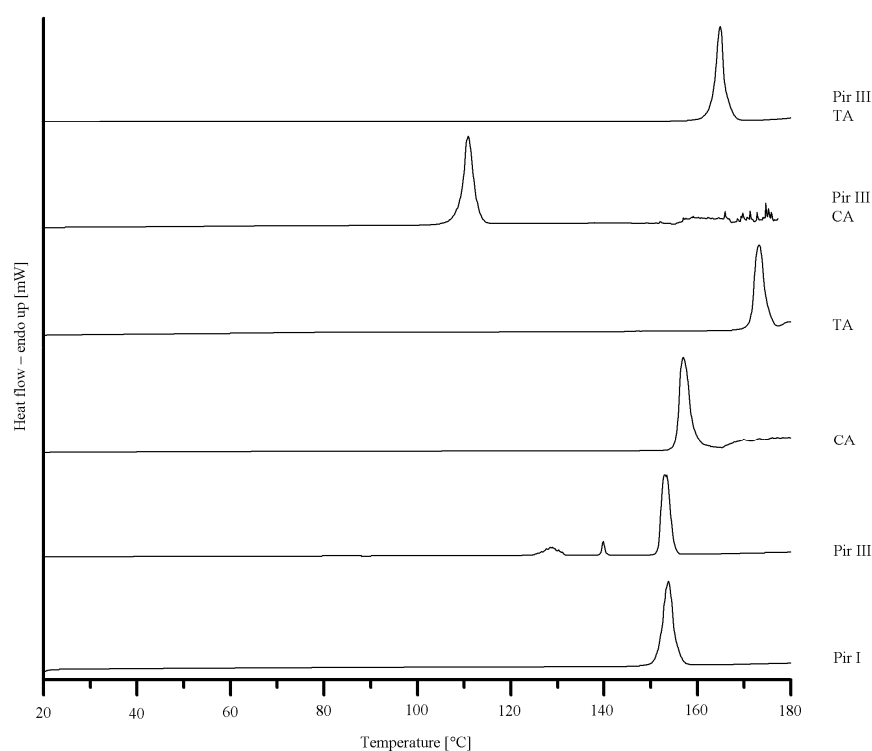


Fig. 13: DSC thermograms of piracetam form I (Pir I) and form III (Pir III), citric acid (CA), tartaric acid (TA), piracetam-citric acid cocrystal Pir III CA), and piracetam-tartaric acid cocrystal (Pir III TA).

In Fig. 14 the characteristic Raman bands of the pure substances and the physical mixtures are highlighted by red dotted lines; the cocrystal peaks are highlighted by green dotted lines. The cocrystal spectra can easily be differentiated from the physical mixtures' spectra, since they show peaks which are not observed for the physical mixtures.

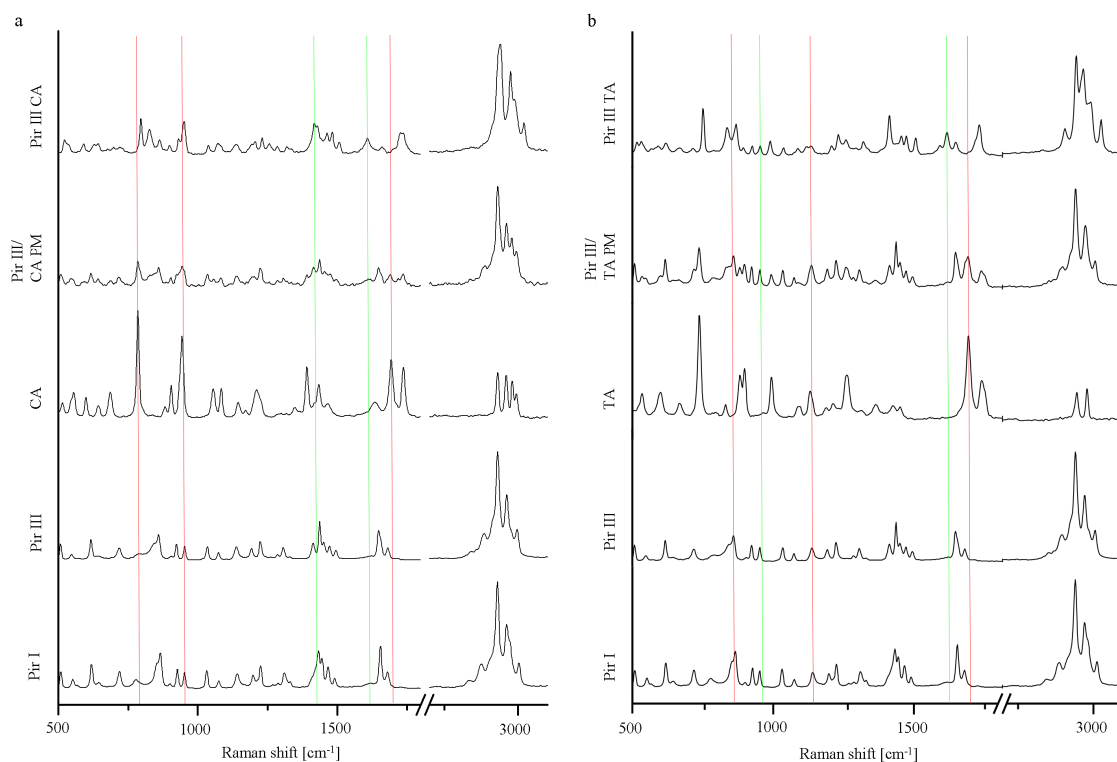


Fig. 14: (a) Raman spectra of piracetam form I (Pir I) and form III (Pir III), citric acid (CA), physical mixture of piracetam form III and citric acid (Pir III/ CA PM), and piracetam-citric acid cocrystal (Pir III CA). (b) Raman spectra of piracetam form I (Pir I) and form III (Pir III), tartaric acid (TA), physical mixture of piracetam form III and tartaric acid (Pir III/ TA PM), and piracetam-tartaric acid cocrystal (Pir III TA).

In the first part of the study the formation speeds of piracetam-citric acid cocrystals and piracetam-tartaric acid cocrystals were investigated as a function of different grinding techniques on the one hand and different polymorphic forms of piracetam on the other hand. Therefore, piracetam form I or form III were co-ground with citric acid and tartaric acid, respectively, by dry-grinding as well as by liquid-assisted grinding. The samples, milled for predefined time periods, were examined using XRPD and Raman spectroscopy.

In Fig. 15, the XRPD patterns and the Raman spectra of the samples of piracetam form I and form III, dry-ground with citric acid, are shown. The patterns and spectra of the physical mixtures (red dotted lines) and the cocrystal (green dotted lines) are included as references.

Upon milling, significant changes in the XRPD patterns and in the Raman spectra can be detected. The intensity of the characteristic peaks of the physical mixture decreases, while that of the cocrystal peaks increases. After 10 min of milling, regardless of the piracetam polymorph used as starting material, the patterns and spectra only show characteristic cocrystal peaks, indicating complete cocrystal formation. Interestingly, the characteristic XRPD peaks and Raman bands of the cocrystals formed by both piracetam form I-citric acid and piracetam form III-citric acid match, indicating that the resulting cocrystals are identical.

For all samples, a loss of crystallinity of piracetam and citric acid during grinding is observed in the XRPD diffractograms and in the Raman spectra, identifiable by the broader peaks with lower intensity. This is a known phenomenon to occur during grinding [55]. Co-grinding at room temperature leads to partial amorphization, and further grinding can accelerate cocrystal formation. This cocrystal formation mechanism is typical for solids which are not volatile and which interact via hydrogen bonds. It has been suggested that cocrystal formation occurs via an intermediate amorphous stage of high energy and high molecular mobility [65]. Some samples were even completely amorphous after grinding, indicated by a broad halo in the XRPD pattern. These samples crystallised forming the cocrystal.

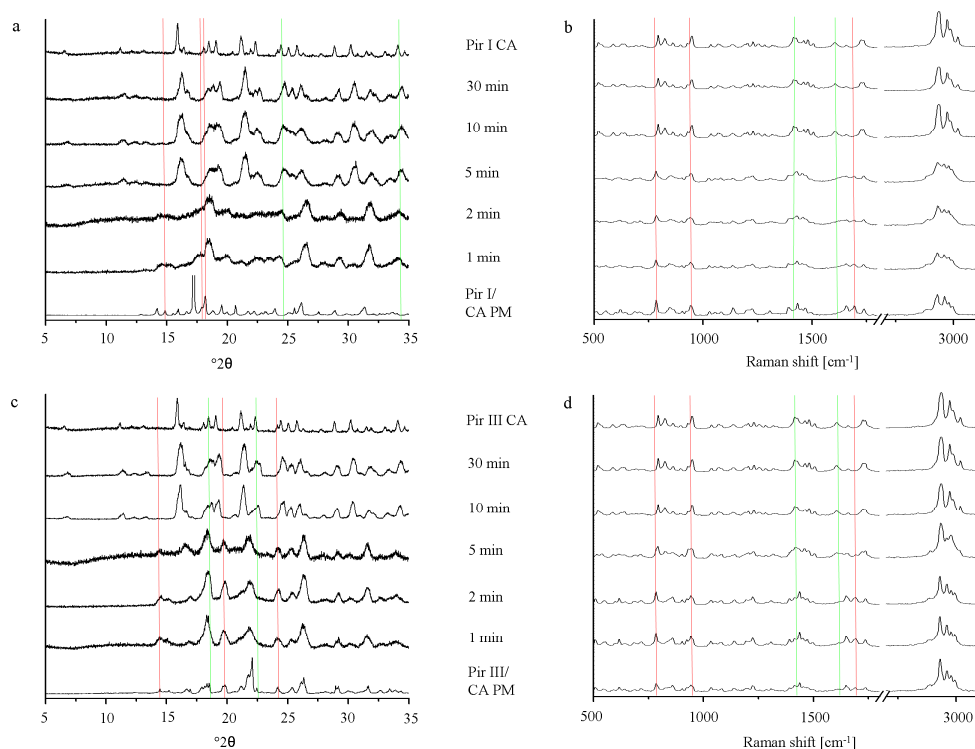


Fig. 15: (a) XRPD patterns of the physical mixture of piracetam form I and citric acid (Pir I/ CA PM), dry-ground for predefined time periods. The piracetam form I-citric acid cocrystal (Pir I CA) reference pattern is included. (b) Raman spectra of the physical mixture of piracetam form I and citric acid (Pir I/ CA PM), dry-ground for predefined time periods. The piracetam form I-citric acid cocrystal (Pir I CA) reference spectrum is included. (c) XRPD patterns of the physical mixture of piracetam form III and citric acid (Pir III/ CA PM), dry-ground for predefined time periods. The piracetam form III-citric acid cocrystal (Pir III CA) reference pattern is included. (d) Raman spectra of the physical mixture of piracetam form III and citric acid (Pir III/ CA PM), dry-ground for predefined time periods. The piracetam form III-citric acid cocrystal (Pir III CA) reference spectrum is included.

In Fig. 16, the XRPD patterns and the Raman spectra of piracetam form I and form III, dry-ground with tartaric acid at predefined milling times, are shown. Again, the intensity of the characteristic peaks of the physical mixture decreases, while the cocrystal peaks become more prominent with increasing milling times. Independent of the polymorphic form of piracetam, the physical mixture peaks disappear after 10 min of grinding and cocrystal formation is completed. This observation is surprising, as Chieng et al. showed that the

thermodynamically less stable polymorph of carbamazepine forms cocrystals with nicotine amide faster during dry-grinding than the stable polymorph because of its higher energy [68]. This trend is not observed in the present study. Again, the cocrystals formed by piracetam form I and form III do not show polymorphism.

In the diffractograms, a loss of crystallinity, as it was shown for piracetam-citric acid cocrystals, cannot be observed with piracetam-tartaric acid. In addition, there was no evidence of amorphous material in the DSC thermograms (not shown) or Raman spectra detectable by the naked eye.

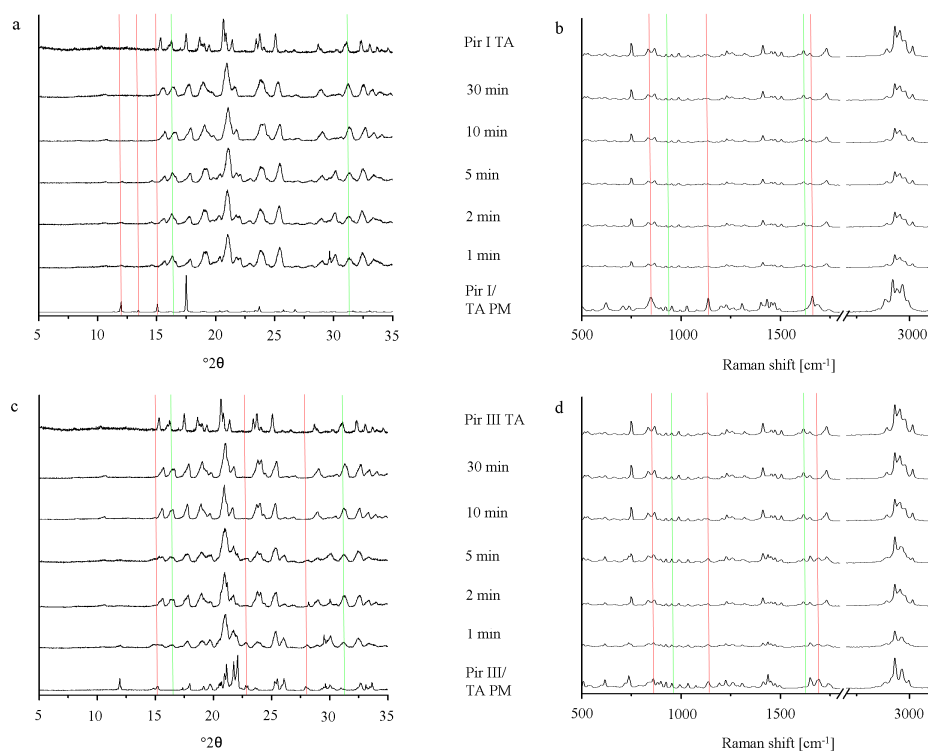


Fig. 16: (a) XRPD patterns of the physical mixture of piracetam form I and tartaric acid (Pir I/ TA PM), dry-ground for predefined time periods. The piracetam form I- tartaric acid cocrystal (Pir I TA) reference pattern is included. (b) Raman spectra of the physical mixture of piracetam form I and tartaric acid (Pir I/ TA PM), dry-ground for predefined time periods. The piracetam form I- tartaric acid cocrystal (Pir I TA) reference spectrum is included. (c) XRPD patterns of the physical mixture of piracetam form III and tartaric acid (Pir III/ TA PM), dry-ground for predefined time periods. The piracetam form III- tartaric acid cocrystal (Pir III TA) reference pattern is included. (d) Raman spectra of the physical mixture of piracetam form III and tartaric acid (Pir III/ TA PM), dry-ground for predefined time periods. The piracetam form III- tartaric acid cocrystal (Pir III TA) reference spectrum is included.

Cocrystal formation during grinding may be enhanced by small amounts of liquid added to the milling jar before the milling process [170]. To compare the rate of cocrystal formation during this liquid-assisted grinding with dry-grinding, the XRPD patterns and the Raman spectra of piracetam form I or form III, co-ground with citric acid and tartaric acid, respectively, were recorded after the same milling times (Figs. 17 and 18). Already after 1 min of milling, the patterns and spectra differ significantly from those of the physical mixture. Peaks characteristic of the physical mixture disappear from the XRPD patterns and the Raman spectra and only cocrystal peaks are detected. Obviously, cocrystal formation is already completed after 1 min of liquid-assisted grinding for both the piracetam-citric acid cocrystal and the piracetam-tartaric acid cocrystal.

On the one hand, the fast cocrystal formation may be explained by the higher molecular mobility of the API and the cocrystal formers as a result of their partial solubility in the liquids used in the experimental setup [170, 171]. On the other hand, Viertelhaus et al. observed a loss of crystallinity in an equimolar mixture of piracetam and citric acid during liquid-assisted grinding [90]. This was not observed in the present study, probably because of the fast cocrystallization process.

As observed with the dry-grinding process, no differences are found between the cocrystal formation rates of the different polymorphic forms of piracetam during liquid-assisted grinding. According to the XRPD patterns, the cocrystals of piracetam and citric acid or tartaric acid obtained by liquid-assisted grinding and dry grinding, respectively, are identical. Raman spectroscopy (Figs. 17 b, 17 d and 18 b, 18 d) and DSC (data not shown) support the XRPD findings.

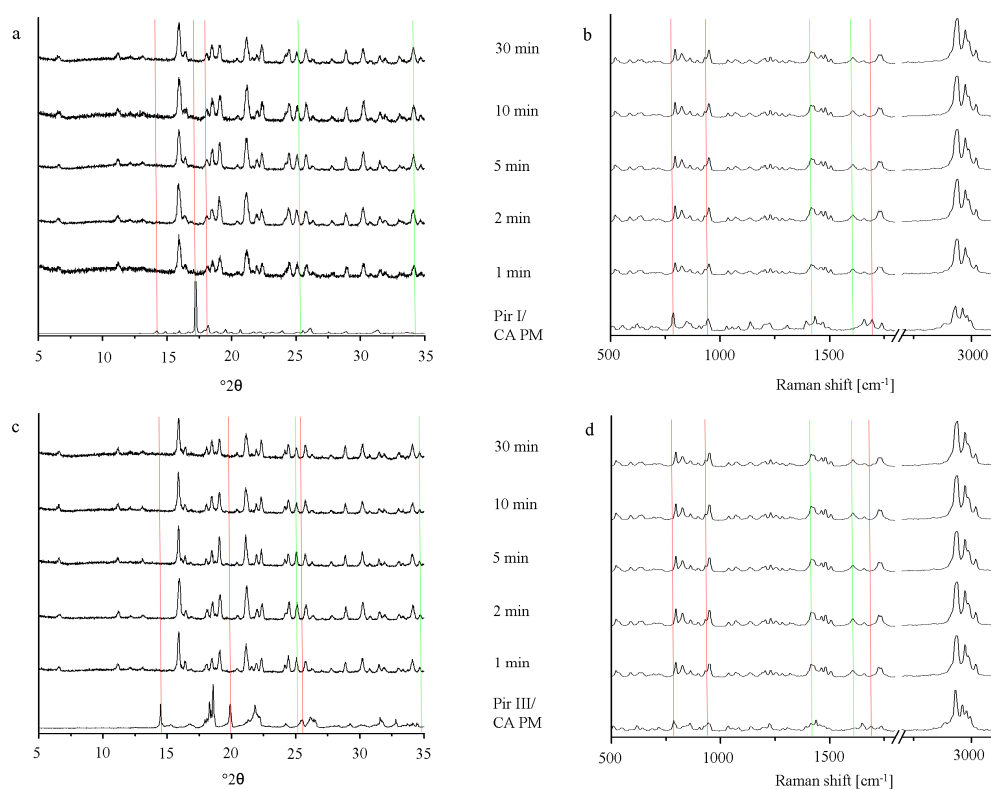


Fig. 17: (a) XRPD patterns of the physical mixture of piracetam form I and citric acid (Pir I/ CA PM), after liquid-assisted grinding for predefined time periods. The piracetam form I-citric acid cocrystal (Pir I CA) reference pattern is included. (b) Raman spectra of the physical mixture of piracetam form I and citric acid (Pir I/ CA PM), after liquid-assisted grinding for predefined time periods. The piracetam form I-citric acid cocrystal (Pir I CA) reference spectrum is included. (c) XRPD patterns of the physical mixture of piracetam form III and citric acid (Pir III/ CA PM), after liquid-assisted grinding for predefined time periods. The piracetam form III-citric acid cocrystal (Pir III CA) reference pattern is included. (d) Raman spectra of the physical mixture of piracetam form III and citric acid (Pir III/ CA PM), after liquid-assisted grinding for predefined time periods.

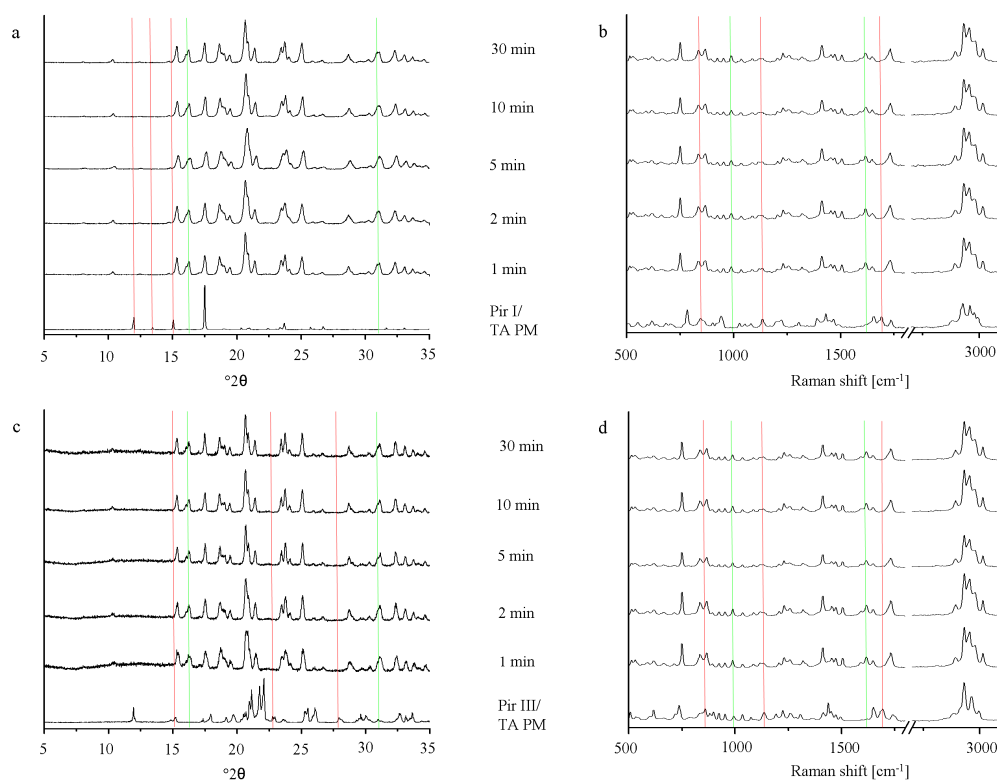


Fig. 18: (a) XRPD patterns of the physical mixture of piracetam form I and tartaric acid (Pir I/TA PM), after liquid-assisted grinding for predefined time periods. The piracetam form I-tartaric acid cocrystal (Pir I TA) reference pattern is included. (b) Raman spectra of the physical mixture of piracetam form I and tartaric acid (Pir I/TA PM), after liquid-assisted grinding for predefined time periods. The piracetam form I-tartaric acid cocrystal (Pir I TA) reference spectrum is included. (c) XRPD patterns of the physical mixture of piracetam form III and tartaric acid (Pir III/TA PM), after liquid-assisted grinding for predefined time periods. The piracetam form III-tartaric acid cocrystal (Pir III TA) reference pattern is included. (d) Raman spectra of the physical mixture of piracetam form III and tartaric acid (Pir III/TA PM), after liquid-assisted grinding for predefined time periods.

In summary, it was found with both cocrystal systems that liquid-assisted grinding results in very fast cocrystal formation, which is completed within the first minute of grinding. Cocrystal formation during dry-grinding is a slower process and is completed only after 10 minutes. In the present study, the type of polymorphic form does not have a significant influence on the cocrystal formation rate, which is in contrast to findings published by Chieng et al. in 2009 for carbamazepine cocrystals [68]. Different polymorphic cocrystals

are not obtained by dry-grinding or liquid-assisted grinding. Dry-grinding of piracetam and citric acid leads to partial amorphization, which is suggested to be the cocrystallization mechanism. Amorphization is not obvious for formation of the piracetam-tartaric acid cocrystal.

To gain a deeper insight into the transformation of the physical mixture into the cocrystal during dry-grinding, principal component analysis (PCA) of the Raman spectra was performed. PCA is a valuable technique to visualise differences in the cocrystal formation rate and can help to provide insight into solid-state transformation processes taking place during grinding [68]. In Fig. 19 a, the PCA 2D score plot of piracetam-citric acid cocrystal formation is presented. Of the total variance, 70 % is explained by the first two components. Principal component 1 (PC-1, 50 % of the total variance) distinguishes between the cocrystal and non-cocrystal systems: It correlates negatively with non-cocrystal and positively with cocrystal systems. Comparison of the PC-1 loadings plot with the Raman spectra of the physical mixture and the cocrystal supports this interpretation of the score plot (Fig. 19 b). Scores of samples dry-ground for less than 5 min cluster in the left part of the score plot (black symbols). XRPD confirms that these samples remain as physical mixtures of the original crystalline components. Scores of samples ground for more than 5 min forming cocrystals (confirmed by XRPD) cluster on the right hand side of the score plot (blue symbols). In some cases, the samples are completely X-ray amorphous after different milling periods (red symbols). When these amorphous samples were stored for 24 hours at ambient conditions, they crystallised and clustered with the cocrystal scores, indicating cocrystal formation (green symbols). PC-2 (20 % of the total variance) describes spectral differences between the physical mixtures of citric acid and piracetam form I or form III (PC-2 loadings plot Fig. 19 c). After completion of the cocrystal formation, no differences between the spectra of the cocrystals formed by form I and form III are detected with PCA.

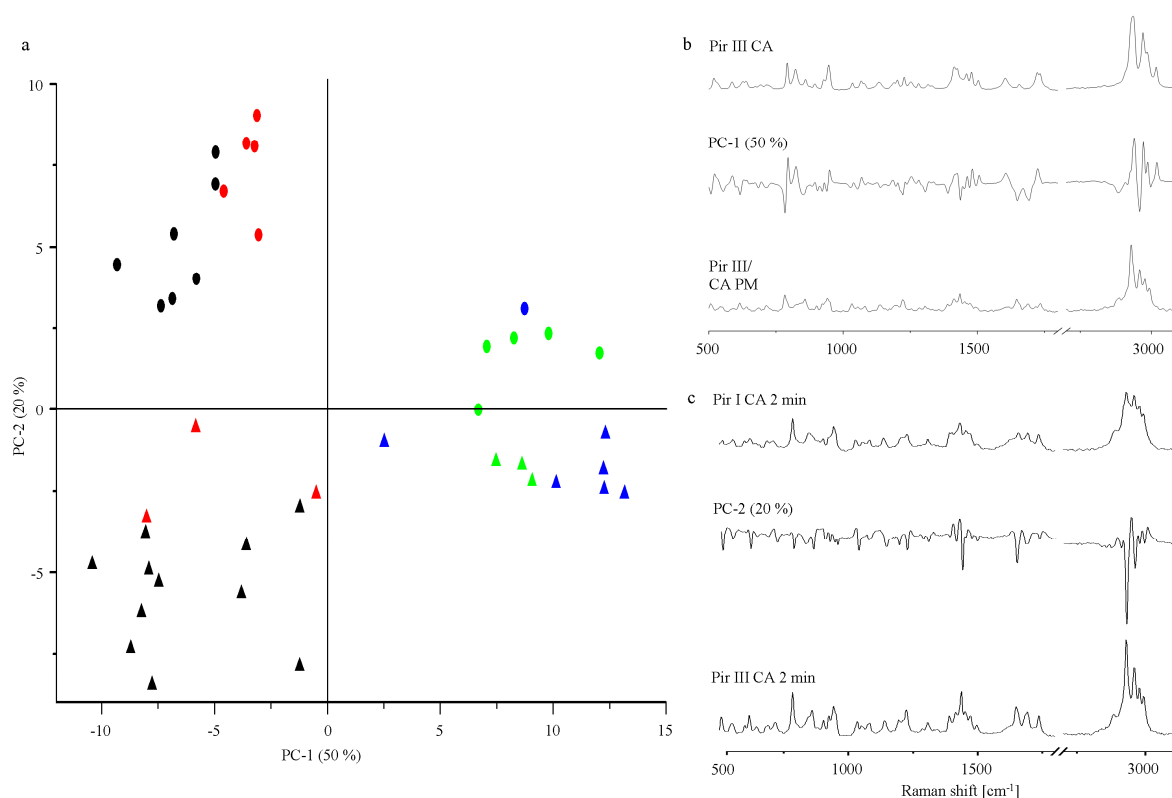


Fig. 19: (a) PCA 2D score plot of piracetam form I (circles) or form III (triangles) dry-ground with citric acid. Black symbols represent non-cocrystal systems ground for less than 5 min, blue symbols represent cocrystal systems, red symbols represent samples being X-ray amorphous after various grinding times, green symbols represent the amorphous samples after crystallization, forming the cocrystal. (b) Loadings plot of PC-1 (c) Loadings plot of PC-2.

In Fig. 20 a the PCA 2D score plot of piracetam-tartaric acid cocrystal formation is displayed. The first two PCs explain 85 % of the total variance: PC-1 with 58 % and PC-2 with 27 %. PC-1 differentiates between cocrystal and non-cocrystal systems and correlates negatively with cocrystal and positively with non-cocrystal spectral information. This interpretation is confirmed if the PC-1 loadings plot is compared with the Raman spectra of both the physical mixture and the cocrystal (Fig. 20 b). The differences in PC-2 space are harder to attribute, and are discussed below. Interestingly, the mixtures prepared with form I at less than one minute of milling occupy the same PCA space as those prepared with form III at the same period of milling. XRPD analysis revealed that form I crystallised to form III

within this time period. With increasing milling time for form III, the score clusters move from the physical mixture cluster in quadrant IV towards the cocrystal cluster in quadrant III. After 10 min of grinding, the scores cluster with the cocrystal reference scores suggesting completed cocrystallization. Despite form I converting to form III, the mixtures originally consisting of forms I and III take different paths in PCA space and the rate of cocrystal formation is different, with the original form I mixtures taking longer than 30 min to form cocrystals. This suggests some sort of residual structural differences (e.g. in morphology or degree of disorder) of the piracetam crystals in the samples even though both contained form III during the first minute of milling.

XRPD analysis of the samples during milling while diverging in the PC-2 space was also performed. Interestingly, XRPD analysis did not reveal any solid-state differences between the mixtures prepared with the two different polymorphs during the milling process, and the PC-2 loadings of the Raman spectra did not provide evidence that the Raman spectra were the result of different solid-state forms. Therefore, the structural differences associated with this divergence in PCA space are subtle, and may be due to slight differences in the degree of disorder. Nevertheless, the differences in cocrystal formation kinetic are substantial, suggesting that subtle structural differences can have a significant impact on cocrystal formation kinetics.

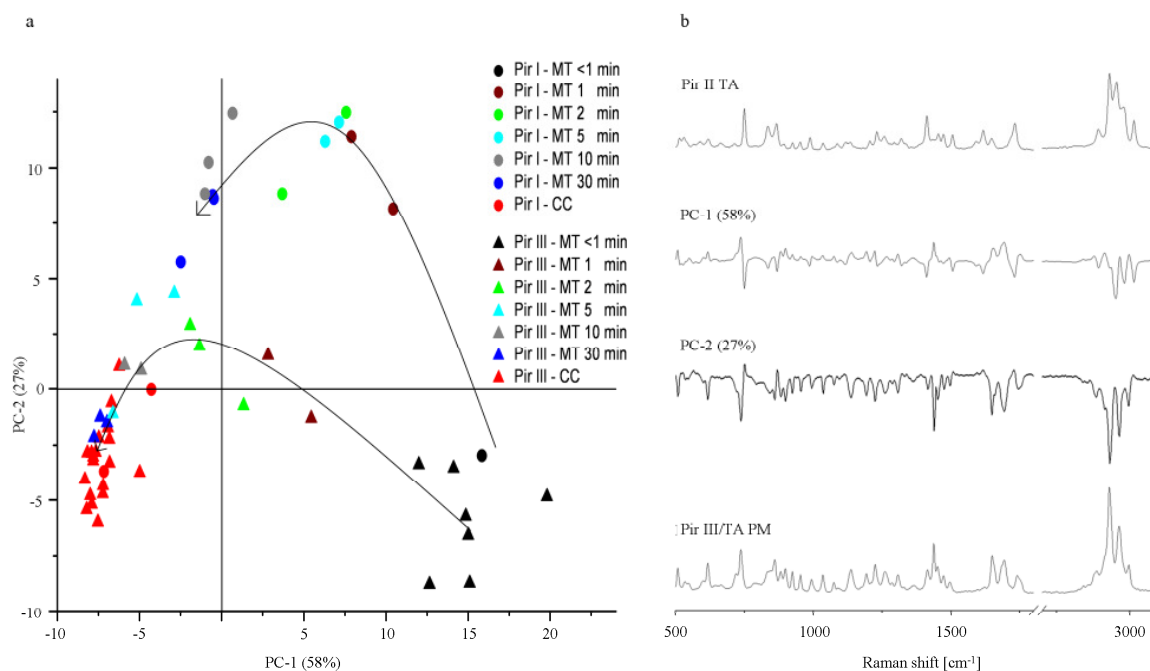


Fig. 20: (a) PCA 2D score plot of piracetam form I or form III dry-ground with tartaric acid. (b) Loadings plots of PC-1 and PC-2, Raman spectra of Pir III / TA PM and Pir III TA for comparison.

3.4 Conclusion

Piracetam cocrystals containing citric acid and tartaric acid, respectively, can be prepared by dry-grinding as well as liquid-assisted grinding. The rate of cocrystal formation is independent of the polymorphic form of the API, but differs with the applied grinding technique. As expected, the cocrystal formation during liquid-assisted grinding is faster than that during dry-grinding. Piracetam-citric acid cocrystals are formed via an amorphous intermediate stage. This could not be confirmed for the tartaric acid cocrystals. However, subtle structural differences were found to influence the piracetam-tartaric acid cocrystal formation process. This study shows that Raman spectroscopy in combination with principal component analysis is a valuable tool to follow cocrystallization processes during different milling techniques.

4. High-shear granulation as a manufacturing method for cocrystal granules

High-shear granulation as a manufacturing method for cocrystal granules

Abstract

Cocrystal formation allows the tailoring of physicochemical as well as of mechanical properties of an API. However, there is a lack of large-scale manufacturing methods of cocrystals. Therefore, the objective of this work was to examine the suitability of high-shear wet granulation as a manufacturing method of model cocrystal system in a batch scale and their pharmaceutical characterization.

High-shear wet granulation was found to be a feasible manufacturing method for cocrystal granules. Cocrystal formation depended on the exposure time of the solids to the granulation liquid (water), the amount of liquid, the impeller speed of the granulator, and on the excipients (hydroxyl propylcellulose, microcrystalline cellulose, calcium hydrogenphosphate) used in the formulation. Storage stability was strongly influenced by the excipients, since in presence of calcium hydrogenphosphate the poorly water-soluble salt calcium tartrate monohydrate was formed at high relative humidity. Interestingly, compactability was increased by cocrystal formation compared to that of the reference granules (piracetam and the respective excipients). The drug release was slightly decreased by cocrystal formation, most likely due to the lower solubility of the cocrystal. In the presence of calcium hydrogenphosphate however, no influence of cocrystal formation on either compactability or on drug release were observed, compared with the reference tablets.

It was concluded that high-shear wet granulation is a valuable, however complex, manufacturing method for cocrystals. Cocrystal formation may influence compactability and drug release and thus affect drug performance and should be investigated during pre-formulation.

4.1 Introduction

The most common orally administered drug formulations are solid dosage forms such as capsules and tablets, as their manufacture is fast, inexpensive, and straight-forward. Usually the active pharmaceutical ingredient (API) is processed in its crystalline form, most preferably as the stable polymorph, salt, or hydrate. In recent years another solid-state form has attracted interest, namely the cocrystal systems. These systems can be defined as a stoichiometric multicomponent system, formed by an API and a cocrystal former, which both are solid under ambient conditions [34]. Cocrystals offer multiple options to vary the physicochemical properties of an API such as stability [159, 160], dissolution behaviour [50], bioavailability [161], hygroscopicity [178], and mechanical properties [179], without chemical modification of the API [180]. The API and cocrystal former molecules interact via van-der-Waals forces, π - π interactions and, most commonly, hydrogen bonds [158, 173]. Although a better understanding of cocrystal formation allowed a more specific cocrystal design by predicting the intermolecular interactions by modelling approaches [181], cocrystal formation is not yet fully predictable and has to be confirmed experimentally. Cocrystals may be prepared for example by solvent evaporation [182], slurring [183], liquid-assisted grinding [170, 184, 185], and dry-grinding [65, 68]. To differentiate between solution-based and mechano-chemical preparation methods Frišćić introduced the empirical parameter η [$\mu\text{l}/\text{mg}$], defined as the ratio of the volume of the grinding liquid V [μl] and the sum of the masses of the API and cocrystal former m [mg] (Eq. (6)):

$$\eta = \frac{V (\text{granulation liquid})}{m (\text{API} + \text{cocrystal former})} \quad \text{Eq. (6)}$$

An η value of Zero represents dry-grinding, η between Zero and 2 liquid-assisted grinding, between 2 and 12 slurring, and larger than 12 solution synthesis [186]. In the past years liquid-assisted grinding has emerged to the method of choice for cocrystal preparation,

exhibiting significant advantages over the other techniques, including an increased formation rate, higher yields, and higher crystallinity of the product [65, 170]. The mechanistic role of the grinding liquid however is not yet fully understood. While in some cases the liquid appears to act as a lubricant and increases molecular mobility during cocrystallization [65], in other cases the properties of the liquid seem to have an impact on the cocrystal formation process [185]. In 2007, Zhang et al. reported a solution-mediated cocrystal formation mechanism, which was developed based on the mechanism suggested for hydrate formation of an anhydrous API, for example as observed by Mirza et al. for baclofen [83]. Zhang et al. assumed a critical cocrystal former activity (α_{CCF_c}), at which the API and the cocrystal are in equilibrium, showing the same thermodynamic stability. If the API is exposed to an environment with a higher α_{CCF} than α_{CCF_c} , the cocrystal is more stable than the API and is therefore formed. The same assumption is true with respect to the activity of the API. In a slurry where both portions of the API and the cocrystal former remain solid the activities of both are higher than their critical activities, leading to formation of the respective cocrystal. Upon nucleation, the remaining API and the cocrystal former will dissolve and crystallize as the cocrystal until the activities of the cocrystal former or the API fall below the critical activity [92-94]. Mechanical agitation such as sonicating or vortexing may facilitate the solution-mediated cocrystal formation process [93, 94].

While the above-mentioned preparation methods are well-suited for lab-scale experiments, up-scaling of these processes is limited [187]. A few attempts have been undertaken to produce cocrystals on a large-scale by pharmaceutical standard operations. Hot-melt extrusion, using a combination of controlled heat and shear deformation, has recently been used for cocrystal preparation [187-189]. Alhalaweh and Velaga spray-dried solutions of various APIs and cocrystal formers as stoichiometric mixtures to obtain the respective cocrystals [190]. Interestingly, high-shear granulation as a cocrystal manufacturing method

has not been extensively investigated [89], which is surprising, because cocrystal formation via a solution-mediated mechanism as well as a mechanism suggested for liquid-assisted grinding in terms of the combination of mechanical energy introduced into the system and moisture are expectable.

High-shear granulation is a common manufacturing process in the pharmaceutical industry where small particles are agglomerated by means of a granulation liquid. The main reasons are to improve flowability, increase uniformity in drug distribution, prevent segregation, and reduce dust exposure to the environment [70]. The high-shear granulation process can be divided into three different steps: First, the materials are mixed and the granulation liquid is added. Subsequently, the moist mixture is wet-massed, followed by a drying step [70]. During every step process-induced solid-state transformations [72] can occur, which may be examined by XRPD [79], near infrared [78], and Raman spectroscopy [20]. These process-induced transformations can result from water exposure and thermal as well as mechanical stress. They are usually undesired, as they are difficult to control and may alter the physicochemical properties of the API [86].

Nevertheless, the objective of this work was to examine cocrystal formation during high-shear granulation and to investigate its suitability as a manufacturing method of the well-described piracetam-tartaric acid cocrystal (Cambridge Structural Database (CSD) reference code: RUCDUP) [90] on a batch scale. Furthermore, the influence of different excipients on the cocrystallization process was investigated. The manufactured cocrystal granules were characterized with regard to their pharmaceutical properties and were compared to piracetam reference granules.

4.2 Materials and methods

4.2.1 Materials

Piracetam (Pir) was kindly donated by the Northeastern Pharmaceutical Group, China. L-tartaric acid (TA) was purchased from Carl Roth, Germany. Hydroxypropyl cellulose (HPC) and calcium hydrogenphosphate anhydrate (CaHPO_4) were supplied by Nycomed, Denmark. Microcrystalline cellulose (MCC) was donated by Lehmann and Voss, Germany. All substances were of pharmaceutical grade.

4.2.2 Methods

4.2.2.1 Manufacturing of the granules

Three different granule formulations (Table 3) were prepared. Each mixture contained a 1:1 molar ratio of Pir and TA with HPC as binder. 30.0 g of each mixture were granulated with 4.0 ml of purified water as granulation liquid.

The components of the three formulations were mixed in a Turbula mixer (Bachofen, Switzerland) for 10 min. Granules were manufactured with a Bohle Mini Granulator (Bohle, Germany). The volume of the granulation jar was 300 ml. Two different factors were analysed at two levels with respect to the response (cocrystal formation), the impeller speed and the granulation period. While the chopper speed was constant during granulation with 1000 rpm, two different impeller speed levels were applied: low (100 rpm) and high impeller speed (800 rpm). Furthermore, cocrystal formation over two different granulation time levels was investigated, at a low (15 min) and at a high level (60 min) after the water was added drop-wise with a pipette. As categorical variable, three different excipients were used in the granule formula. After the granulation process large agglomerates were disassembled by a sieve with a mesh size of 800 μm . Each granulation procedure was performed in duplicate.

For comparative purposes Pir/HPC and Pir/HPC/CaHPO₄ granules were prepared as described for the Pir/TA/HPC and Pir/TA/HPC/CaHPO₄ granules, but without the addition of TA. All granules were stored for two days at 21 °C and 45 % RH.

Table 3: Formulas of the investigated granules.

| | Pir | TA | HPC | MCC | CaHPO ₄ |
|-------------------------------|------|------|-----|-----|--------------------|
| | [%] | [%] | [%] | [%] | [%] |
| Pir/TA/HPC | 47.5 | 47.5 | 5 | - | - |
| Pir/TA/HPC/MCC | 27.5 | 27.5 | 5 | 45 | - |
| Pir/TA/HPC/CaHPO ₄ | 27.5 | 27.5 | 5 | - | 45 |

4.2.2.2 Preparation of the cocrystal reference

The cocrystal reference was prepared by grinding 600 mg of a 1:1 molar ratio of Pir and TA and addition of 20 µl of water in a 25 ml milling jar with two 9 mm stainless steel balls for 15 min using a Retsch ball mill 200 (Retsch, Germany). The milling frequency was 25 Hz [25, 90].

4.2.2.3 Characterization of the granules

4.2.2.3.1 Raman spectroscopy

The amount of cocrystal formed during granulation was determined at-line using a Raman spectrometer (Control Development, USA) equipped with a thermostatically cooled CCD detector and a fibre optic sampling probe (RamanProbeTM, InPhotonics, USA). Samples were excited using a laser with a wavelength of 785 nm and a laser power of 300 mW (Starbright 785S, Torsana Laser Technologies, Denmark). For each spectrum 8 scan

interferograms were recorded from 81 to 2209 cm^{-1} with a resolution of 8 cm^{-1} and 1 s integration time. Spectra were collected before and 1, 5, 10, and 15 min after the addition of the granulation liquid. For each time point, spectra were recorded at three representative spots of the granulation mass.

Calibration samples for quantitative Raman spectroscopy were prepared by accurately weighing of Pir, TA, cocrystal reference and the excipients. The samples were gently mixed in a glass mortar with a glass rod. One calibration set was prepared for each excipient, containing a constant amount of the respective excipient and 0/100, 25/75, 50/50, 75/25, and 100/0 % cocrystal/Pir-TA physical mixture. All calibration samples were prepared in triplicate.

Quantitative analysis of the cocrystal in the granules was performed by Partial Least Squares regression (PLS) models [136], calculated with The Unscrambler 10.2 software (Camo, Norway). The spectra were pre-processed with standard normal variate (SNV) correction [140] and mean-centring, leading to the highest model quality with the lowest root-mean-square error of calibration (RMSEC) and root-mean-square error of cross-validation (RMSECV) values. The PLS models based on the full spectral range from 600 to 1650 cm^{-1} were compared to forward interval PLS (iPLS) models, suggesting a narrow spectral range to exclude noisy or irrelevant variables. iPLS was performed with Mat-Lab version 7.9.0 (R2009b; MathWorks, USA) installed with PLS_Toolbox version 6.2 (Eigenvector Research, USA). The calibration models were validated by leave-one-out cross-validation. The number of latent variables (LV) of each PLS and iPLS model was determined by evaluation of the coefficient of determination (R^2), the RMSEC, and the RMSECV values as a function of the number of LVs.

4.2.2.3.2 X-ray powder diffractometry (XRPD)

Differences in solid forms were examined using a Panalytical MPD X'PERT Pro X-ray diffractometer (Philips, The Netherlands) using CuK α radiation with 1.54 Å, equipped with a PIXcel detector in continuous scanning mode. Step size was 0.013 °2 θ . Powder samples were analyzed on silicon sample holders and scanned at 45 KV and 40 mA from 5 to 35 °2 θ .

4.2.2.4 Drying and storage stability of the cocrystal granules

To investigate the drying and storage stability of the manufactured granules, the granules were stored at 0 % relative humidity (RH) and 40 °C as well as at 75 % RH and 40 °C. The solid-state form was analyzed directly after granulation and after 1, 2, 3, 7, 14, 21, and 28 d of storage.

4.2.2.5 Pharmaceutical characterization of the cocrystal granules

4.2.2.5.1 Particle shape and size

Particle shape and approximate size were determined by stereomicroscopy. Scanning electron microscopy (SEM) was used to investigate the granule shape in detail. Stereomicroscopic images were taken with a Stereo Discovery V8 Microscope (Zeiss, Germany), equipped with a Zeiss Axio Cam ICc1. The lens was a Zeiss Achromat S 1.0x FWD 63 mm. The approximate size was determined as Feret diameter, ten particles were measured. SEM pictures were taken with a Leo 1525 scanning electron microscope (Zeiss, Germany) with a working voltage of 5.00 kV.

4.2.2.5.2 Flowability

Flowability of the granules was determined by measurement of the granule flow rate. The granule flow rate was determined as the time needed for 50 g to flow through a funnel with an orifice diameter of 7 mm (Ph. Eur. 7). Each experiment was performed in triplicate.

4.2.2.5.3 Friability

The mechanical stability of the granules was tested by assessing the friability (method modified from the Ph. Eur. 7 monograph 'Friability of granules and spheroids'). An amount of 2.50 g of the granules was sieved (mesh 355 μm) to remove fines and shaken by a Retsch ball mill MM 200 (Retsch, Germany) in a 25 ml stainless steel jar without balls for 120 s at a frequency of 3 Hz. Before and after the experiment the granules were dried at 105 °C in a drying chamber to determine the loss on drying. The friability was calculated by Eq. (7)

$$F = \frac{m_1(100 - T_1) - m_2(100 - T_2)}{m_1} \quad \text{Eq. (7)}$$

where F is the friability, m_1 and m_2 are the masses of the granules before and after the experiment, respectively, and T_1 and T_2 are the losses on drying before and after the experiment, respectively. Each granule formulation was tested in triplicate to determine the friability.

4.2.2.5.4 Residual moisture content

The residual moisture content of the granules was determined after drying by Karl-Fischer titration, using a Schott Titroline KF titrator, standardized with hydranal water standard 10.0. Three replicate measurements were performed for each granule formulation.

4.2.2.5.5 Compactability

The granules were compressed to tablets with an E XI eccentric press, instrumented with strain gauges and displacement transducer (Fette, Germany), equipped with 8 mm diameter flat-faced punches. The die wall and the punch surfaces were pre-lubricated with magnesium stearate before each compression act. 150.0 mg of the respective sample were hand-filled into the die. The granules were compressed at compaction forces of approximately 65, 130, 190, 255, and 320 MPa, respectively. Thickness, diameter, and hardness of the tablets were determined by a multi-functional tablet analyser (TBH 525 WTD, Erweka, Germany) after 24 h of relaxing time. All experiments were performed in triplicate at ambient conditions (21 °C/45 % RH). Compactability of the granules was characterized by plotting the tensile strength of the tablets as a function of compaction pressure. The tensile strength was calculated according to Eq. (8) [191, 192],

$$\sigma = \frac{2F}{\pi Dh} \quad \text{Eq. (8)}$$

where σ is the tensile strength, F is the applied compaction force, D the tablet diameter, and h the tablet height.

4.2.2.5.6 Drug release

The tablets were further investigated regarding the influence of the solid-state form of the API on the drug release behaviour. Each tablet (compaction pressure approximately 200 MPa) was dissolved in 75 ml of phosphate buffer (pH 6.8, 0.05 M) and stirred with a magnetic stirrer at 100 rpm at 21 °C. Samples of 2 ml were taken manually with a syringe, equipped with a 0.45 µm membrane filter, after 30 s, 1, 2, 5, 10, and 15 min. The extracted volume was replaced by phosphate buffer. As Pir is UV-inactive, analysis was performed with an infrared spectrometer (Tensor 37, Bruker, Germany), equipped with a calcium

fluoride AquaSpec 1110 M flow-through cell (Bruker, Germany) with a path length of 6.5 μm and a nitrogen-cooled photovoltaic MCT detector. 50 μl of each sample were injected into the flow-through cell. For each spectrum 128 scan interferograms were recorded from 3100 to 1000 cm^{-1} with a resolution of 4 cm^{-1} . The blank buffer spectrum was subtracted from the Fourier-transformed sample spectra using the OPUS 6.4 software. Each spectrum was corrected with regard to baseline as well as to the water and CO_2 signals with OPUS algorithms.

Quantification of the released Pir as a function of time was performed by a Partial Least Squares regression (PLS) model [136], calculated with The Unscrambler 10.2 software (Camo, Norway). The spectral range of the amide I bands of Pir between 1725 and 1630 cm^{-1} was chosen to build the PLS model. The calibration model was validated by leave-one-out cross-validation. The number of latent variables (LV) of the PLS model was determined as described in section 2.2.3.1. Four calibration samples were prepared in triplicate containing a 1:1 molar ratio of Pir and TA with Pir concentrations of 0.237, 0.474, 0.948, and 1.896 mg per ml phosphate buffer.

4.3 Results and discussion

4.3.1 Cocrystal formation during high-shear granulation

4.3.1.1 Cocrystal granules prepared at low impeller speed and low granulation time

Raman spectroscopy has successfully been applied to characterize cocrystals and is an established technique for at-line and in-line monitoring of wet granulation processes [18, 20, 79]. In the present study, during in-line monitoring the wetted mass adhered to the Raman probe during granulation, and led to unreliable data. Thus, the process was monitored at-line.

In Fig. 21 the SNV-corrected and mean-centred Raman spectra of Pir, TA as well as their physical mixture, and the spectra of plain HPC, MCC, CaHPO₄, and of the cocrystal reference are displayed. The obtained cocrystal and physical mixture spectra were in good agreement with the literature spectra [25]. To determine the cocrystal formation rate during high-shear granulation and the amount of cocrystal in the granules, calibration models based on Raman spectroscopy in combination with PLS regression were developed. Development of a universal calibration model for the different granule formulas was not realizable because of the spectral influence of the excipients. Therefore, three different calibration models were established, one for each formulation: Pir/TA/HPC, Pir/TA/HPC/MCC, and Pir/TA/HPC/CaHPO₄.

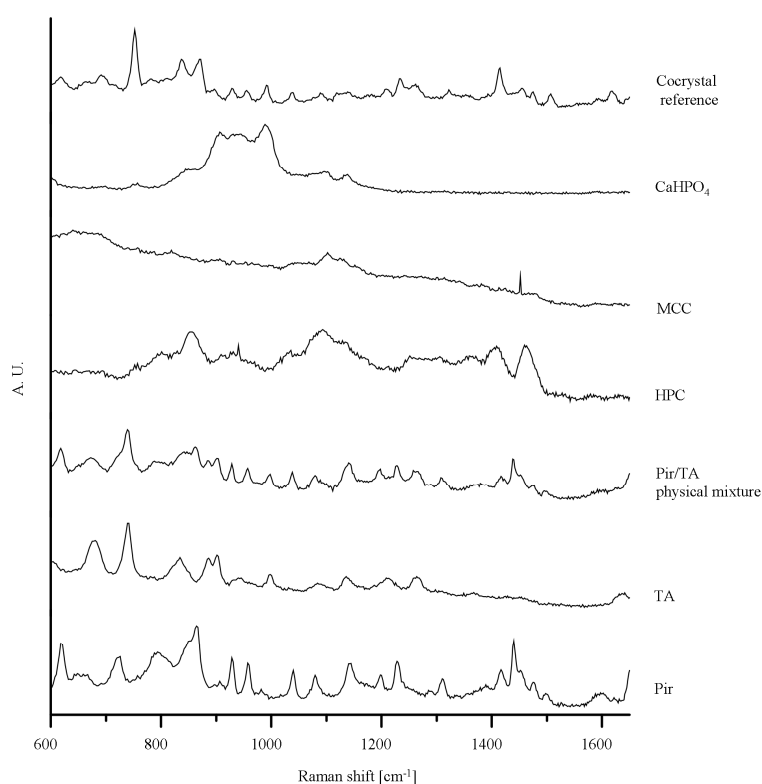


Fig. 21: SNV-corrected and mean-centred Raman spectra of Pir, TA, their physical mixture, HPC, MCC, CaHPO₄, and the cocrystal reference.

In Table 4 the different PLS regression models are evaluated with regards to the spectral window the respective model is based on, the number of LVs, the R^2 , the RMSEC, and the RMSECV. For the full spectral model of the Pir/TA/HPC formula, two LVs were used and resulted in a R^2 of 0.974, a RMSEC of 4.05 %, and a RMSECV of 6.14. To further improve the calibration models, forward iPLS was employed, which excludes noisy or irrelevant spectral ranges from calculating the respective model, and combining the spectral intervals with the lowest RMSECVs, until the model is not further improved. The risk of this method is losing robustness of the model by excluding too many variables, therefore the models need to be evaluated carefully. This method was recently successfully employed to investigate the amount of lactose monohydrate in whey permeate powder [193] and to examine piroxicam hydrate formation during high-shear wet granulation [18]. In the present study, selection of only one spectral interval resulted in the best calibration models. For Pir/TA/HPC, the spectral window between 675 and 928 cm^{-1} highly corresponded to the amount of cocrystal in the calibration samples. Two LVs were used; the R^2 was 0.981, the RMSEC value was 3.78, the RMSECV was 5.20. Compared to the full spectral model the choice of the spectral window between 675 and 928 cm^{-1} resulted in a better calibration model.

With Pir/TA/HPC/MCC the same spectral interval was chosen according to the forward iPLS results, showing a slightly increased model quality compared to the full spectral model. Two LVs were used to build the iPLS model, resulting in a R^2 of 0.966, a RMSEC of 4.35, and a RMSECV of 7.40. The full spectral model (2 LVs) showed a R^2 of 0.961, a RMSEC of 4.06, and a RMSECV of 8.00.

With Pir/TA/HPC/ CaHPO_4 , the spectral range between 1516 and 1737 cm^{-1} resulted in the best calibration model, using two LVs. The R^2 was 0.977, the RMSEC was 3.20 %, and the RMSECV was 5.77 %.

Table 4: Evaluation of PLS regression models, based on Raman spectroscopy.

| | Pre- processing | Spectral window | Latent variables | R ² | RMSEC | RMSECV |
|-------------------------------|--------------------|--------------------|---------------------|----------------|-------|--------|
| Pir/TA/HPC | SNV | 600-1650 | 2 | 0.974 | 4.05 | 6.14 |
| Pir/TA/HPC | SNV | 675-928 | 2 | 0.981 | 3.78 | 5.20 |
| Pir/TA/HPC/MCC | SNV | 600-1650 | 2 | 0.961 | 4.06 | 8.00 |
| Pir/TA/HPC/MCC | SNV | 675-928 | 2 | 0.966 | 4.35 | 7.40 |
| Pir/TA/HPC/CaHPO ₄ | SNV | 600-1650 | 2 | 0.971 | 3.52 | 6.41 |
| Pir/TA/HPC/CaHPO ₄ | SNV | 675-928 | 2 | 0.961 | 5.35 | 7.49 |
| Pir/TA/HPC/CaHPO ₄ | SNV | 1516-1737 | 2 | 0.977 | 3.20 | 5.77 |

The above-described results show that variable selection can improve the prediction quality of PLS models. The improved models were used to investigate the cocrystal formation rate and to determine the amount of cocrystal in the granules at-line during the wet-massing step of the high-shear wet granulation process.

The predicted amount of cocrystal in the manufactured granules as a function of granulation time is presented in Fig. 22. With Pir/TA/HPC and Pir/TA/HPC/CaHPO₄, respectively, the cocrystal formation rate was very fast and a significant difference in cocrystal formation rate or amount was not observable: Approximately 70 % of the physical mixture of drug and cocrystal former converted into the cocrystal within the first min of granulation. After 5 min approximately 95 % of the physical mixture was transformed into the cocrystal (Fig. 22, green curve – Pir/TA/HPC, blue curve – Pir/TA/HPC/CaHPO₄).

Although the prediction error was relatively high with Pir/TA/HPC/MCC, a clear trend was observable: Within 15 min of high-shear granulation, only about 70 % of the physical mixture was converted into the cocrystal (Fig. 22, red curve).

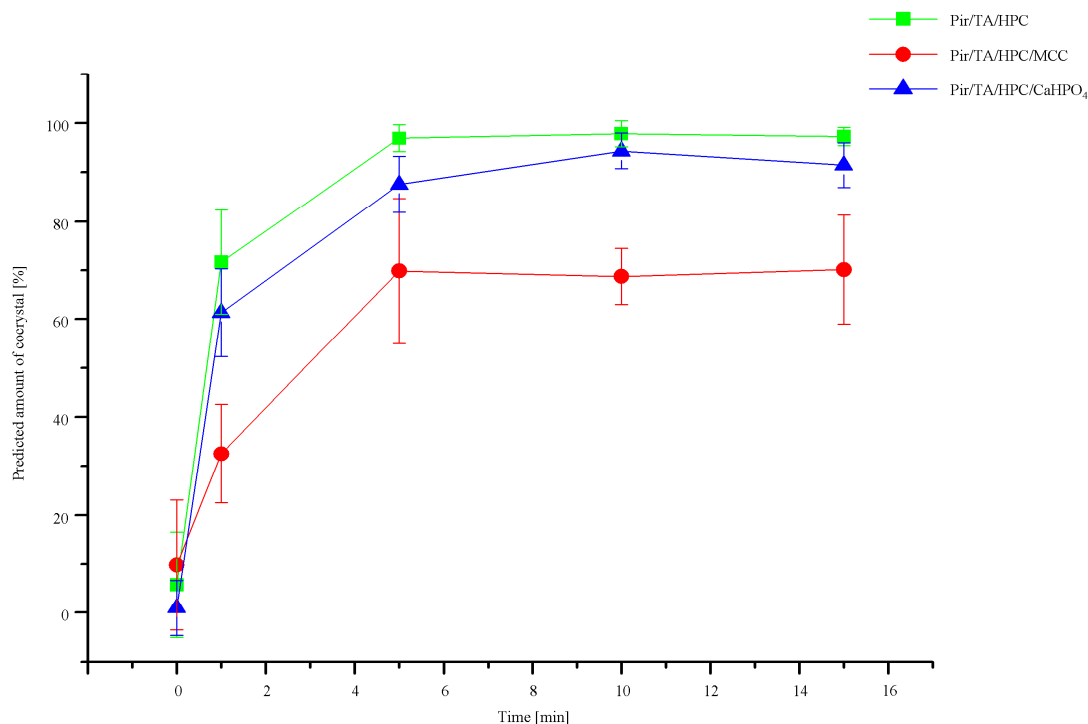


Fig. 22: Predicted amount of cocrystal as a function of granulation time. Granulation was performed in duplicate; each time point represents the mean predicted amount of cocrystal \pm SD at three representative sampling spots. Green curves: Pir/TA/HPC. Red curves: Pir/TA/HPC/MCC. Blue curves: Pir/TA/HPC/CaHPO₄.

To confirm the results of Raman spectroscopy qualitatively, the solid form of the granules was further investigated with XRPD. The XRPD diffractograms of the freshly prepared granules are shown in Fig. 23. The pattern of the Pir/TA/HPC granules is almost identical with the cocrystal reference, exhibiting characteristic cocrystal reflections at 15.2, 17.4, 20.5, and 24.9 $^{\circ}2\theta$ (green lines) [25, 90]. Only one very small reflection at 21.6 $^{\circ}2\theta$ indicates remaining Pir (Fig. 23 a, b), showing an incomplete cocrystal formation with very small remaining amounts of physical mixture. This could not be observed with Raman spectroscopy and iPLS models, because the model quality was not sufficient.

The diffractogram of the Pir/TA/HPC/MCC granules shows besides the characteristic cocrystal reflections (green lines) two Pir reflections at 21.6 and 27.7 $^{\circ}2\theta$ (red lines), again

leading to the conclusion that the cocrystal formation was not complete, confirming the Raman spectroscopic results.

In the XRPD diffractogram of the Pir/TA/HPC/CaHPO₄ granules cocrystal reflections (green lines) and CaHPO₄ reflections at 26.5 and 30.2 °2θ (blue lines), can be observed. Neither Pir nor TA reflections can be identified in the diffractogram.

It can be summarized that with Pir/TA/HPC and with Pir/TA/HPC/MCC cocrystal formation is not complete at the low impeller speed over the low granulation time, while with Pir/TA/HPC/CaHPO₄ the cocrystal is completely formed.

The degree of solid-state transformations during high-shear granulation depends on the respective mechanism and may correspond to the solubility differences, processing temperature, the amount of granulation liquid, the impeller speed, and the exposure time (i. e. the granulation time) of the solids to the granulation liquid [32, 86]. As temperature was not controllable in the experimental setup and larger amounts of water led to sticking of the granulation mass to the granulation jar, the impeller speed and the granulation time were increased to achieve complete cocrystal formation of the investigated granule formulations.

4.3.1.2 Cocrystal granules prepared at high impeller speed over high granulation time

In Fig. 23 c the XRPD patterns of the granules prepared at the high impeller speed level (800 rpm) over the high granulation time level (60 min) are displayed. The diffractogram of the Pir/TA/HPC granules is identical to the cocrystal reference diffractogram, proving complete cocrystal formation (Fig. 23 d). In the XRPD pattern of the Pir/TA/HPC/MCC granules however, the Pir reflection at 21.6 °2θ can still be observed, showing that the cocrystal is not completely formed, despite the higher impeller speed and the longer granulation time (Fig. 23 c). In contrast, the diffractogram of the Pir/TA/HPC/CaHPO₄

indicates complete cocrystal formation, as already observed at the low impeller speed over the low granulation time (Fig. 23 c).

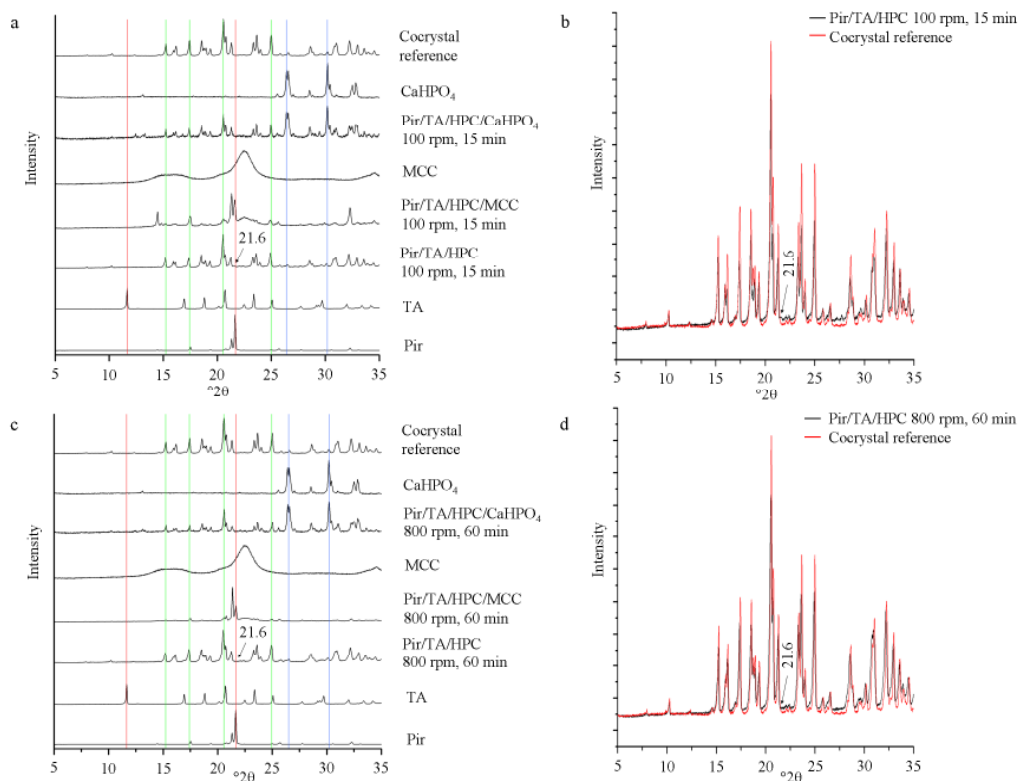


Fig. 23: (a) XRPD patterns of the pure compounds and the freshly prepared granules at an impeller speed of 100 rpm over 15 min. (b) XRPD patterns of the freshly prepared Pir/TA/HPC granules at an impeller speed of 100 rpm over 15 min. (c) XRPD patterns of the pure compounds and the freshly prepared granules at an impeller speed of 800 rpm over 60 min. (d) XRPD patterns of the freshly prepared Pir/TA/HPC granules at an impeller speed of 800 rpm over 60 min.

From the presented results it is concluded that cocrystal formation during high-shear granulation depends on the impeller speed and the granulation time on the one hand and on the excipient used in the granule formula on the other hand.

Formation of the Pir/TA cocrystal during high-shear wet granulation could follow two possible mechanisms: Either a mechanism as assumed for liquid-assisted grinding, where a very small amount of liquid catalyses the cocrystal formation in presence of high mechanical energy put into the system [171], or a solution-mediated mechanism, which is discussed for hydrate formation of high drug-load formulations during high-shear wet granulation [5, 32]

and for cocrystal formation during slurring [92-94]. The solution-mediated mechanism involves three steps: initially dissolution of the metastable form of the API, subsequently nucleation of the stable form, followed by crystal growth. As the majority of the mechanical energy provided by the impeller is dissipated by translational movement of the particles, it may be speculated that the mechanical energy is not sufficient for the cocrystal formation mechanism compared to that observed for liquid-assisted grinding. Furthermore, Pir as well as TA are better water soluble than the cocrystal [90] which could result in dissolution of Pir and TA until reaching supersaturation of the cocrystal, thus nucleation of the cocrystal, and finally cocrystal growth. In a recently published study it has been shown that formation of the Pir/TA cocrystal is time-dependent during dry-grinding ($\eta = 0 \mu\text{l mg}^{-1}$) in a ball mill at 30 Hz [25]. Full transformation into the cocrystal was achieved after 10 min. Small amounts of water ($\eta = 0.033 \mu\text{l mg}^{-1}$) however, acting as a catalyst (most likely by increasing the molecular mobility of the API and the cocrystal former molecules) increased the cocrystal formation rate significantly: Complete cocrystal formation was achieved within the first minute of this so-called liquid-assisted grinding process [25]. However, in the current study, high-shear granulation of Pir/TA/HPC did not result in complete cocrystal formation at an impeller speed of 100 rpm over 15 min ($\eta = 0.13 \mu\text{l mg}^{-1}$), although η was approximately 4-fold higher than during the described liquid-assisted grinding process and thus a higher molecular mobility was expected. An increased impeller speed and granulation time led to complete cocrystal formation, because firstly a prolonged granulation time results in a prolonged exposition of Pir and TA to the granulation liquid, and secondly, it is suggested that an increased impeller speed influences cocrystallization mainly by increasing water distribution and wetting of the granulation mass. The increased shear forces applied to the particles most likely only play a minor role, as most of the energy provided by the impeller is dissipated in translational movement of the particles [5, 32]. This interpretation is in good agreement with the results

reported by Wikström et al. on the influence of the impeller speed on the hydrate formation of theophylline during high-shear granulation: An increased impeller speed resulted in an enhanced transformation rate of anhydrous theophylline to the monohydrate form [76]. However, if η was increased to $0.27 \mu\text{l mg}^{-1}$, cocrystal formation was already complete at an impeller speed of 100 rpm over 15 min as a result of higher molecular mobility due to the presence of a higher amount of water, but the granulation mass was too wet for the granulation process. This supports a solution-mediated mechanism as the driving force for cocrystal formation, as the mechanical energy provided by the impeller could not significantly influence the cocrystal formation due to sticking.

With Pir/TA/HPC/MCC, cocrystal formation was incomplete at an η value of $0.27 \mu\text{l mg}^{-1}$ at an impeller speed of 100 rpm over 15 min as well as at 800 rpm over 60 min. As a result of its partially amorphous nature MCC absorbed large amounts of the granulation liquid (water), and hence competed with the cocrystallization process. Therefore, the volume of water originally present in the granulation mass was not completely available for the cocrystallization process. However, the cocrystal formation process was not totally hindered. This was also observed with theophylline hydrate formation during wet granulation with silicified MCC as filler [86].

The standard deviations of predicted amount of cocrystal in the Pir/TA/HPC/MCC formulation were comparably high, because the reproducibility of the cocrystal formation process was poor. The reason for this could be the complex water sorption mechanism of MCC [194] and can further be affected by the rate of water addition during the granulation process.

Interestingly, with CaHPO_4 as filler cocrystal formation was already complete at an impeller speed of 100 rpm over 15 min with a similar η value as during the granulation process with MCC as filler. It is suggested that crystalline CaHPO_4 did not detract water from

the cocrystallization process due to its minimal water-absorbing potential and thus did not have a significant influence on the cocrystal formation. Airaksinen et al. reported comparable results for the hydrate formation of nitrofurantoin during high-shear wet granulation: While crystalline lactose monohydrate (first filler) did not affect hydrate formation, silicified MCC (second filler) absorbed water and hence hindered hydrate formation at low amounts of water [85].

In summary, it can be stated that cocrystal formation during high-shear granulation is very complex and depends on the volume of the granulation liquid, the water absorption capacity of the excipients used in the formulation, and on the impeller speed and granulation time.

4.3.2 Storage stability the granules

4.3.2.1 Storage stability of the MCC granules

As cocrystals can be formed during storage [169, 195], the Pir/TA/HPC/MCC granules were dried at 40 °C and 0 % RH and stored at 40 °C and 75 % RH, respectively. The solid-state form of the granules was determined with XRPD (Fig. 24, green lines represent characteristic cocrystal peaks, red lines represent characteristic physical mixture peaks). Independent of the applied conditions, the Pir peak at 21.6 °2θ was observable over at least 28 d. Thus, cocrystal formation was not completed under the applied storage conditions, neither with the granules prepared at 100 rpm over 15 min nor with the granules prepared at 800 rpm over 60 min.

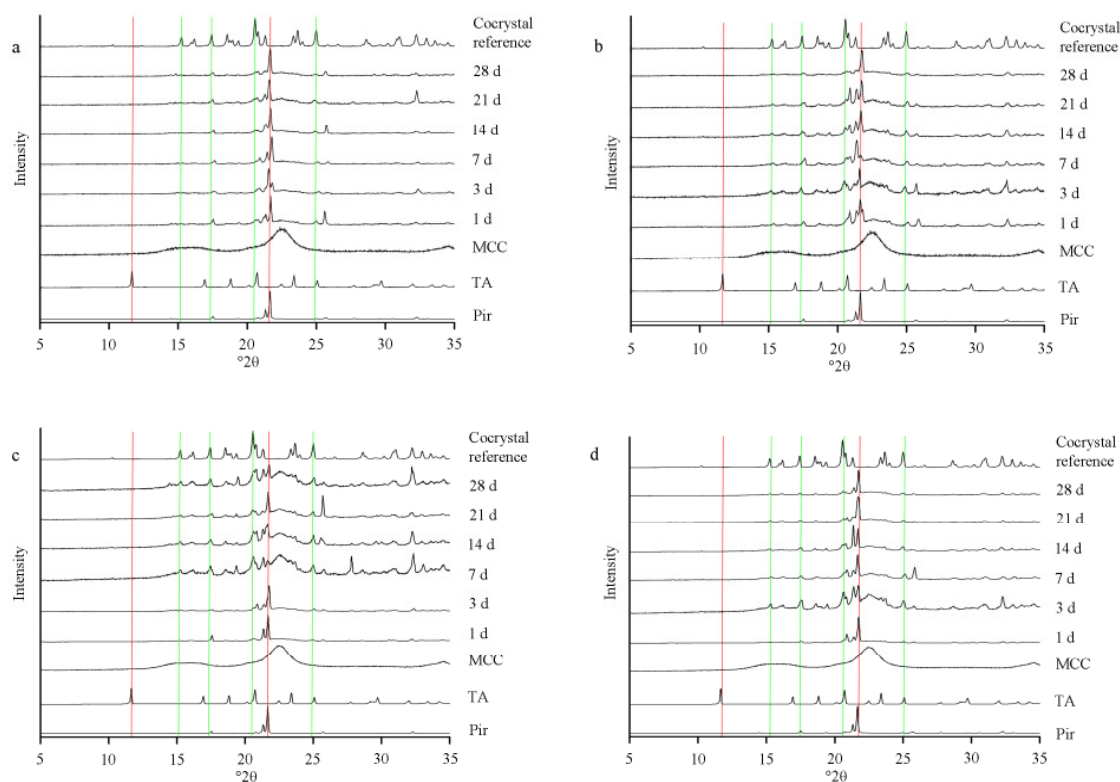


Fig. 24: XRPD patterns of the stored Pir/TA/HPC/MCC granules.

- (a) granules prepared at an impeller speed of 100 rpm over 15 min, stored at 40 °C/0 % RH.
- (b) granules prepared at an impeller speed of 100 rpm over 15 min, stored at 40 °C/75 % RH.
- (c) granules prepared at an impeller speed of 800 rpm over 60 min, stored at 40 °C/0 % RH.
- (d) granules prepared at an impeller speed of 800 rpm over 60 min, stored at 40 °C/75 % RH.

4.3.2.2 Storage stability of the cocrystal granules

The last step of wet granulation is the drying of the granules. As solid-state transformations can occur during drying [18, 68, 97], the manufactured cocrystal granules were dried at 40 °C and 0 % RH for up to 28 d to determine the drying stability of the cocrystal. The solid-state form was investigated using XRPD. As presented in the XRPD diffractograms (Figs. 25 a, c, e. green lines represent cocrystal peaks, red line physical mixture peaks, blue lines CaHPO₄ peaks), in all cases the cocrystal was stable at least over 28 d.

For the manufacturing as well as for the shelf life, the storage stability of the cocrystal granules at high relative humidity is also of interest. As many solid-state transformations proceed relatively slowly under ambient conditions, accelerated storage conditions were applied in this study: The granules were stored for 28 d at 40 °C and 75 % RH. XRPD proved that the cocrystal in the Pir/TA/HPC granules manufactured at 800 rpm over 60 min was stable (Figs. 25 b).

Interestingly, with Pir/TA/HPC/CaHPO₄ granules, distinct changes in the diffractograms were observed when the granules were stored at 40 °C and 75 % RH (Fig. 25 d, f). While the cocrystal peaks decreased and the granules exhibited a wet state, new peaks appeared in the patterns over time. These observations can be explained by the deliquescence of the cocrystal and partly of the CaHPO₄ as well as the simultaneous formation of the poorly water soluble salt calcium tartrate monohydrate (CSD reference code: CATART, peaks marked with an asterisk). Cocrystal formation as a result of deliquescence was observed for various cocrystal systems and could be transferred to the presented case. The formation mechanism may be divided into three steps: (1) moisture uptake (in the present case by anhydrous CaHPO₄), (2) dissolution of the cocrystal and partially of the CaHPO₄, and (3) nucleation and growth of calcium tartrate monohydrate [196].

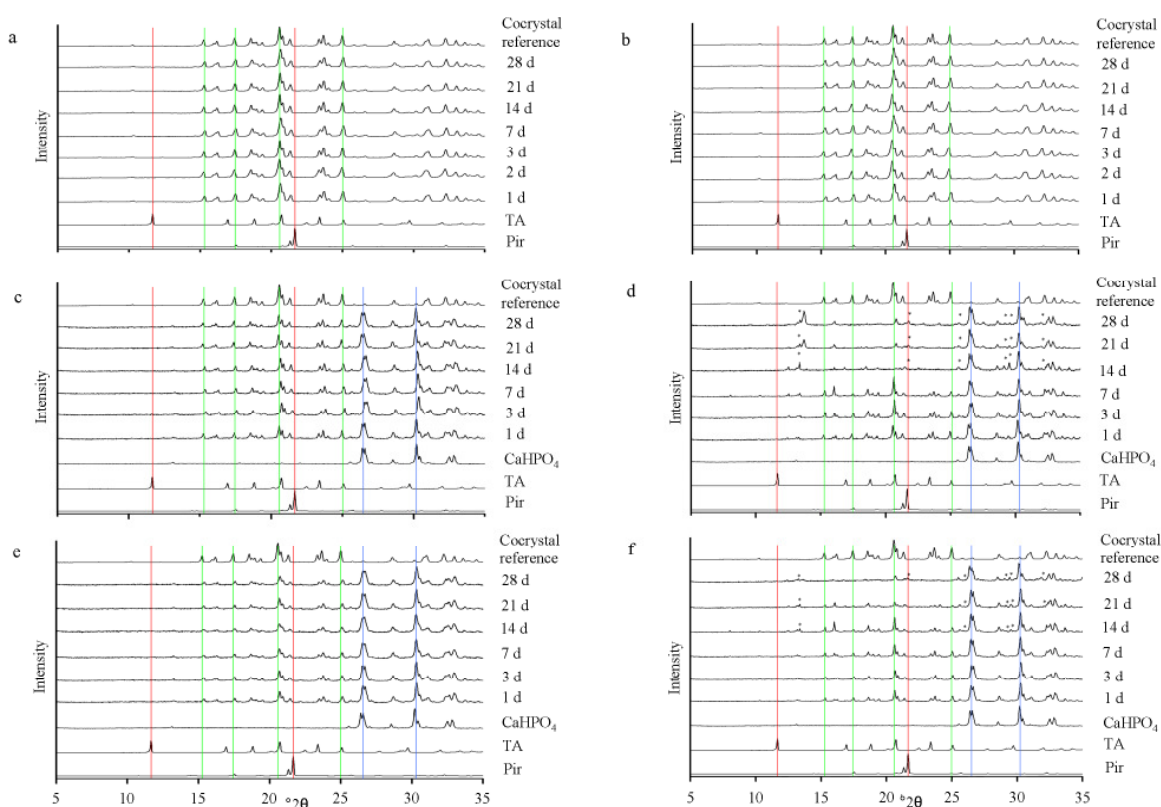


Fig. 25: XRPD patterns of the stored cocrystal granules. (a) Pir/TA/HPC granules, prepared at an impeller speed of 800 rpm over 60 min, stored at 40 °C/0 % RH. (b) Pir/TA/HPC granules, prepared at an impeller speed of 800 rpm over 60 min, stored at 40 °C/75 % RH. (c) Pir/TA/HPC/CaHPO₄ granules, prepared at an impeller speed of 100 rpm over 15 min, stored at 40 °C/0 % RH. (d) Pir/TA/HPC/CaHPO₄ granules, prepared at an impeller speed of 100 rpm over 15 min, stored at 40 °C/75 % RH. (e) Pir/TA/HPC/CaHPO₄ granules, prepared at an impeller speed of 800 rpm over 60 min, stored at 40 °C/0 % RH. (f) Pir/TA/HPC/CaHPO₄ granules, prepared at an impeller speed of 800 rpm over 60 min, stored at 40 °C/75 % RH.

The stability study showed that drying of the prepared cocrystal granules did not affect cocrystal stability, while storage under high relative humidity resulted in deliquescence of the cocrystal and in the formation of calcium tartrate monohydrate.

4.3.3 Technological characterization of the cocrystal granules

4.3.3.1 Particle shape and size

The shape and approximate size of the cocrystal granules were determined by stereomicroscopy. In Fig. 26 a, d, and g the stereomicrographs of the different cocrystal

granules are presented. All granules were approximately between 450 and 1000 μm in diameter and almost spherical. SEM provided a more detailed impression of the surface of the granules. Pir/TA/HPC granules (800 rpm, 60 min) appear porous with clearly observable rhombic cocrystals in the SEM images (Fig. 26 b and c). The Pir/TA/HPC/CaHPO₄ granules, prepared at an impeller speed of 100 rpm over 15 min, are very porous and large cocrystals are visible (Fig. 26 e and f). An increased impeller speed (800 rpm) and a prolonged granulation time (60 min) resulted in round-shaped, dense Pir/TA/HPC/CaHPO₄ granules with a smooth surface, exhibiting very small cocrystals (Fig. 26 h and i).

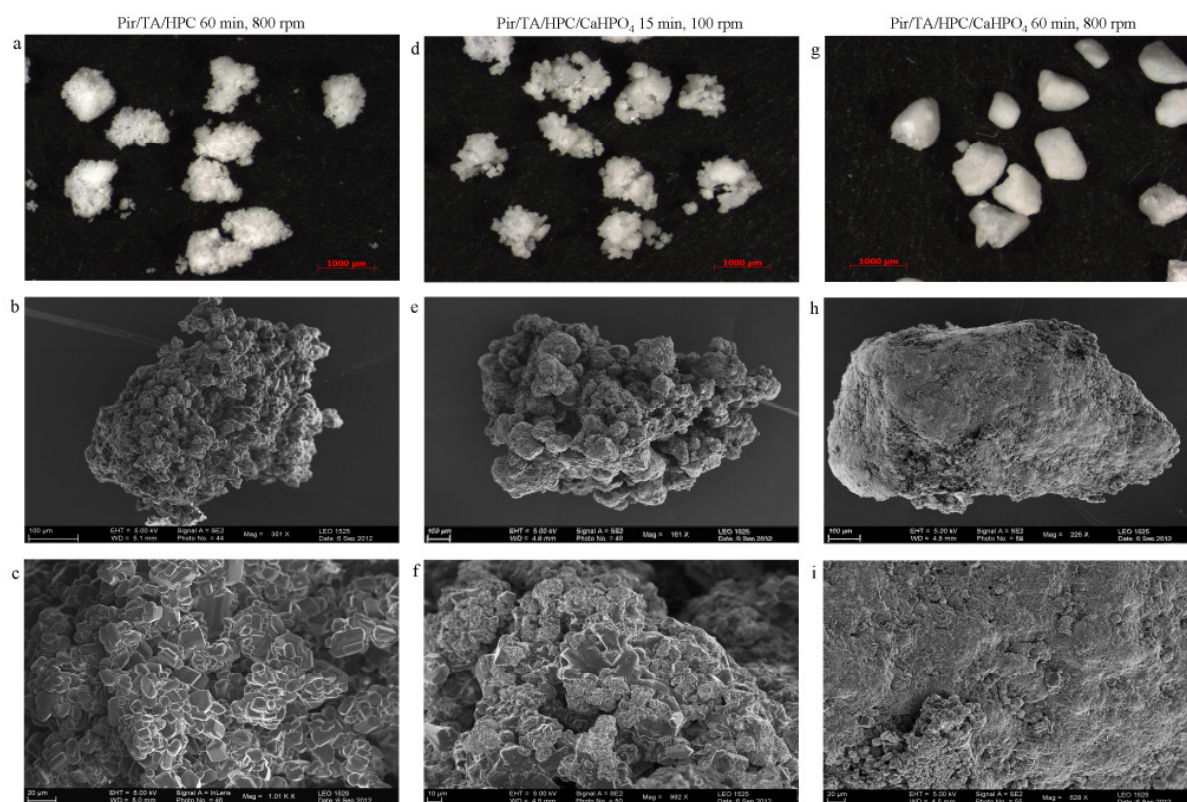


Fig. 26: Stereomicrographs and SEM images of (a-c) Pir/TA/HPC granules, prepared at an impeller speed of 800 rpm over 60 min. (d-f) Pir/TA/HPC/CaHPO₄ granules, prepared at an impeller speed of 100 rpm over 15 min. (g-i) Pir/TA/HPC/CaHPO₄ granules, prepared at an impeller speed of 800 rpm over 60 min.

The structure of the granules is not only influenced by the processing parameters and the excipients used in the formulation, but is further affected by the solid-state form of the

API. Therefore, the stereomicrographs and the SEM images of the reference granules are shown in Fig. 27. The size of the reference granules was comparable to that of the cocrystal granules. Interestingly, the Pir/HPC reference granules appear dense with only very small Pir crystals present (Figs. 27 a-c), while the Pir/TA/HPC cocrystal granules are porous with clearly observable rhombic cocrystals. The Pir/HPC/CaHPO₄ reference granules are microscopically comparable to those containing the cocrystal: The granules prepared at 100 rpm over 15 min are more porous and larger crystals are observable (Figs. 27 d-f) compared to the granules prepared at an impeller speed of 800 rpm over 60 min (Figs. 27 g-i).

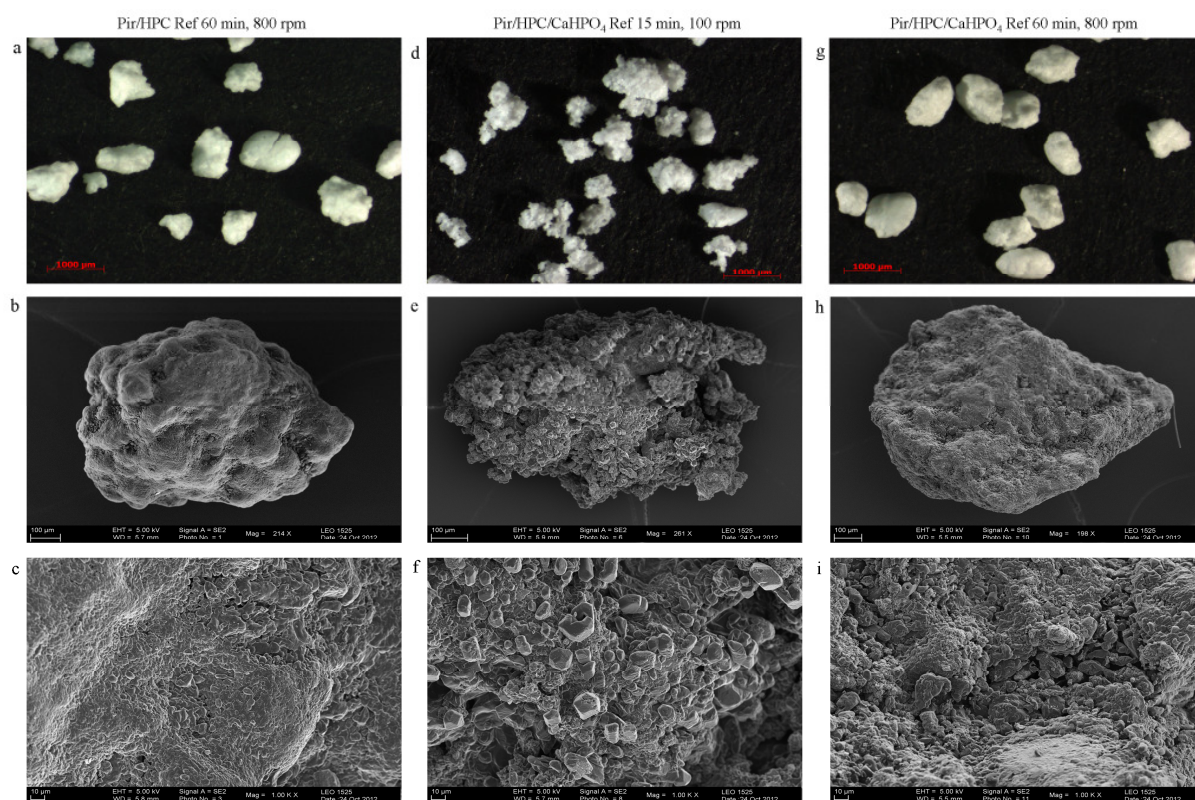


Fig. 27: Stereomicrographs and SEM images of (a-c) Pir/HPC reference granules, prepared at an impeller speed of 800 rpm over 60 min. (d-f) Pir/HPC/CaHPO₄ reference granules, prepared at an impeller speed of 100 rpm over 15 min. (g-i) Pir/HPC/CaHPO₄ reference granules, prepared at an impeller speed of 800 rpm over 60 min.

The granule morphology influences pharmaceutically important particulate properties of the granules such as flowability, friability, and compactability [187]. Therefore, the cocrystal

granules were characterized regarding these properties and compared to the Pir/HPC and Pir/HPC/CaHPO₄ reference granules, respectively. The results of the technological characterization are summarized in Table 5.

4.3.3.2. Flowability

The flowability of all examined granules was characterized by the granule flow rate and was acceptable (Table 5). However, the Pir/TA/HPC granules showed a lower granule flow rate than the reference granules, which can be explained by the rough surface of the cocrystal granules compared to the smooth surface of the reference granules. By addition of CaHPO₄, the differences between cocrystal and reference granules became less pronounced and flowability was improved compared to the Pir/TA/HPC granules, again resulting from the differences in surface roughness. As expected, an increase in impeller speed and granulation time resulted in an increase in the granule flow rate.

4.3.3.3 Friability

The friability is a measure of the mechanical strength of the granules. Although the standard deviations of the friability data were comparably high, trends could be observed (Table 5). The friability of the cocrystal granules (mass loss of between 2.75 and 12.90 %) was higher compared to the reference granules (mass loss between 0.81 and 2.83 %). The differences in friability between cocrystal and reference granules can be explained by the particle morphology: granules with a smooth surface showed a lower friability compared to particles with a rough surface [197]. The friability correlated negatively with the impeller speed and the granulation time.

4.3.3.4 Residual moisture content

The residual moisture content of the granules was determined by Karl-Fischer titration after the drying step. The sorbed water can influence the tensile strength of tablets manufactured with the respective granules. A low water content increases the plastic deformation of the particles by formation of a monolayer around the particles, while a high water content results in a poor compactability because of sticking. The residual moisture of the cocrystal granules was higher compared to the reference granules (Table 5). However, in all cases the residual moisture content was within an acceptable range.

Table 5: Technological properties of the examined granules.

| | Flowability [s/50g] (n = 3 ± SD) | Friability [%] (n = 3 ± SD) | Residual moisture [%] (n = 3 ± SD) |
|---------------------------------------|-------------------------------------|--------------------------------|---------------------------------------|
| Pir/TA/HPC 60 min, 800 rpm | 10.20 ± 0.72 | 5.73 ± 1.18 | 0.42 ± 0.02 |
| Pir/HPC Ref 60 min, 800 rpm | 6.47 ± 0.07 | 1.88 ± 0.63 | 0.38 ± 0.01 |
| Pir/TA/HPC/CaHPO4 15 min, 100 rpm | 6.35 ± 0.1 | 12.90 ± 6.31 | 1.57 ± 0.10 |
| Pir/HPC/CaHPO4 Ref 15 min, 100 rpm | 7.10 ± 0.07 | 2.83 ± 0.49 | 0.51 ± 0.01 |
| Pir/TA/HPC/CaHPO4 60 min, 800 rpm | 4.22 ± 0.09 | 2.75 ± 0.63 | 1.08 ± 0.04 |
| Pir/HPC/CaHPO4 Ref 60 min, 800 rpm | 4.09 ± 0.10 | 0.81 ± 0.06 | 0.64 ± 0.01 |

4.3.3.5 Compactability

The granules were compressed to tablets to examine their mechanical behaviour in dependence of the solid-state form of the API. Compactability was investigated by plotting the tensile strength of the tablets as a function of compaction pressure (Fig. 28). To minimize the influence of particle size distribution, a granule size range between 350 μm and 800 μm was selected for tableting.

Interestingly, tablets prepared with the Pir/TA/HPC cocrystal granules had a higher tensile strength at the investigated compaction pressures than the Pir/HPC reference granules (Fig. 28 a). This observation can be explained by either TA or the cocrystal formation changing the tableting behaviour of the Pir. To exclude the influence of TA, a physical mixture of Pir/HPC and TA/HPC granules was tableted at different compaction pressures (blue triangles in Fig. 28 a). It is obvious that the compactability of this physical mixture was lower compared to that of the cocrystal granules. This implies that in this case the formation of the cocrystal changes the mechanical properties of the granules. The reason is most likely the parallel arrangement of the Pir/TA chains in the cocrystal lattice [90]. These so-called slip plains can be shifted in parallel, resulting in a higher plasticity. Improved compactability due to introduction of slip plains into the crystalline lattice has been described for various cocrystal systems, for example for paracetamol/oxalic acid [6], for caffeine/methyl gallate [179], and for ibuprofen/nicotinamide [178].

In contrast, with granules consisting of 50 % CaHPO_4 , the solid-state form of the API did not have a significant impact on the compactability, as the tensile strengths of the cocrystal and the reference tablets were comparable. It is suggested that the very high brittle fracture and thus high compactability of CaHPO_4 minimized the influence of the solid-state form of the API on the compactability (Fig. 28 b and c). The higher tensile strength of tablets manufactured with Pir/TA/HPC/ CaHPO_4 granules, prepared at a impeller speed of 800 rpm

over 60 min, compared to those prepared at a impeller speed of 100 rpm over 15 min, can be explained by the higher density of the former granules.

These results show that the compactability of granules not only depends on its technological properties, but is also highly influenced by the solid-state form of the API which therefore needs to be taken into account during pre-formulation.

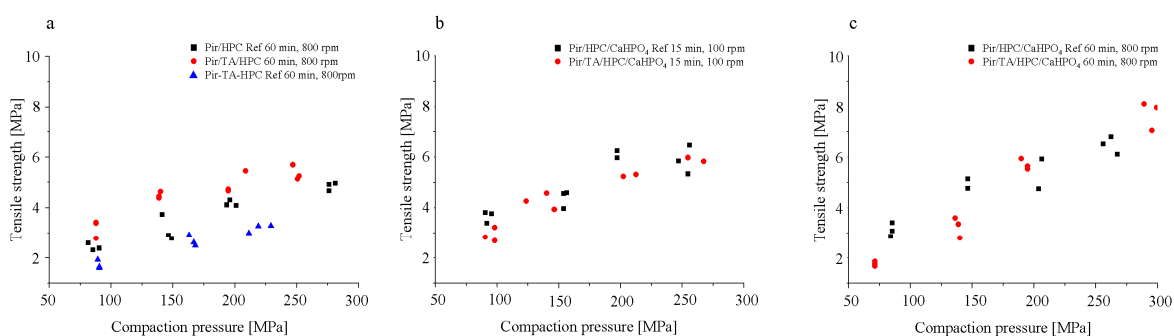


Fig. 28: Compactability of the granules, displayed as tensile strength as a function of compaction pressure ($n=3$). (a) Compactability of Pir/TA/HPC granules, prepared at an impeller speed of 800 rpm over 60 min. (b) Compactability of Pir/TA/HPC/CaHPO₄ granules, prepared at an impeller speed of 100 rpm over 15 min. (c) Compactability of Pir/TA/HPC/CaHPO₄ granules, prepared at an impeller speed of 800 rpm over 60 min.

4.3.3.6 Drug release

Cocrystal formation can alter the release of a drug from its formulation and may affect the bioavailability of the API. Therefore, drug release from the tablets manufactured with the cocrystal granules was measured and compared to that from the tablets manufactured with the reference granules. As Pir is UV-inactive, standard dissolution tests with flow-through cells and UV quantification could not be performed. Thus, the samples were analysed using an infrared spectrometer, equipped with a flow-through cell, which is usually employed for protein analysis [198]. This equipment allows quantification of UV-inactive but IR-active APIs in solution and is easier to handle and less time-consuming than HPLC. For quantification, a PLS model was established. In Fig. 29 a, the IR spectra of Pir, TA, and the

physical mixture of both are displayed. The spectra are corrected with regard to baseline as well as to the water and CO₂ signals. For quantification purposes the spectral region between 1725 and 1630 cm⁻¹ covering the Pir amide I bands at 1685 and 1656 cm⁻¹ were used to establish the PLS model (Fig. 29 b). One LV resulted in the best calibration model with a R² of 0.992, a RMSEC of 0.053, and a RMSECV of 0.062.

The calibration model was used to predict the amount of Pir released in the phosphate buffer as a function of time. In Fig. 9c-e the drug release profiles of the tablets are shown. As shown in Fig. 29 c, the Pir release from the Pir/HPC reference tablets was slightly higher compared to that from the Pir/TA/HPC cocrystal tablets, most likely due to the somewhat lower solubility of the cocrystal [90]. With CaHPO₄ as filler this trend was not observed (Figs. 29 d and e).

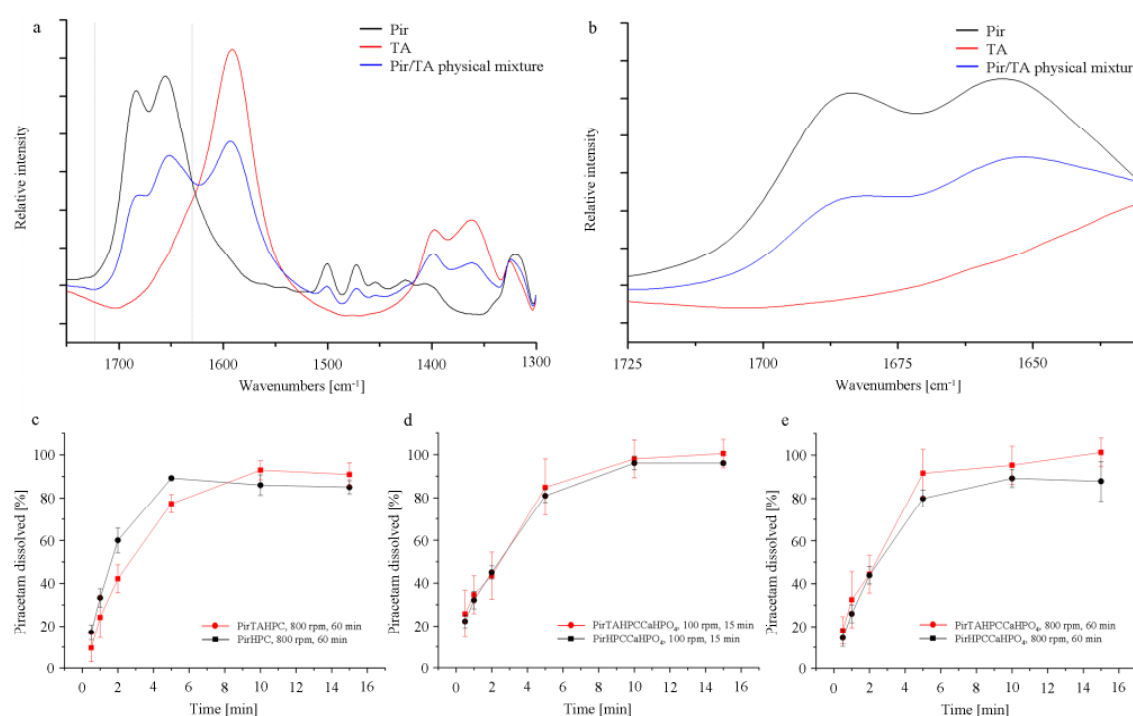


Fig. 29: (a, b) FT-IR spectra of Pir, TA, and the Pir/TA physical mixture in phosphate buffer (pH 6.8, 0.05 M). (c-e) Dissolution profiles of tablets prepared at a compaction pressure of approx. 190 MPa (n=3), containing (c) Pir/TA/HPC granules, prepared at an impeller speed of 800 rpm over 60 min. (d) Pir/TA/HPC/CaHPO₄ granules, prepared at an impeller speed of 100 rpm over 15 min. (e) TA/HPC/CaHPO₄ granules, prepared at an impeller speed of 800 rpm over 60 min.

4.4 Conclusion

High-shear granulation could be established as a suitable technique to produce cocrystal granules on a batch scale. Cocrystal formation during high-shear granulation depends on the amount of granulation liquid added, on the impeller speed, and on the excipients used in the formulation. Cocrystal formation during high-shear wet granulation can, on the one hand, be beneficial for pharmaceutical manufacturers, as downstream-processing can be facilitated. On the other hand, one has to be aware of accidental, unwanted cocrystal formation, as it may influence for example compactability and drug release and thus affect drug performance.

**5. Recrystallization of amorphous glibenclamide in tablets –
a multi-factorial investigation**

Recrystallization of amorphous glibenclamide in tablets – a multi-factorial investigation***Abstract***

The recrystallization of an amorphous drug in a solid dosage form is a complex process and is affected by different influencing parameters during manufacturing and storage. However, these parameters may not only have an impact on the physical stability of the drug, the chemical stability also may be affected.

The aim of the present study was to investigate the influence of the preparation method of amorphous glibenclamide, the compaction pressure applied during tableting as well as the storage conditions on its physical and chemical stability.

Amorphous glibenclamide was prepared by ball-milling and quench-cooling, respectively. While the drug remained chemically intact during ball-milling, it partially degraded during the melting step before quench-cooling. However, tablets containing either quench-cooled or ball-milled glibenclamide, tableted with MCC and Mg stearate at high and low compaction pressure, did not show immediate recrystallization of the drug. During storage of the tablets at 20 °C/0 % RH recrystallization was not observed in any case. An increase in relative humidity resulted in recrystallization of the amorphous ball-milled glibenclamide. Interestingly, a higher degree of crystallinity was observed with tablets compacted at a low pressure. This was also observed at 60 °C/0 % RH and was explained by the reduced molecular mobility of the amorphous drug molecules due to “mechanical trapping” by the MCC molecules. This effect was less pronounced at 60 °C/75 % RH, possibly the result of water vapour absorption by MCC, resulting in swelling and thus softening of the tablets, which might lead to recrystallization. Quench-cooled glibenclamide only recrystallized at high relative humidity. Furthermore, the degree of recrystallized glibenclamide was higher at 60 °C compared to 20 °C. However, at 60 °C/75 % quench-

cooled glibenclamide degraded significantly, while the ball-milled samples remained chemically intact.

It could be concluded that not only the physical but also the chemical stability of an amorphous drug may be affected by manufacturing and storage of the respective solid dosage forms, and therefore needs to be taken into account during pre-formulation as well as during manufacturing.

5.1 Introduction

About 80 % of the drugs on the market are manufactured as solid dosage forms such as tablets and capsules [199]. The bioavailability of the active pharmaceutical ingredient (API) in these dosage forms can be predicted by to the biopharmaceutical classification system (BCS), classifying the API with regard to its membrane permeability and water solubility [200]. A recently published study revealed that between 60 and 70 % of the drug candidates in the pipeline belong to class II of the BCS with a sufficient membrane permeability but a poor water solubility, ultimately leading to a decrease in bioavailability after oral administration [201]. Different approaches have been undertaken to improve the water solubility and thus the bioavailability of BCS class II drugs. One of the most promising propositions was to formulate the API in its amorphous form instead of its thermodynamically stable crystalline form. The molecules in the amorphous state are not organized in a crystal lattice, therefore only showing short range order [38]. Thus, the amorphous form of an API may have a higher water solubility compared to the crystalline forms [202]. However, an amorphous system shows a higher Gibbs energy relative to that of its crystalline counterpart, which is the thermodynamic driving force for recrystallization. Recrystallization counteracts the solubility advantage of the amorphous API [39]. The recrystallization tendency of an

amorphous drug is correlated with environmental influences such as temperature and relative humidity [39] and may also be influenced by the preparation process of the amorphous phase [40]. Furthermore, pharmaceutical down-stream processing steps such as tableting may induce recrystallization [5, 32]. For example, recrystallization of amorphous indomethacin was found to be pressure-induced by tableting and could be reduced by different tableting excipients used in the formula [113]. Polymers with a large elastic deformation reduced the pressure-induced recrystallization most effectively, as a large amount of the compaction energy is taken up by elastic deformation of the polymer.

The quantitative determination of solid-state forms of an API in the presence of excipients is complex. Nevertheless, the suitability of different analytical techniques for quantification of the API in tablets has been examined in several studies [23, 203, 204]. Spectroscopic methods such as Raman spectroscopy [204] and solid-state nuclear magnetic resonance [203] have been shown to allow the identification of the solid-state forms of the API in tablets. Furthermore, parallel-beam X-ray powder diffractometry was found to provide an insight into the solid-state form of the API in tablets [23].

Not only the physical stability in terms of recrystallization behaviour is affected by the manufacturing process and the storage parameters, the chemical stability may also be influenced. The influencing parameters affecting the physical as well as the chemical stability of drugs in tablets are multi-factorial and thus complex, often showing a significant impact on drug performance. Therefore, the ICH Q8 guideline [2] and the FDA PAT guidance [1] recommend a detailed investigation of the process parameters, which influence the product quality, allowing an improved understanding and controlling of the process.

Thus, the aim of this study was to investigate the influence of different processing parameters, namely the preparation method of the amorphous API, the compaction pressure during tableting, and the storage conditions of the tablets, on the recrystallization behaviour

as well as on the chemical stability of amorphous glibenclamide. Glibenclamide was chosen as a model drug because the amorphous as well as the polymorphic forms of this API are thoroughly investigated and described in detail in the literature [205-209].

5.2 Materials and methods

5.2.1 Materials

Glibenclamide was kindly donated by Berlin Chemie (Germany), microcrystalline cellulose (MCC) by Lehmann & Voss (Germany), and magnesium stearate (Mg stearate) by Baerlocher (Germany).

5.2.2 Methods

5.2.2.1 Amorphization of glibenclamide

5.2.2.1.1 Ball-milling

Amorphization of glibenclamide by ball-milling has already been described by Patterson et al. [57]; this method was modified in the present study. Approximately 500 mg of crystalline glibenclamide were milled using a MM 200 ball mill (Retsch, Germany) in 25 ml stainless steel milling jars with three 9 mm and three 6 mm stainless steel balls over 60 min. The milling frequency was 25 Hz. The experiments were performed in a cold room at 4 °C.

5.2.2.1.2 Quench-cooling

Quench-cooling as a preparation method of amorphous glibenclamide was investigated by Hassan et al. [206]. Crystalline glibenclamide was heated in an oil bath at 178 °C until the sample was completely molten. Immediately afterwards the melt was poured into liquid

nitrogen and subsequently gently ground with mortar and pestle before sieving (mesh size: 250 μm).

The amorphous character of each batch was confirmed by XRPD to guarantee the absence of crystalline material. The amorphous material was stored in an airtight container at $-18\text{ }^{\circ}\text{C}$ at 0 % RH until further processing.

5.2.2.2 Tableting of amorphous glibenclamide

The tablet formula consisted of 50 % amorphous glibenclamide prepared by either ball-milling or quench-cooling, 45 % MCC, and 5 % Mg stearate. The powder blends were mixed in a Turbula mixer (Bachofen, Switzerland) for 10 min. Tablets were compacted with an E XI eccentric press, instrumented with strain gauges and displacement transducer (Fette, Germany), and equipped with 10 mm flat-faced punches. 100.0 mg of the respective sample were manually filled into the die. The powder was compacted at forces of approximately 65 and 320 MPa, respectively. All experiments were performed at ambient conditions ($21\text{ }^{\circ}\text{C}/45\text{ } \% \text{RH}$).

5.2.2.3 Storage of the tablets

The tablets were stored at $20\text{ }^{\circ}\text{C}/0\text{ } \% \text{RH}$, $20\text{ }^{\circ}\text{C}/75\text{ } \% \text{RH}$ as well as at $60\text{ }^{\circ}\text{C}/0\text{ } \% \text{RH}$ and at $60\text{ }^{\circ}\text{C}/75\text{ } \% \text{RH}$.

The solid-state form of the API was analyzed directly after tableting as well as after 10 d and 30 d of storage.

5.2.2.4 Solid-state analysis of the tablets

5.2.2.4.1 *Differential scanning calorimetry (DSC)*

The thermal behaviour of the samples was investigated by DSC. DSC scans were recorded in triplicate using a DSC 7 (Perkin Elmer, Germany) between 0 °C and 250 °C at a heating rate of 10 K/min. For temperature calibration, a two-level calibration was performed with indium and water. Enthalpy calibration was done with indium.

5.2.2.4.2 *X-ray powder diffractometry (XRPD)*

The solid-state of the API in the tablets was examined with a Panalytical MPD X'PERT Pro X-ray diffractometer (Philips, The Netherlands) using CuK α radiation with 1.54 Å, equipped with a PIXcel detector in continuous scanning mode. Step size was 0.013 °2 θ . The tablets were gently ground with an achate mortar and pestle, carefully paying attention to not alter the solid-state form of the glibenclamide. Powder samples were analyzed on silicon sample holders and scanned at 45 kV and 40 mA from 5 to 35 °2 θ .

Quantification of the amount of crystalline glibenclamide in the tablets was determined by evaluating the Standard Normal Variate (SNV)-corrected XRPD data with a PLS model consisting of 5 calibration points with a variable amount of amorphous and crystalline glibenclamide (100 % amorphous/0 % crystalline, 75 %/25 %, 50 %/50 %, 25 %/75 %, 0 %/100 %) and a constant amount of MCC and Mg stearate. The calibration model was validated by leave-one-out cross-validation. The number of latent variables (LV) was determined by evaluation of the coefficient of determination (R^2), the root-mean-square error of calibration (RMSEC), and the root-mean-square error of cross validation (RMSECV) as a function of the number of LVs.

5.3 Results and discussion

5.3.1 Characterization of the investigated solid-state forms of glibenclamide

The thermal behaviour of crystalline glibenclamide and its amorphous form, prepared by ball-milling and quench-cooling, respectively, was examined by DSC. The thermogram of the raw crystalline material revealed one single endothermic event, namely the melting point (T_m) at an onset temperature of 174 °C. Typically for amorphous materials, the ball-milled sample showed a glass transition temperature (T_g) of approximately 74 °C and recrystallized at 102 °C. The recrystallized substance melted at 169 °C. Interestingly, the quench-cooled glibenclamide neither showed a recrystallization nor a melting event. Only a T_g was observable at 48 °C. The differences in the glass transition temperatures of the ball-milled and the quench-cooled samples have been explained by a partial thermal degradation of the glibenclamide during melting before the quench-cooling process, resulting in small molecular fragments, acting as plasticizers, which decrease the T_g [57, 207, 209]. Applying the HPLC method developed by Patterson et al. [57], the degradation behaviour of the quench-cooled glibenclamide was confirmed by an additional peak at a retention time R_f of 14.0 min at a wavelength of 230 nm, while the ball-milled substance only showed the glibenclamide peak (R_f : 17.5 min). Thus, already the preparation method of the amorphous glibenclamide has an impact on the chemical stability of the drug. Nevertheless, the partially degraded material was used for further processing to examine the physical and chemical stability of the quench-cooled substance.

In Fig. 30 the XRPD patterns of the plain glibenclamide (crystalline, ball-milled, quench-cooled) as well as the powder blends to be tableted containing amorphous and crystalline glibenclamide, respectively, are presented. The reflections of the crystalline form correspond to the XRPD pattern published for the most stable polymorphic form I [57, 205-208]. In contrast to the crystalline glibenclamide, the ball-milled as well as the quench-cooled

samples only show a halo, demonstrating that the API is completely amorphous. The powder blend containing amorphous glibenclamide and MCC as well as Mg stearate does not show any XRPD reflections either, also proving complete X-ray amorphousness. The differences in the shapes of the halos of plain amorphous glibenclamide and the powder blend containing amorphous glibenclamide result from MCC. However, in the XRPD pattern of the powder blend consisting of crystalline glibenclamide and MCC as well as Mg stearate, the characteristic glibenclamide reflexes are clearly observable despite the amorphous background. Thus, XRPD can be used to detect crystalline glibenclamide in a powder blend containing X-ray amorphous excipients.

5.3.2 Tableting of amorphous glibenclamide

The powder blends containing MCC, Mg stearate and amorphous glibenclamide, either prepared by quench-cooling or by ball-milling, were tableted at a low and a high compaction pressure with an eccentric press to investigate the influence of the compaction energy on the recrystallization behaviour of the amorphous API. The tablets were examined by XRPD directly after compaction to determine the degree of recrystallized API. As a loss of crystallinity may already be observed during particle size reduction [26], the tablets were only crushed by using an achate mortar and pestle for XRPD analysis, carefully paying attention to not alter the solid-state form of the glibenclamide. In Fig. 30 the XRPD patterns of tablets consisting of MCC, Mg stearate, and amorphous glibenclamide, prepared by quench-cooling or ball-milling and tableted at 65 or 320 MPa, respectively, are shown. None of the XRPD patterns showed any reflections, indicating that amorphous glibenclamide, independent of its preparation method, does not recrystallize during tableting. This has also been observed with amorphous indomethacin, prepared by quench-cooling [113]. However, during storage it

could be shown that compacted indomethacin recrystallized faster as compared to the uncompacted drug. It was concluded that the compaction energy transferred into the amorphous drug during tableting induced recrystallization.

Thus, the prepared glibenclamide tablets were stored under different conditions to investigate the recrystallization behaviour.

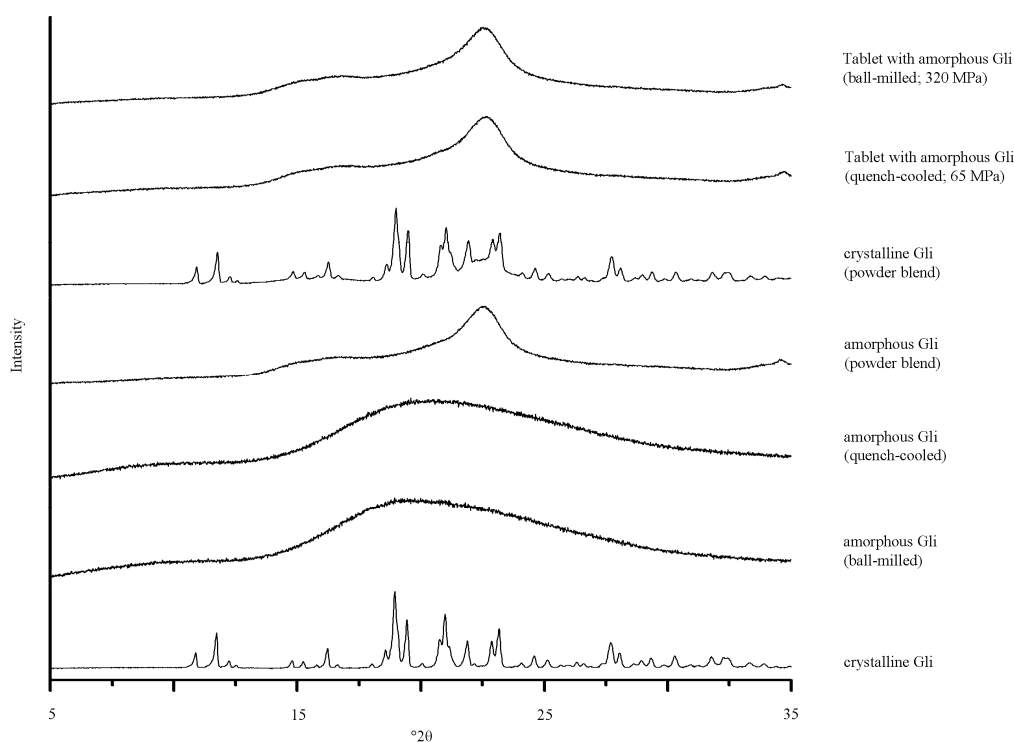


Fig. 30: XRPD patterns of crystalline glibenclamide, ball-milled glibenclamide, quench-cooled glibenclamide, powder blend amorphous glibenclamide (50 % amorphous glibenclamide / 45 % MCC / 5 % Mg stearate), powder blend crystalline glibenclamide (50 % crystalline glibenclamide / 45 % MCC / 5 % Mg stearate), tablet with amorphous glibenclamide (quench-cooled, 65 MPa), tablet with amorphous glibenclamide (ball-milled, 320 MPa).

5.3.3 Storage of the prepared glibenclamide tablets

In Figs. 31 a-d the XRPD patterns of the glibenclamide tablets stored at different conditions for 10 d (Figs. 31 a and c) and 30 d (Figs. 31 b and d), respectively, are displayed. At 20 °C and 0 % RH the XRPD patterns only show halos, demonstrating that the

glibenclamide remained amorphous over 30 d of storage, independent of the preparation method of the amorphous substance and the compaction pressure of the tablets. At higher relative humidity (20 °C/75 % RH), after 10 d of storage small peaks are observable, which increased with prolonged storage. Interestingly, in the patterns of the ball-milled samples more peaks are present than in the diffractograms of the quench-cooled tablets, indicating a higher amount of crystalline drug in the tablets. Furthermore, the amorphous glibenclamide in tablets containing ball-milled substance recrystallized faster if compacted at only 65 MPa compared to 320 MPa.

At 60 °C storage temperature, these trends were even more pronounced. Moreover, the amorphous glibenclamide prepared by ball-milling already recrystallized at 0 % RH, which was not observed with quench-cooled glibenclamide. Again, tablets compacted at 65 MPa showed a higher degree of crystallinity compared to tablets compacted at 320 MPa. Interestingly, the XRPD patterns of tablets containing quench-cooled samples show reflections which do not correspond to the stable polymorphic form I of glibenclamide at 10.0, 15.1, and 17.4 °2θ. As the surface of the tablets turned yellow over 30 d, it is assumed that degradation of the API took place during storage. This hypothesis could be confirmed by HPLC, the chromatograms showing the same peak of the degradation product which was already observed after preparation of the amorphous form (R_f : 14.0), and in addition a second peak at R_f of 16.5 min (R_f : 16.5 min). Thus, not only the physical but also the chemical stability is influenced by the storage conditions.

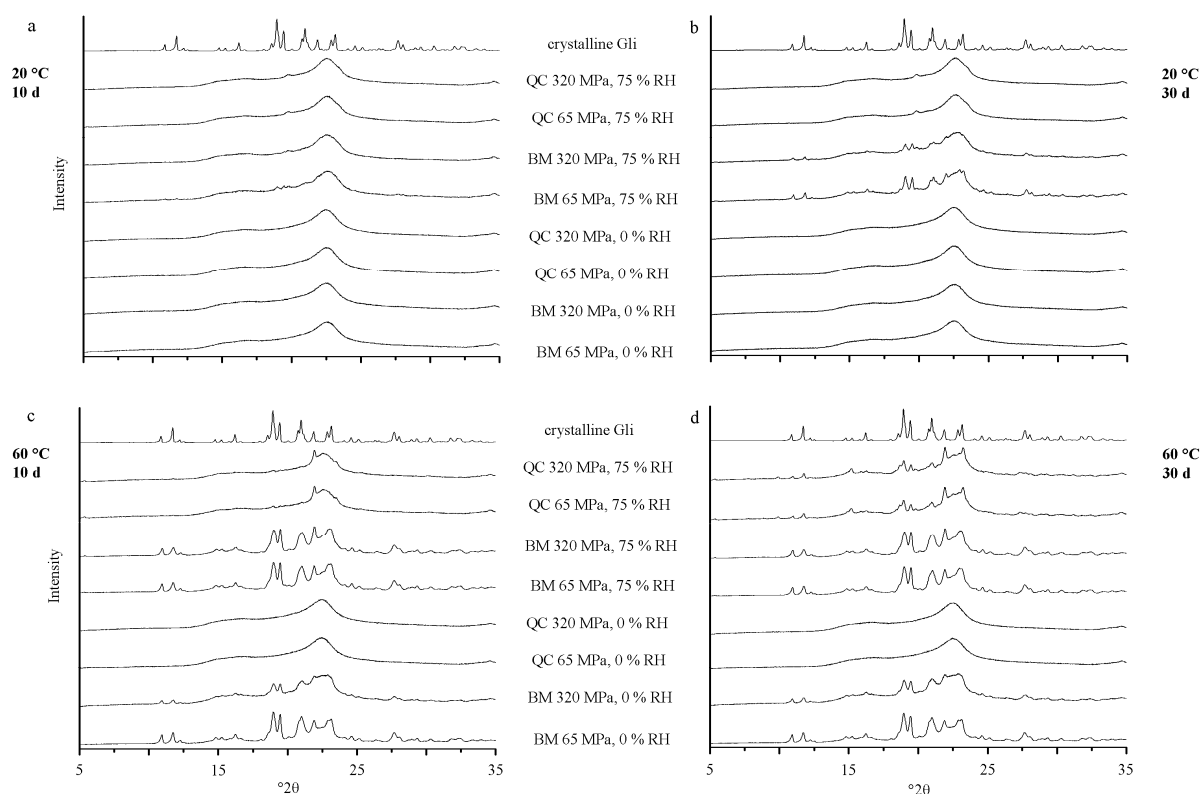


Fig. 31: XRPD patterns of tablets containing differently prepared amorphous glibenclamide, compacted at low/high level of compaction pressure and stored under different conditions. (a) 20 °C/ 10 d. (b) 20 °C/ 30 d. (c) 60 °C/ 10 d. (d) 60 °C/ 30 d.

5.3.4 Quantification model and prediction of crystalline glibenclamide in the stored tablets

To obtain a more detailed insight into the recrystallization behaviour of amorphous glibenclamide after tableting, quantification of the amount of crystalline glibenclamide with respect to different processing parameters and storage conditions was performed. Thus, a prediction model was established by PLS regression on the basis of the SNV-corrected XRPD patterns of 5 calibration points. Three LVs were used to build the model, resulting in an R^2 of 0.992, an RMSEC of 1.78, and an RMSECV of 3.39.

In Fig. 32 the amount of recrystallized glibenclamide predicted by the PLS model is presented. Tablets stored at 20 °C and 0 % RH did not recrystallize within 30 d, independent of the preparation method of the amorphous glibenclamide and the applied compaction pressure during tableting (Fig. 32 a). As expected, at 20 °C and 75 % RH tablets originally

containing amorphous glibenclamide prepared by ball-milling partially recrystallized during storage over 30 d. Interestingly, tablets compacted at 65 MPa showed a higher amount of recrystallized glibenclamide (about 30 % after 30 d) than those compacted at 320 MPa (about 12 % after 30 d). In contrast, the drug in the tablets containing quench-cooled glibenclamide stored at 20 °C and 75 % RH remained almost completely amorphous.

As many solid-state transformations are known to proceed faster under accelerated conditions, tablets were also stored at 60 °C/0 % RH and at 60 °C/75 % RH, respectively. The predicted amount of recrystallized drug is presented in Fig. 32 b. At dry conditions, 75 % of the ball-milled drug recrystallized in tablets compacted at the low pressure, while only approximately 22 % recrystallization was observed with the tablets compacted at the high pressure. Interestingly, there was no significant difference in the degree of recrystallization after 10 and 30 d of storage, respectively. In contrast, the tablets with quench-cooled glibenclamide did not show recrystallization at dry conditions. At 75 % RH, over 60 % of the drug recrystallized in the tablets containing ball-milled glibenclamide. A slightly higher amount of recrystallized glibenclamide was found in tablets compacted at the lower compaction pressure compared to those compacted at the higher pressure, without showing any differences in degree of recrystallization over 30 d of storage. Tablets containing quench-cooled glibenclamide however showed a time-dependent recrystallization at 75 % RH with an increasing degree of crystalline glibenclamide during storage.

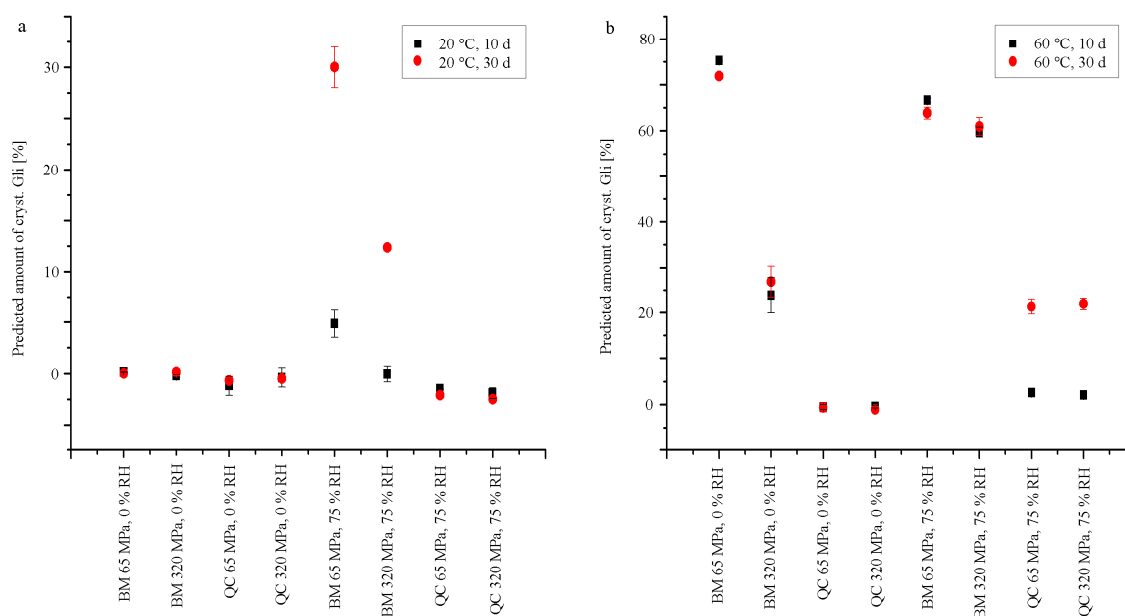


Fig. 32: Amount of recrystallized glibenclamide in tablets during storage, predicted by PLS model based on SNV-corrected XRPD data, 3 LVs. (a) 20 °C storage temperature. (b) 60 °C storage temperature. (BM: ball-milled glibenclamide; QC: quench-cooled glibenclamide).

The recrystallization of amorphous glibenclamide in the prepared tablets was affected by the influencing factors investigated in this study, i. e. preparation method of the amorphous glibenclamide, compaction pressure, storage temperature, and storage relative humidity of the glibenclamide tablets.

As discussed above, HPLC revealed that glibenclamide partially degraded during the melting step before the quench-cooling process. Patterson et al. determined the amount of degraded glibenclamide during melting to be approximately 16 % [57]. Thus, in the present study only tendencies regarding the recrystallization behaviour of quench-cooled glibenclamide could be observed. However, quench-cooled glibenclamide was found to be more stable with respect to recrystallization compared to the ball-milled substance, an observation which was also recently published for amorphous indomethacin, which is

chemically stable during quench-cooling [40]. In this study the stability and differences in the molecular structure of differently prepared amorphous indomethacin were compared. These stability differences were explained by variations in relaxation time and not by structural differences, as it could have been anticipated [40]. This interpretation is thought to also be applicable to amorphous glibenclamide but was not investigated. Furthermore, it is speculated that the recrystallization behaviour of amorphous glibenclamide may also be influenced by the chemical degradation products occurring during melting before the quench-cooling process.

Storage conditions are known to affect recrystallization of an amorphous API in tablets, as high temperature as well as high humidity may increase the recrystallization rate [39]. The amorphous glibenclamide in the tablets did not recrystallize at mild storage conditions (20 °C/0 % RH), independent of the preparation methods of the amorphous glibenclamide as well as the compaction pressure applied during tableting. This was expected, as amorphous substances are regarded as stable with respect to their recrystallization tendency at storage temperatures of more than 50 °C below their T_g [210]. However, an increase of RH resulted in significant recrystallization, most likely as a result of an increase in molecular mobility of the amorphous glibenclamide molecules due to adsorbed water vapour. Interestingly, tablets compacted at low pressure showed a higher amount of recrystallized glibenclamide compared to those compacted at high pressure. The compaction pressure applied during the tableting process may induce recrystallization of amorphous drugs, as described by Schmidt et al., who observed a higher recrystallization tendency not during tableting but during storage after tableting of amorphous indomethacin at higher compaction pressures [113]. As observed with indomethacin, amorphous glibenclamide does not recrystallize during tableting. However, in contrast to indomethacin, in the present study the degree of recrystallization of amorphous

glibenclamide during storage was found to be lower in tablets compacted at a high pressure. Thus, recrystallization of amorphous glibenclamide is not pressure-induced.

As observed at 20 °C and 75 % RH, at high temperature and low humidity (60 °C/0 %) the ball-milled glibenclamide in the tablets compacted at low pressure recrystallized faster compared to the glibenclamide in tablets prepared with high compaction pressure. As intermolecular interactions between amorphous glibenclamide and MCC were ruled out by FTIR, it may be hypothesized that the variances in the recrystallization behaviour of amorphous glibenclamide in tablets compacted at different pressures result from “mechanical trapping” of the amorphous glibenclamide molecules by the MCC, reducing their molecular mobility, and thus decreasing recrystallization.

After 10 days as well as 30 days of storage approximately 75 % of the ball-milled drug were recrystallized, while 25 % of glibenclamide most likely remained amorphous, as chemical degradation did not occur (HPLC data not shown). The quench-cooled drug remained amorphous at 60 °C/0 % RH.

Storage at harsh conditions (60 °C/75 %) also led to fast recrystallization of approximately 62 % of the ball-milled glibenclamide within 30 days. The differences in the amount of recrystallized glibenclamide depending on the compaction pressure were less pronounced at high humidity compared to low humidity. This might be explained by the water absorbing ability of the MCC, which swells and leads to a softening of the tablets, allowing for recrystallization of the amorphous API. Furthermore, the molecular mobility of the amorphous glibenclamide is increased due to high temperature and high RH, also leading to faster recrystallization.

5.4 Conclusion

The physical as well as the chemical stability of amorphous glibenclamide was shown to depend on the preparation method of the amorphous drug and, as expected, on the storage conditions such as temperature and relative humidity. Interestingly, with a higher compaction pressure during tableting, lower degree of recrystallization was observed, most likely due to a reduction of the molecular mobility of the amorphous glibenclamide, induced by the MCC in the compact.

The present study shows that the physical as well as the chemical stability of an amorphous drug is multi-factorial and needs to be evaluated thoroughly, as it may strongly affect drug performance and possibly even drug toxicity.



6. Thermal degradation of amorphous glibenclamide

Thermal degradation of amorphous glibenclamide

Abstract

A glibenclamide polymorph published by Panagopoulou-Kaplani and Malamataris (2000) [211], obtained by sublimation of amorphous glibenclamide, was analysed. A new interpretation of the data is presented and experimentally confirmed by X-ray powder diffractometry, Fourier transform infrared spectroscopy, differential scanning calorimetry, and mass spectrometry. The crystals formed during sublimation of amorphous glibenclamide do not represent a glibenclamide polymorph, but a thermal degradation product, namely 1,3-dicyclohexylurea. The reaction mechanism is suggested to be an elimination of cyclohexylisocyanate from glibenclamide. Cyclohexylisocyanate may decompose to carbon monoxide and cyclohexylamine, which may react in an addition reaction with another cyclohexylisocyanate molecule forming 1,3-dicyclohexylurea.

6.1 Introduction

Glibenclamide (5-chloro-*N*-(4-[*N*-(cyclohexylcarbamoyl)sulphamoyl]phenethyl)-2-methoxy-benzamide) (Fig. 33) is an orally administered sulphonylurea antidiabetic drug. As a result of its good biomembrane permeability and its very poor water solubility, it is rated as a class II drug of the Biopharmaceutics Classification System [212]. Since bioavailability is a major concern with class II drugs, Blume et al. investigated the in vitro dissolution and the bioavailability of marketed glibenclamide tablets. Significant differences between tablets manufactured by different companies were observed, the reasons of which remained unclear [213].

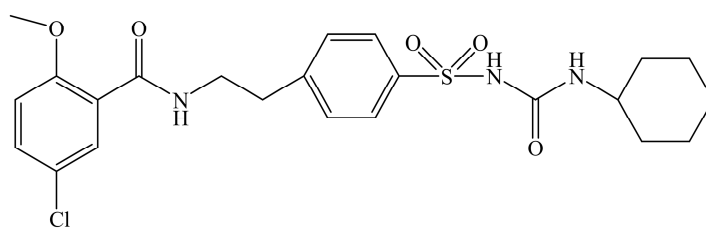


Fig. 33: Chemical structure of glibenclamide

Glibenclamide is a drug with sulphonylurea structure containing two moieties, which are susceptible to degradation at least under harsh conditions: on the one hand the benzamide group and on the other hand the sulphonylurea moiety, which can be split at the urea amide bonds. Bansal et al. investigated the degradation of glibenclamide in acidic and basic media as well as under influence of UV light and at elevated temperatures (50 °C). While glibenclamide degradation occurred in hot acidic and basic media, UV light-induced decomposition and thermal degradation at 50 °C was not observed [214]. Wojnarowska et al. observed thermal degradation during analysis of glibenclamide by thermal Fourier transformation infrared spectroscopy (FTIR) only at temperatures above approximately 190 °C [209].

Sulphonylureas decompose during dry heating by elimination of isocyanates [215, 216], for example, pyrolysis of the sulphonylurea tolbutamide leads to n-butyl isocyanate [217].

Glibenclamide shows polymorphism. Polymorphism is defined as the ability of a substance to crystallize in more than one crystalline form [14, 16]. Depending on the literature source consulted, between approximately 30 % [218] and 50 % [16] of recently developed drugs exist in at least two different crystalline forms.

There are several reasons why polymorphism plays an important role in preformulation, such as regulatory issues and processing properties. Polymorphs may differ in many of their

physicochemical properties such as melting point, mechanical behaviour, storage stability, solubility, and bioavailability resulting from different thermodynamic energies [14, 16].

In the literature, the amorphous form and four polymorphs of glibenclamide are described. In 1991, Hassan et al. investigated the properties of amorphous glibenclamide, which was obtained by melting the crystalline drug using an oil bath at 185 °C and quickly cooling the melt in liquid nitrogen [206]. According to Patterson et al., 16 % of glibenclamide decomposed during this so-called quench-cooling process, whereas only 0.3 % of the drug degraded during amorphization by ball milling [57]. The amorphous glibenclamide obtained by ball milling showed a glass transition temperature (T_g) of 73 °C, while that of the quench-cooled glibenclamide was 58.5 °C. This decrease in the T_g was explained by thermal degradation products acting as plasticizers [57]. In contrast, Wojnarowska et al. observed complete amorphization without any degradation during melting of glibenclamide at 174 °C with subsequent quench-cooling and by cryo-milling of glibenclamide [209]. The amorphous form of glibenclamide recrystallized within two months dependent on temperature [206] and humidity [57].

In 1989, Suleiman and Najib prepared a new polymorph (form II, recrystallization from acetonitrile) and two solvates (pentanol solvate and toluene solvate) of glibenclamide by recrystallization [208]. The solvates showed higher water solubility than the polymorphs I and II. A third polymorph (form III, recrystallization from a mixture of chloroform and ether) and another solvate (recrystallization from a mixture of carbon tetrachloride and chloroform) were obtained by Hassan et al. [205]. Form III showed a higher solubility than form I and II and a lower melting point (T_m) than form I. The authors concluded that form II and form III are metastable and that form I as the marketed form of the drug is the stable form.

In 2000, Panagopoulou-Kaplani and Malamataris described a new glibenclamide polymorph (form IV), which was obtained by sublimation of the amorphous form [211]. This

new polymorph showed a higher T_m than form I and was even less water soluble than the marketed polymorph. The authors concluded that the new polymorph is more stable than the other three known polymorphs. In the present study, a new interpretation of the data by Panagopoulou-Kaplani and Malamataris [211] is presented and experimentally confirmed.

6.2 Materials and methods

6.2.1 Materials

Crystalline glibenclamide (pharmaceutical grade) was kindly supplied by Berlin Chemie (Germany). 1,3-Dicyclohexylurea as reference substance (DCU) was purchased from TCI Europe (Germany).

6.2.2 Methods

6.2.2.1 Preparation of the sublimate

Glibenclamide was melted at 185 °C using a paraffin bath. The melt was poured into liquid nitrogen. The resulting amorphous glibenclamide was heated in a Petri dish covered by a watch glass on a conventional hot plate at 130-160 °C, as described by Panagopoulou-Kaplani and Malamataris [211]. As expected, crystals resublimated on the watch glass.

6.2.2.2 Stereomicroscopy

Stereomicroscopic pictures were taken with a Stereo Discovery V8 Microscope (Zeiss, Germany), equipped with a Zeiss Axio Cam ICc1. The objective used was a Zeiss Achromat S 1.0x FWD 63 mm.

6.2.2.3 Scanning electron microscopy (SEM)

SEM pictures were taken on a Leo 1525 scanning electron microscope (Zeiss, Germany) with a working voltage of 5.00 kV.

6.2.2.4 X-ray powder diffractometry (XRPD)

Differences in crystal lattice configuration were examined using an X'PERT X-ray diffractometer (Philips, The Netherlands, CuK α radiation 1.54 Å) in continuous scanning mode, and step size was 0.02°2 θ . Powder samples were analysed in aluminium sample holders and scanned at 40 kV and 30 mA from 5 to 35°2 θ .

6.2.2.5 Fourier transform infrared spectroscopy (FTIR)

FTIR spectra were recorded on a Tensor 37 spectrometer (Bruker, Germany), equipped with an Attenuated Total Reflectance module (Pike MIRacle). Spectra were detected by an RT-DLaTGS detector over a 4000-600 cm⁻¹ range with a resolution of 4 cm⁻¹, and 16 scans were obtained. Spectral analysis was done using the OPUS® 6.5 software.

6.2.2.6 Mass spectrometry (MS)

MS was performed with a VG 70-S (VG Analytical, England) coupled with a SEV detector, employing electron impact (70 eV) and a source temperature of 200 °C. The mass range examined in this study was m/z 35-800. The obtained mass spectra were interpreted using the MassLib software (MSP Kofel, Switzerland, MassLib V9.3-106, MPI für Kohleforschung).

6.2.2.7 Differential scanning calorimetry (DSC)

DSC scans were recorded in triplicate using a DSC 7 (Perkin Elmer, Germany) between 0 °C and 250 °C at a heating rate of 10 K/min. For temperature calibration, a two-level calibration was performed using indium and water. Enthalpy calibration was done with indium.

6.3 Results and discussion

In Figs. 34 and 35, the stereomicroscopic and SEM photographs of crystalline glibenclamide, amorphous glibenclamide, the sublimate, and DCU are shown. It is obvious that glibenclamide in its untreated form is an aggregate of very small flaky crystals with a primary particle size of about 10 μm . The quench-cooled amorphous glibenclamide exhibits large glassy particles including a conchate fraction. The sublimate crystals are of feathery-needle shape with a primary particle size of several hundred micrometres and look similar to the crystals found by Panagopoulou-Kaplani and Malamataris in 2000 [211]. DCU crystals exhibit a hexagonal shape.

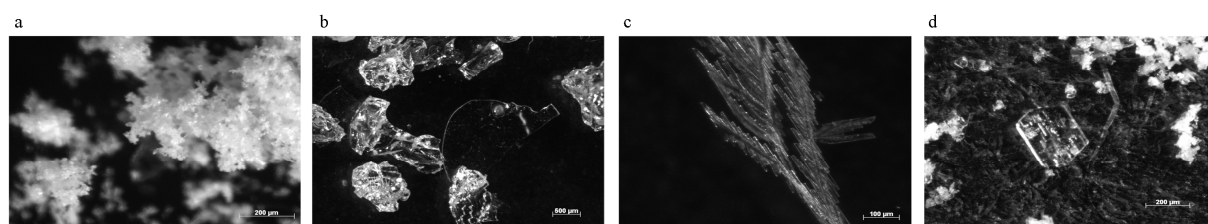


Fig. 34: Stereomicroscopic photographs of (a) crystalline glibenclamide, (b) amorphous glibenclamide, (c) sublimate, and (d) 1,3-dicyclohexylurea reference substance (DCU).

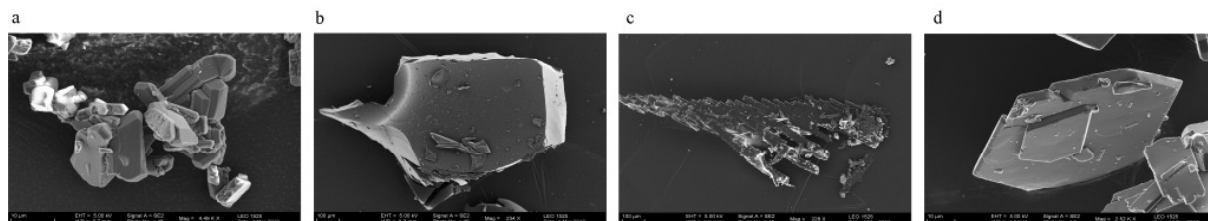


Fig. 35: SEM photographs of (a) crystalline glibenclamide, (b) amorphous glibenclamide, (c) sublimate, and (d) 1,3-dicyclohectylurea reference substance (DCU).

In Fig. 36, the XRPD patterns of crystalline glibenclamide, the amorphous form, the sublimate, and DCU are displayed. The diffractogram of crystalline glibenclamide is consistent with the published pattern with sharp characteristic peaks at $11.6^\circ 2\theta$, $18.9^\circ 2\theta$ and $20.9^\circ 2\theta$ [57, 208]. The halo shape of the diffractogram proves the amorphous structure of the quench-cooled glibenclamide.

The diffractogram of the sublimate is comparable to the diffractogram reported by Panagopoulou-Kaplani and Malamataris [211]. It differs completely from the pattern of crystalline glibenclamide in both intensity and position of the reflexes. Distinct peaks can be identified at $7.6^\circ 2\theta$, $17.3^\circ 2\theta$, and $22.0^\circ 2\theta$. The $7.6^\circ 2\theta$ peak has a high intensity of about 45,000 counts, while the other peaks show intensities between 2000 and 9000 counts.

Comparison of the pattern of the sublimate with an XRPD pattern database (Powder Diffraction File, 2003, The International Centre for Diffraction Data, USA) led to the conclusion that the sublimate represents DCU. The pattern of the DCU reference substance is congruent with the pattern of the sublimate.

Isomorphism, i.e. an identical crystal lattice configuration of two different substances (here a polymorphic form of glibenclamide and DCU), is rarely observed, especially if dealing with organic compounds. Moreover, it is difficult to distinguish different isomorphous forms solely by XRPD.

To exclude isomorphism and to verify the interpretation of the XRPD results, FTIR spectroscopy (Fig. 37), MS (Fig. 38), and DSC (Fig. 39) were performed. The FTIR spectrum of the crystalline glibenclamide is similar to the FTIR spectra of crystalline glibenclamide published previously [57, 206, 211]. The urea NH stretch vibrations can be identified at 3360 cm^{-1} , and the amide NH stretch vibrations are found at 3300 cm^{-1} . The peak slightly above 3000 cm^{-1} results from aromatic CH vibrations, and the peak slightly below 3000 cm^{-1} is caused by aliphatic CH vibrations. The amide carbonyl moiety is responsible for the peak at 1714 cm^{-1} , and the urea carbonyl for the peak at 1615 cm^{-1} . The sulphonyl stretch vibrations are found at wave numbers 1340 cm^{-1} and 1157 cm^{-1} , respectively [147].

The FTIR spectrum of amorphous glibenclamide in Fig. 38 shows significant differences from the crystalline glibenclamide spectrum: While CH and sulphonyl stretch vibrations of the crystalline and amorphous substance remain unchanged, the urea NH stretch vibrations manifest themselves in a rather broad peak and the amide NH band disappeared. The intensity of the amide carbonyl stretch vibrations decreases. Moreover, a peak shoulder at 1654 cm^{-1} appears. This shoulder has been interpreted as C=N stretch vibrations of imidic acid [57, 206, 209]. Glibenclamide has two moieties, which could show this tautomerism of amide and imidic acid: the amide group and the urea group. To determine the moiety being responsible for the tautomerism, the DCU spectrum is recorded. Since there is no amide moiety in DCU, the carbonyl band at 1622 cm^{-1} results from the urea carbonyl. This means that the 1714 cm^{-1} band of the glibenclamide spectrum is likely to be caused by the amide carbonyl stretch vibrations. As the 1714 cm^{-1} band decreases in favour of the appearance of

the 1654 cm^{-1} shoulder, it may be concluded that in fact the amide is converted into the imidic acid form, which was confirmed by Wojnarowska et al. [209]. These observations lead to the assumption that the conversion of crystalline glibenclamide into its amorphous form changes the drug's predominantly amide conformation to a predominantly imidic acid conformation. The amide form is thermodynamically more stable and seems to be stabilized by $\text{NH}\cdots\text{O}$ intermolecular hydrogen bonding. The thermodynamically less stable imidic acid structure appears to be stabilized by intramolecular hydrogen bonding between the imidic acid and the aryl ether oxygen [57, 206, 209].

The spectrum of the sublimate is identical to the spectrum published by Panagopoulou-Kaplani and Malamataris in 2000 [211]. It shows several characteristic differences compared to the spectrum of crystalline glibenclamide: While the urea NH stretch vibration at 3320 cm^{-1} , the aliphatic CH stretch vibrations at wave numbers directly below 3000 cm^{-1} , and the urea carbonyl peak at 1622 cm^{-1} can still be identified, the aromatic CH stretch vibrations at 3000 cm^{-1} , the amide carbonyl peak at 1714 cm^{-1} , and the sulphonyl peaks at 1340 cm^{-1} and 1157 cm^{-1} disappeared. As this spectrum does not show any aromatic and sulphonyl bands and because it is congruent to that of DCU, the XRPD results are confirmed: The sublimate represents 1,3-dicyclohexylurea.

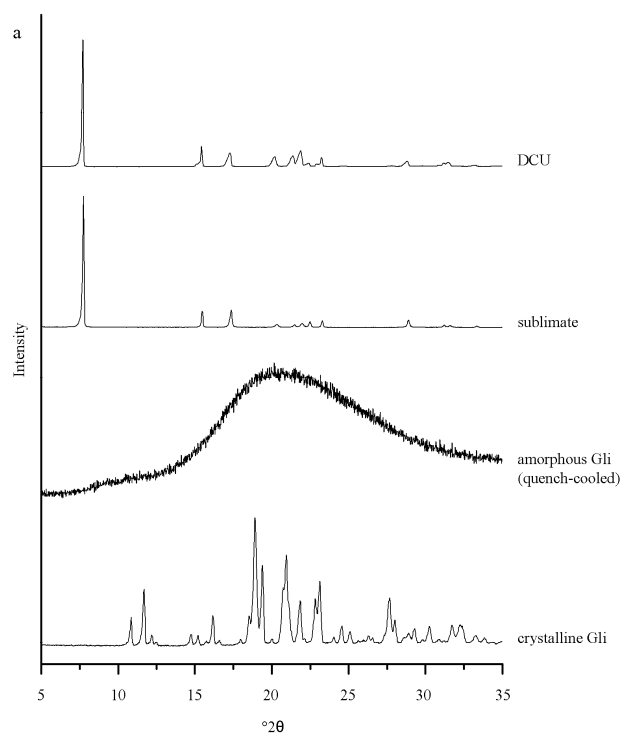


Fig. 36: XRPD pattern of crystalline glibenclamide, amorphous glibenclamide, sublimate, and 1,3-dicyclohectylurea reference substance (DCU).

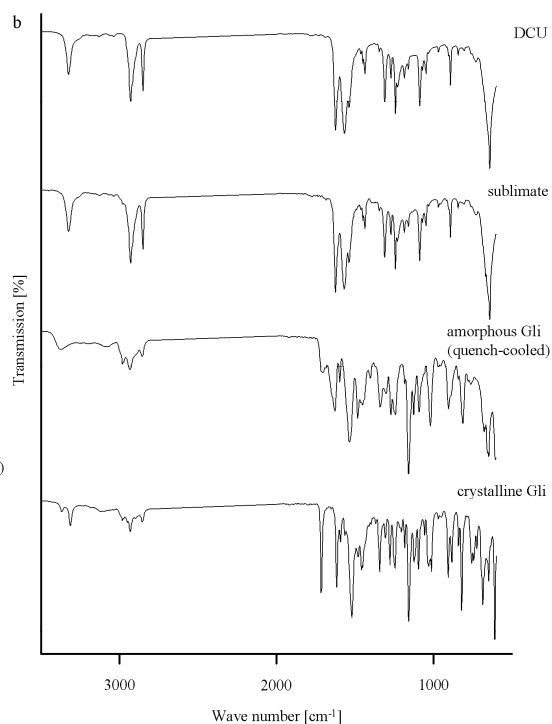


Fig. 37: FTIR spectra of crystalline glibenclamide, amorphous glibenclamide, sublimate, and 1,3-dicyclohectylurea reference substance (DCU).

The mass spectrum of the resublimated crystals is presented in Fig. 38.

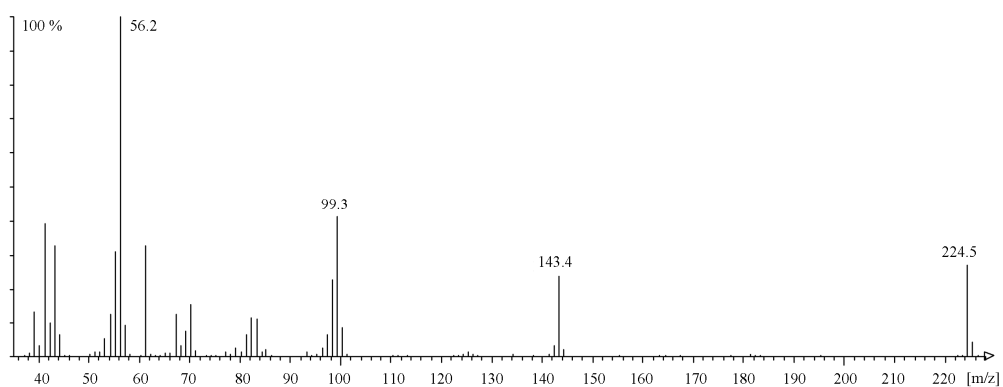


Fig. 38: Mass spectrum of the sublimate.

Again, comparison of the spectrum with a database (NIST/EPA/NIH Mass Spectral Database, Standard Reference Database 1, 1992, National Institute of Standards and

Technology, USA) reveals that the sublimate is 1,3-dicyclohexylurea. The m/z 224.5 peak is identified as the DCU peak.

DSC thermograms of the investigated compounds are presented in Fig. 39. The thermograms are evaluated with regard to the position of the thermal events and the melting/sublimation enthalpies (ΔH). The crystalline glibenclamide shows a melting incidence at a mean onset temperature of 169.7 ± 0.3 °C and a mean ΔH of 114.9 ± 3.1 J/g. This corresponds to the onset melting behaviour of the stable anhydrous form of crystalline glibenclamide as found in the literature [57, 206, 211, 219].

The thermogram of amorphous glibenclamide shows a glass transition temperature (T_g) of approximately 42 °C, which is in good agreement with the T_g of 40-56 °C determined for the quench-cooled substance [211]. Interestingly, the T_g of amorphous glibenclamide determined in this study is approximately 30 °C lower than the T_g of ball milled glibenclamide and about 10 °C lower than the T_g of amorphous glibenclamide obtained by quench-cooling [57]. These observed T_g shifts might be explained by differences in the duration of the melting process at 185 °C before quench-cooling. As it was shown in this study as well as by Wojnarowska et al. [209] that glibenclamide decomposes around 190 °C, thermal degradation during melting in the quench-cooling process is expected. Small molecules resulting from degradation, which are miscible with the sample, could act as plasticizers and lower the T_g . Another reason for the T_g depression might be condensed water vapour from the quench-cooling process on the surface of the amorphous glibenclamide also acting as a plasticizer [220].

The thermograms of the sublimate and of DCU show two endothermic events at about 222 °C and 234 °C, respectively. Since there is no exothermic event observable, polymorphic transition can be excluded. Hot stage microscopy revealed that the first endothermic event results from a partial sublimation of DCU and the second event represents the melting point

of the remaining substance. Panagopoulou-Kaplani and Malamataris [211] detected the first peak at 218 °C, the second peak was not found. In the present study, the sublimation peak has an onset temperature of 222.4 ± 0.3 °C and a ΔH of 68.61 ± 1.15 J/g, whereas the sublimation peak of DCU shows an onset temperature of 223.4 ± 0.7 °C and a ΔH of 73.73 ± 0.94 J/g. The temperature and enthalpy differences between the sublimation events of the sublimate and of DCU are about 1.0 °C and approximately 5 J/g, respectively. The melting peak of the sublimate shows an onset temperature of 233.1 ± 0.6 °C and a ΔH of 86.11 ± 3.15 J/g, while the melting peak of DCU exhibits an onset temperature of 235.3 ± 0.5 °C and a ΔH value of 96.28 ± 2.02 J/g. The temperature and enthalpy differences between the melting events are about 2.0 °C and approximately 10 J/g, respectively. The melting point is in good agreement with the literature value of DCU of 236 °C (Safety Data Sheet of 1,3-dicyclohexylurea, 2007, TCI Europe NV, The Netherlands).

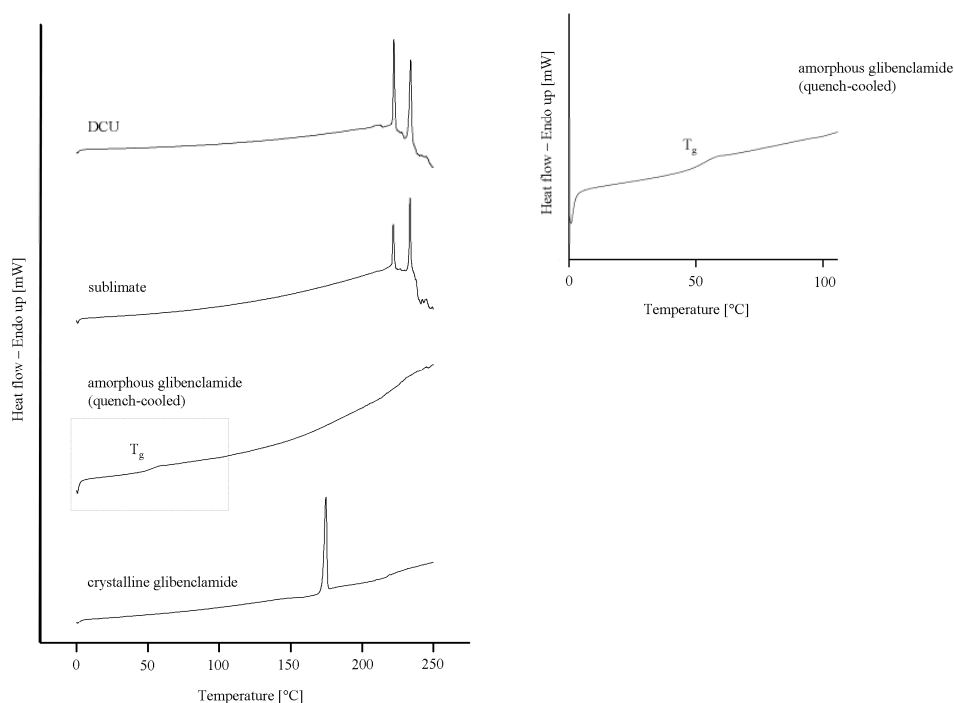


Fig. 39: DSC thermograms of crystalline glibenclamide, amorphous glibenclamide, sublimate, and 1,3-dicyclohexylurea reference substance (DCU). Insert: glass transition temperature of amorphous glibenclamide.

DCU is obviously formed by thermal degradation of amorphous glibenclamide during dry heating. The baseline shift of amorphous glibenclamide in Fig. 40 b at temperatures above 190 °C is an indication for thermal degradation. This observation is in good agreement with the results by Wojnarowska et al. [209], who observed thermal degradation of amorphous glibenclamide at temperatures above approximately 190 °C confirmed by thermal FTIR. Thermal degradation is also observed with crystalline glibenclamide (Fig. 39) at temperatures of above 200 °C.

Surprisingly, in this study, as well as in the study by Panagopoulou-Kaplani and Malamataris [211], thermal degradation is observed on a hot plate set to temperatures of only 130-160 °C. To explain this inconsistency regarding the degradation temperature, the actual hot plate temperature in our laboratory was determined over two hours with an external IR thermometer. It could be shown that setting the temperature to 145 °C leads to a plate and sample temperature of over 300 °C, possibly because of energy loss resulting from the small size of the Petri dish as well as the sample compared to the hot plate diameter. As a result of thermal degradation and formation of DCU, sublimation could already be observed after approximately 15 min of heating. If the hot plate temperature was set to only 65 °C, the measured hot plate and sample temperature was of about 145 °C. In this case, no degradation and thus no sublimation occurred within six hours.

The XRPD, FTIR, MS, and DSC results prove that the sublimate obtained in the described sublimation process is not a polymorphic form of glibenclamide, but its thermal degradation product 1,3-dicyclohexylurea (DCU) **4**.

Dry heating of sulphonylureas leads to the formation of an isocyanate and a primary sulphonamide [215, 217]. Thus, cyclohexylisocyanate **1** is eliminated from glibenclamide. The suggested reaction mechanism of the formation of DCU is displayed in Fig. 40; in presence of small amounts of water **1** may form carbamic acid **2**, which is instable and

decomposes to cyclohexylamine **3** and carbon dioxide. **3** can react with another cyclohexylisocyanate molecule **1** in an addition reaction to **4**.

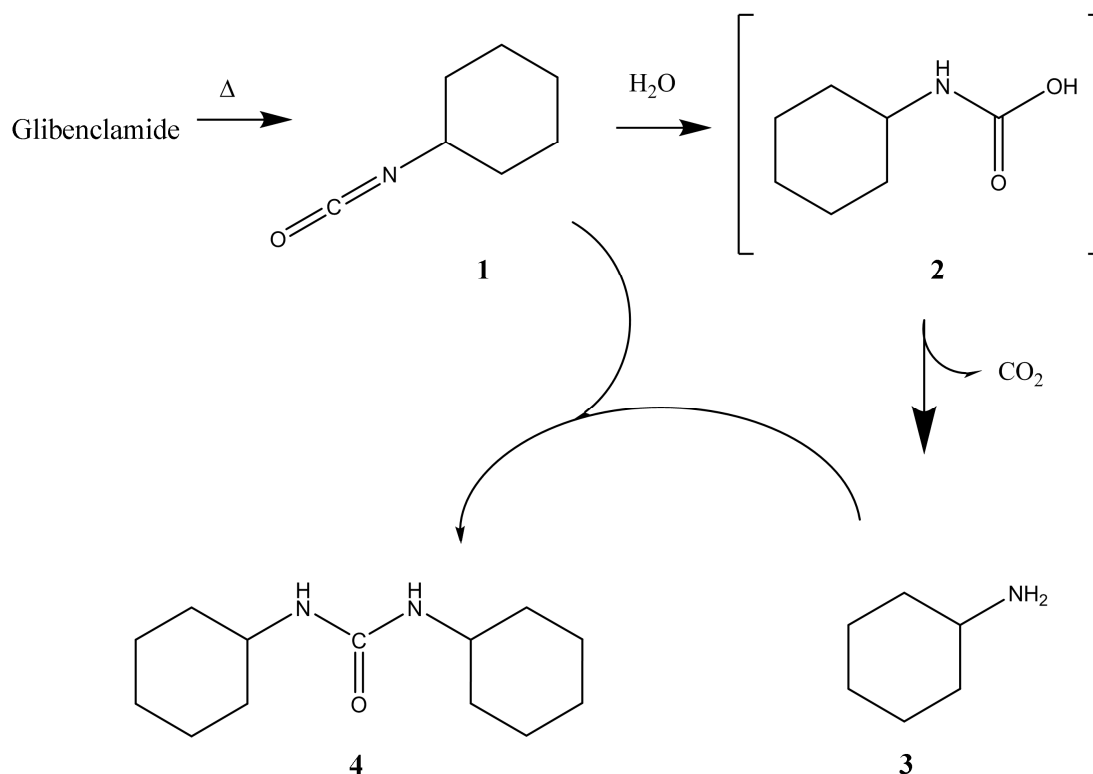


Fig. 40: Decomposition of glibenclamide into cyclohexylisocyanate. In the presence of small amounts of water carbamic acid is formed, which decomposes to cyclohexylamine and carbon dioxide. In a subsequent additive reaction of cyclohexylisocyanate and cyclohexylamine 1,3-dicyclohexylurea is formed.

6.4 Conclusion

The results of this study are in contrast to the observations of Panagopoulou-Kaplani and Malamataris [211]. The substance obtained by sublimation of amorphous glibenclamide is not a further polymorphic form of glibenclamide, but the thermal degradation product 1,3-dicyclohexylurea **4**.

If there was a more stable glibenclamide form than the commercially available form I, polymorphic transformation into the more stable crystalline form during processing or shelf

life should occur. Consequently, this should lead to a decrease in water solubility and, thus, a potentially reduced bioavailability. From the results of this study, it may be concluded that the differences in in vitro dissolution and bioavailability between various marketed glibenclamide tablets reported by Blume et al. [213] are not caused by polymorphic transformation into a thermodynamically more stable polymorph, as stated by Panagopoulou-Kaplani and Malamataris [211].

Der Lebenslauf entfällt aus datenschutzrechtlichen Gründen.

Publications list

Publications

- Rehder, S.; Klukkert, M.; Löbmann, K. A. M.; Strachan C. J.; Gordon, K. C.; Sakmann, A.; Rades, T.; Leopold, C. S.
Investigation of the formation process of two piracetam cocrystals during grinding
Pharmaceutics Special Issue: Pharmaceutical salts and co-crystals (2011), 3, 706-722.
- Rehder, S.; Sakmann, A.; Rades, T.; Leopold C. S.
Thermal degradation of amorphous glibenclamide
Eur. J. Pharm. Biopharm. (2012), 80 (1), 203-208.
- Rehder, S.; Wu, J. X.; Laackmann, J.; Moritz, H.-U.; Rantanen, J.; Rades, T.; Leopold, C. S.
A case study of real-time monitoring of solid-state phase transformations of acoustically levitated particles using near infrared and Raman spectroscopy
Eur. J. Pharm. Sci. (2013), 48, 97-103.
- Rehder, S.; Christensen, N. P. A.; Rantanen, J.; Rades, T.; Leopold, C. S.
High-shear granulation as a manufacturing method for cocrystal granules
Eur. J. Pharm. Biopharm., accepted for publication.

| Title | Journal | Authors | Anteil | Aufgaben |
|---|--|--|---------------------|--|
| Investigation of the formation process of two piracetam cocrystals during grinding | Pharmaceutics Special Issue: Pharmaceutical salts and co-crystals (2011), 3, 706-722 | Rehder, S.; Klukkert, M.; Löbmann, K. A. M.; Strachan C. J.; Gordon, K. C.; Sakmann, A.; Rades, T.; Leopold, C. S. | 60 % 35 % 5 % | Planung, Betreuung, Auswertung, Publikation Experimente Experimente |
| Thermal degradation of amorphous glibenclamide | Eur. J. Pharm. Biopharm. (2012), 80 (1), 203-208. | Rehder, S.; Sakmann, A.; Rades, T.; Leopold C. S. | 100 % | Planung, Experimente, Auswertung, Publikation |
| A case study of real-time monitoring of solid-state phase trans-formations of acoustically levitated particles using near infrared and Raman spectroscopy | Eur. J. Pharm. Sci. (2013), 48, 97-103 | Rehder, S.; Wu, J. X.; Laackmann, J.; Moritz, H.-U.; Rantanen, J.; Rades, T.; Leopold, C. S. | 75 % 20 % 5 % | Planung, Experimente, Auswertung, Publikation Auswertung Experimente |
| High-shear granulation as a manufacturing method for cocrystal granules | Eur. J. Pharm. Biopharm., Accepted for publication | Rehder, S.; Christensen, N. P. A.; Rantanen, J.; Rades, T.; Leopold, C. S. | 95 % 5 % | Planung, Experimente, Auswertung, Publikation Experimente |

| | | | |
|--|---------------------------------|---|-----------------------------------|
| Recrystallization of amorphous glibenclamide in tablets – a multifactorial approach | Research article in preparation | Rehder, S.; Rades, T.; Leopold, C. S. | 100 % Supervisor Supervisor |
| Solid-state transformations induced by pharmaceutical processes during manufacturing | Review article in preparation | Rehder, S.; Rades, T.; Leopold, C. S. | 100 % Supervisor Supervisor |

Unterschrift Frau Prof. Dr. Leopold

Conference
contributions –
oral presentations

Rehder, S.; Wu, J. X.; Laackmann J.; Rantanen, J.; Rades, T.;
Moritz, H.-U.; Leopold, C. S.

Real-time monitoring of solid-state phase transformation of
acoustically levitated particles using near infrared spectroscopy
8th World Meeting on Pharmaceutics, Biopharmaceutics and
Pharmaceutical Technology, Istanbul, Turkey (2012)

Rehder, S.; Klukkert, M.; Strachan, C. J.; Sakmann, A.; Rades, T.;
Leopold, C. S.

Investigation of piracetam cocrystals formation during different
grinding procedures by Raman spectroscopy
38th Meeting of the Controlled Release Society, National Harbour,
Maryland, USA (2011)

Rehder, S.; Sakmann, A.; Rades, T.; Leopold, C. S.

Thermal degradation of amorphous glibenclamide
In-house-Präsentation Berlin Chemie AG, Berlin, Germany (2010)

Conference
contributions –
poster presentations

Rehder, S.; Rades, T.; Leopold, C. S.

Recrystallization of amorphous glibenclamide in tablets –
a multifactorial approach
40th Meeting of the Controlled Release Society, Honolulu, Hawaii,
USA (2013)

Rehder, S.; Christensen, N. P. A.; Rantanen, J.; Rades, T.;
Leopold, C. S.

Technological characterization of cocrystal granules formed by
high-shear granulation
26th Meeting of the American Association of Pharmaceutical
Scientists, Chicago, Illinois, USA (2012)

Conference
contributions –
poster presentations

Rehder, S.; Kniese, M.; Sakmann, A.; Rades, T.; Leopold, C. S.
Formation of piracetam-tartaric acid cocrystals during high shear
granulation
Jahrestagung der Deutschen Pharmazeutischen Gesellschaft
Innsbruck, Österreich (2011)

Rehder, S.; Laackmann, J.; Rantanen, J.; Moritz, H.-U.; Rades, T.;
Leopold, C. S.
Emulation of spray-freeze drying in a fluidized bed by acoustic
levitation
25th Meeting of the American Association of Pharmaceutical
Scientists, Washington D.C., USA (2011)

Klukkert, M.; Rehder, S.; Löbmann, K. A. M.; Strachan, C.;
Sakmann, A.; Rades, T.; Leopold, C. S.
Investigation of cocrystal formation during storage, using Raman
spectroscopy and chemometrics
25th Meeting of the American Association of Pharmaceutical
Scientists, Washington D.C., USA (2011)

Rehder, S.; Sakmann, A.; Rades, T.; Leopold, C. S.
Characterization of the sublimate of amorphous glibenclamide
during dry heating
24th Meeting of the American Association of Pharmaceutical
Scientists, New Orleans, Louisiana, USA (2010)

Rehder, S.; Sakmann, A.; Rades, T.; Leopold, C. S.
Stability of triturations containing amorphous ketoprofen during
tableting
37th Meeting of the Controlled Release Society, Portland, Oregon,
USA (2010)

Hazardous materials

| Substance | Supplier | Danger symbol | Code letter | Hazard statements | Precautionary statements |
|----------------------|----------------------|---|-------------|----------------------|---|
| Acetone | Merck Germany |  | F | H 225-319-336 | P 210-233-305-351+338 |
| Acetonitrile | Baker Germany |  | F, Xn | H225-332-302-312-319 | P 210-305+351+338-403+235 |
| Citric acid | Roth Germany |  | Xi | H 318 | P 305+351+338-311 |
| Dichloromethane | Merck Germany |  | Xn | H 351 | P 281-308+313 |
| Hydrochloric acid | Roth Germany |  | C | H 314-335 | P 260-301+330+331-303+361+353+305+351+338-405-501 |
| Ibuprofen | BASF Germany |  | Xn | H 302 | P 301-312 |
| Ketoprofen | Kreussler Germany |  | T | H 301-315-319-335 | P 261-301+310-305+351+338 |
| Sodium hydroxide | Roth Germany |  | C | H 314-290 | P 280-301+330+331-309+310-305+351+338 |
| Tartaric acid | Roth Germany |  | Xi | H 315-319-335 | P 261-305+351+338 |
| Trifluoroacetic acid | RdH Germany |  | C | H 332-314-412 | P 271-273-301+330+331-305+351+338-309+310 |

Eidesstattliche Versicherung

Hiermit versichere ich an Eides statt, dass ich die vorliegende Arbeit selbstständig und ohne fremde Hilfe sowie nur mit den angegebenen Hilfsmitteln und Quellen erstellt habe. Ich versichere zudem, keinen weiteren Promotionsversuch an einer anderen Einrichtung unternommen zu haben.

Hamburg, den

Sönke C. Rehder

References

- [1] FDA, Guidance for Industry PAT - A framework for innovative pharmaceutical development, manufacturing, and quality assurance, (2004).
- [2] International Conference on Harmonization of Technical Requirements for Registration of Pharmaceuticals for Human Use, Pharmaceutical development - Q8, (2008).
- [3] Mutschler E., Geisslinger G., Kroemer H. K., Ruth P., Schäfer-Korting M., Mutschler Arzneimittelwirkungen, Wissenschaftliche Verlagsgesellschaft Stuttgart, Stuttgart, 2008.
- [4] Bauer J., Spanton S., Henry R., Quick J., Dzinki W., Porter W., Morris J., Ritonavir: An extraordinary example of conformational polymorphism, *Pharm. Res.* 18 (2001) 859-866.
- [5] Wildfong P. L. D., Effects of pharmaceutical processing on the solid form of drug and excipient materials, in: Brittain H. G. (Ed.) *Polymorphism in pharmaceutical solids*, Informa Healthcare, New York, 2009, pp. 510-559.
- [6] Karki S., Frišćić T., Fábíán L., Laity P. R., Day G. M., Jones W., Improving mechanical properties of crystalline solids by cocrystal formation: new compressible forms of paracetamol, *Adv. Mater.* 21 (2009) 3905-3909.
- [7] Crookes D. L., Process of forming form 2 ranitidine hydrochloride, *Pat. Appl. No.* 406710, 1987
- [8] Perman J., Structure of the week - The \$ 30 billion dollar polymorph, in, *American Chemical Society Network*, (2010).
- [9] Schickaneder H., Nikodopoulos A., Process for preparing form 1 ranitidine hydrochloride, *Pat. Appl. No.* 08/426,930, 1995.
- [10] Goyal S., Thorson M. R., Zhang G. G. D., Gong Y., Kenis P. J. A., Microfluid approach to cocrystal screening of pharmaceutical parent compounds, *Cryst. Growth Des.* 12 (2012) 6023-6034.
- [11] Benmore C. J., Weber J. K. R., Amorphization of molecular liquids of pharmaceutical drugs by acoustic levitation, *Phys. Rev. X* 1 (2011) 011004/1-011004/7.
- [12] Rehder S., Wu J. X., Laackmann J., Moritz H.-U., Rantanen J., Rades T., Leopold C. S., A case study of real-time monitoring of solid-state phase transformations in acoustically levitated particles using near infrared and Raman spectroscopy, *Eur. J. Pharm. Sci.* 48 (2013) 97-103.
- [13] Welter E., Neidhart B., Acoustically levitated droplets - a new tool for micro and trace analysis, *Fresenius J. Anal. Chem.* 357 (1997) 345-350.
- [14] Brittain H. G., Theory and principles of polymorphic systems, in: H.G. Brittain (Ed.) *Polymorphism in Pharmaceutical Solids*, Informa Healthcare, Milford, New Jersey, USA, 2009.
- [15] Chieng N., Rades T., Aaltonen J., An overview of recent studies on the analysis of pharmaceutical polymorphs, *J. Pharm. Biomed. Anal.* 55 (2011) 618-644.
- [16] Hilfiker R., Blatter F., v. Raumer M., Relevance of solid state properties for pharmaceutical products, in: R. Hilfiker (Ed.) *Polymorphism in the Pharmaceutical Industry*, Wiley-VCH Verlag GmbH & Co. KGaA, Weinheim, 2006.
- [17] McGoverin C. M., Rades T., Gordon K. C., Recent pharmaceutical applications of Raman and terahertz spectroscopies, *J. Pharm. Sci.* 97 (2008) 4598-4621.
- [18] Christensen N. P. A., Cornett C., Rantanen J., Role of excipients on solid-state properties of piroxicam during processing, *J. Pharm. Sci.* 101 (2012) 1202-1211.
- [19] Rantanen J., Process analytical applications of Raman spectroscopy, *J. Pharm. Pharmacol.* 59 (2007) 171-177.

- [20] Jørgensen A., Rantanen J., Karjalainen M., Khriachtchev L., Räsänen E., Yliruusi J., Hydrate formation during wet granulation studied by spectroscopic methods and multivariate analysis, *Pharm. Res.* 19 (2002) 1285-1291.
- [21] Reich G., Near-infrared spectroscopy and imaging: Basic principles and pharmaceutical applications, *Adv. Drug Deliv. Rev.* 57 (2005) 1110-1137.
- [22] Chakravarty P., Bhardwaj S. P., King L., Suryanarayanan R., Monitoring phase transformations in intact tablets of trehalose by FT-Raman spectroscopy, *AAPS Pharm. Sci. Tech.* 10 (2009) 1420-1426.
- [23] Cao W., Bates S., Peck G. E., Wildfong P. L. D., Qiu Y., Morris K. R., Quantitative determination of polymorphic composition in intact compacts by parallel-beam X-ray powder diffractometry, *J. Pharm. Biomed. Anal.* 30 (2002) 1111-1119.
- [24] Heinz A., Gordon K. C., McGoverin C. M., Rades T., Strachan C. J., Understanding the solid-state forms of fenofibrate - a spectroscopic and computational study, *Eur. J. Pharm. Biopharm.* 71 (2009) 100-108.
- [25] Rehder S., Klukkert M., Löbmann K. A. M., Strachan C. J., Sakmann A., Gordon K. C., Rades T., Leopold C. S., Investigation of the formation process of two piracetam cocrystals during grinding, *Pharmaceutics* 3 (2011) 706-722.
- [26] Chieng N., Rehder S., Saville D., Rades T., Aaltonen J., Quantitative solid-state analysis of three solid forms of ranitidine hydrochloride in ternary mixtures using Raman spectroscopy and X-ray powder diffraction, *J. Pharm. Biomed. Anal.* 49 (2009) 18-25.
- [27] Amigo J. M., Bastús N. G., Hoen R., Vázquez-Campos S., Varón M., Royo M., Puentes V., Analysis of time-dependent conjugation of gold nanoparticles with an antiparkinsonian molecule by using curve resolution methods, *Anal. Chim. Acta* 683 (2011) 170-177.
- [28] Wu J. X., Xia D., Van Den Berg F., Amigo J. M., Rades T., Yang M., Rantanen J., A novel image analysis methodology for online monitoring of nucleation and crystal growth during solid state phase transformation, *Int. J. Pharm.* 433 (2012) 60-70.
- [29] Sun C. C., Materials science tetrahedron - A useful tool for pharmaceutical research and development, *J. Pharm. Sci.* 98 (2009) 1671-1687.
- [30] Aaltonen J., Sandler N., Monitoring of phase transformations during processing of solid dosage forms, *Pharm. Tech. Eur.* 19 (2007) 27-28, 31-32.
- [31] Brittain H. G., Theory and principles of polymorphic systems, in: Brittain H. G. (Ed.) *Polymorphism in pharmaceutical solids*, Informa Healthcare, New York City, 2009, pp. 1-23.
- [32] Zhang G. G. D., Law D., Schmitt E. A., Qiu Y., Phase transformation considerations during process development and manufacture of solid oral dosage forms, *Adv. Drug. Dev. Rev.* 56 (2004) 371-390.
- [33] Brittain H. G., Morris K. R., Boerrigter S. X. M., Structural aspects of solvatomorphic systems, in: Brittain H. G. (Ed.) *Polymorphism in pharmaceutical solids*, Informa Healthcare, New York City, 2009, pp. 233-281.
- [34] Shan N., Zaworotko M. J., The role of cocrystals in pharmaceutical science, *Drug Discov. Today* 13 (2008) 440-446.
- [35] Ruscica R., Bianchi M., Quintero M., Martinez A., Vega D. R., Solid-state forms of zoledronic acid: Polymorphism in hydrates, *J. Pharm. Sci.* 99 (2010) 4962-4972.
- [36] Aitipamula S., Chow P. S., Tan R. B. H., Polymorphs and solvates of a cocrystal involving an analgesic drug, ethenzamide, and 3,5-dinitrobenzoic acid, *Cryst. Growth Des.* 10 (2010) 2229-2238.
- [37] Willart J. F., Descamps M., Solid state amorphization of pharmaceuticals, *Mol. Pharm.* 5 (2008) 905-920.

- [38] Bates S., Zografi G., Engers D., Morris K., Crowley K., Newman A., Analysis of amorphous and nanocrystalline solids from their X-ray diffraction pattern, *Pharm. Res.* 23 (2006) 2333-2349.
- [39] Taylor L. S., Shamblin S. L., Amorphous solids, in: H.G. Brittain (Ed.) *Polymorphism in pharmaceutical solids*, Informa Healthcare, New York City, 2009.
- [40] Karmwar P., Graeser K., Gordon K. C., Strachan C. J., Rades T., Investigation of properties and recrystallization behaviour of amorphous indomethacin samples prepared by different methods, *Int. J. Pharm.* 417 (2011) 94-100.
- [41] Konno H., Taylor L. S., Influence of different polymers on the crystallization tendency of molecularly dispersed amorphous felodipine, *J. Pharm. Sci.* 95 (2006) 2692-2705.
- [42] Konno H., Taylor L. S., Ability of different polymers to inhibit the crystallization of amorphous felodipine in the presence of moisture, *Pharm. Res.* 25 (2008) 969-978.
- [43] Miyazaki T., Yoshioka S., Aso Y., Kojima S., Ability of polyvinylpyrrolidone and polyacrylic acid to inhibit the crystallization of amorphous acetaminophen, *J. Pharm. Sci.* 93 (2004) 2710-2717.
- [44] Allesø M., Chieng N., Rehder S., Rantanen J., Rades T., Aaltonen J., Enhanced dissolution rate and synchronized release of drugs in binary systems through formulation: Amorphous naproxen-cimetidine mixtures prepared by mechanical activation, *J. Control. Release* 136 (2009) 45-53.
- [45] Chieng N., Aaltonen J., Saville D., Rades T., Physical characterization and stability of amorphous indomethacin and ranitidine hydrochloride binary systems prepared by mechanical activation, *Eur. J. Pharm. Biopharm.* 71 (2009) 47-54.
- [46] Löbmann K., Laitinen R., Grohganz H., Gordon K. C., Strachan C., Rades T., Coamorphous drug systems: enhanced physical stability and dissolution rate of indomethacin and naproxen, *Mol. Pharm.* 8 (2011) 1919-1928.
- [47] Yamamura S., Gotoh H., Sakamoto Y., Momose Y., Physicochemical properties of amorphous precipitates of cimetidine-indomethacin binary system, *Eur. J. Pharm. Biopharm.* 49 (2000) 259-265.
- [48] Yamamura S., Gotoh H., Sakamoto Y., Momose Y., Physicochemical properties of amorphous salts of cimetidine and diflunisal system, *Int. J. Pharm.* 241 (2002) 213-221.
- [49] Feeley J. C., York P., Sumby B. S., Dicks H., Determination of surface properties and flow characteristics of salbutamol sulfate, before and after micronization, *Int. J. Pharm.* 172 (1998) 89-96.
- [50] Remenar J. F., Morissette S. L., Peterson M. L., Moulton B., MacPhee J. M., Guzmán H. R., Almarsson Ö., Crystal engineering of novel cocrystals of a triazole drug with 1,4-dicarboxylic acids, *J. Am. Chem. Soc.* 125 (2003) 8456-8457.
- [51] Govindarajan R., Suryanarayanan R., Processing-induced phase transformations and their implications on pharmaceutical product quality, in: Hilfiker (Ed.) *Polymorphism in the pharmaceutical industry*, Wiley-VCH, Weinheim, 2006.
- [52] Wildfong P. L. D., Hancock B. C., Moore M. D., Morris K. R., Towards an understanding of the structurally based potential for mechanically activated disordering of small molecule organic crystals, *J. Pharm. Sci.* 95 (2006) 2645-2656.
- [53] Otsuka M., Matsumoto T., Kaneniwa N., Effect of the environmental temperature on polymorphic solid-state transformation of indomethacin during grinding, *Chem. Pharm. Bull.* 34 (1986) 1784-1793.
- [54] Hancock B. C., Shamblin S. L., Zografi G., Molecular mobility of amorphous pharmaceutical solids below their glass transition temperature, *Pharm. Res.* 12 (1995) 799-806.

- [55] Crowley K. J., Zografi G., Cryogenic grinding of indomethacin polymorphs and solvates: assessment of amorphous phase formation and amorphous phase physical stability, *J. Pharm. Sci.* 91 (2002) 492-507.
- [56] Planinšek O., Zednik J., Kunaver M., Srčič S., Godec A., Structural evolution of indomethacin particles upon milling: time-resolved quantification and localization of disordered structure studied by IGC and DSC, *J. Pharm. Sci.* 99 (2009) 1968-1981.
- [57] Patterson J. E., James M. B., Forster A. H., Lancaster R. W., Butler J. M., Rades T., The influence of thermal and mechanical preparative techniques on the amorphous state of four poorly soluble compounds, *J. Pharm. Sci.* 94 (2005) 1998-2012.
- [58] Descamps M., Willart J. F., Dudognon E., Caron V., Transformation of pharmaceutical compounds upon milling and comilling: The role of Tg, *J. Pharm. Sci.* 96 (2007) 1398-1407.
- [59] Tromans D., Meech J. A., Enhanced dissolution of minerals: stored energy, amorphism and mechanical activation, *Miner. Eng.* 14 (2001) 1359-1377.
- [60] Chieng N., Zujovic Z., Bowmaker G., Rades T., Saville D., Effect of milling conditions on the solid-state conversion of ranitidine hydrochloride form I, *Int. J. Pharm.* 327 (2006) 36-44.
- [61] Dunkel U., Rades T., Saville D., in: *Proceedings of the Annual Proceedings of the Australasian Pharmaceutical Science Association: Integrating Research into Practice*, Sydney, 2003, pp. 76.
- [62] Zhang G. G. Z., Gu C., Zell M. T., Burkhardt R. T., Munson E. J., Grant D. J. W., Crystallization and transition of sulfamerazine polymorphs, *J. Pharm. Sci.* 91 (2002) 1089-1100.
- [63] Jørgensen A. C., Strachan C. J., Pöllänen K. H., Koradia V., Tian F., Rantanen J., An insight into water of crystallization during processing using vibrational spectroscopy, *J. Pharm. Sci.* 98 (2009) 3903-3932.
- [64] Petit S., Coquerel G., Mechanism of several solid-solid transformations between dihydrated and anhydrous copper(II) 8-hydroxyquinolates. Proposition for a unified model for the dehydration of molecular crystals, *Chem. Mater.* 8 (1996) 2247-2258.
- [65] Friščić T., Jones W., Recent advances in understanding the mechanism of cocrystal formation via grinding, *Cryst. Growth Des.* 9 (2009) 1621-1637.
- [66] Cheung E. Y., Kitchin S. J., Harris K. D. M., Imai Y., Tajima N., Kuroda R., Direct structure determination of multicomponent molecular crystal prepared by a solid-state grinding procedure, *J. Am. Chem. Soc.* 125 (2003) 14658-14659.
- [67] Chadwick K., Davey R., Cross W., How does grinding produce co-crystals? Insights from the case of benzophenone and diphenylamine, *Cryst. Eng. Comm.* 9 (2007) 732-734.
- [68] Chieng N., Hubert M., Saville D., Rades T., Aaltonen J., Formation kinetics and stability of carbamazepine-nicotinamide cocrystals prepared by mechanical activation, *Cryst. Growth Des.* 9 (2009) 2377-2386.
- [69] Löbmann K., Laitinen R., Grohganz H., Strachan C., Rades T., Gordon K. C., A theoretical and spectroscopical study of co-amorphous naproxen and indomethacin, *Int. J. Pharm.* in press (2012).
- [70] Jørgensen A., Rantanen J., Luukkonen P., Laine S., Yliruusi J., Visualization of a pharmaceutical unit operation: wet granulation, *Anal. Chem.* 76 (2004) 5331-5338.
- [71] Davis T. D., Peck G. E., Stowell J. G., Morris K. R., Byrn S. R., Modeling and monitoring of polymorphic transformations during the drying phase of wet granulation, *Pharm. Res.* 21 (2004) 860-866.
- [72] Morris K. R., Griesser U. J., Eckhardt C. J., Stowell J. G., Theoretical approaches to physical transformations of active pharmaceutical ingredients during manufacturing processes, *Adv. Drug Deliv. Rev.* 48 (2001) 91-114.

- [73] Gokhale R., Trivedi N. R., Wet granulation in low- and high-shear mixers, in: Parikh D. M., (Eds.) Handbook of pharmaceutical granulation technology, Informa Healthcare, New York, 2010, pp. 183-203.
- [74] Shefter E., Higuchi T., Dissolution behavior of crystalline solvated and nonsolvated forms of some pharmaceuticals, *J. Pharm. Sci.* 52 (1963) 781-791.
- [75] Gift A. D., Luner P. E., Luedeman L., Taylor L. S., Manipulating hydrate formation during high shear wet granulation using polymeric excipients, *J. Pharm. Sci.* 98 (2009) 4670-4683.
- [76] Wikström H., Marsac P. J., Taylor L. S., In-line monitoring of hydrate formation during wet granulation using Raman spectroscopy, *J. Pharm. Sci.* 94 (2004) 209-219.
- [77] Jørgensen A., Luukkonen P., Rantanen J., Schæfer T., Juppo A. M., Yliruusi J., Comparison of torque measurements and near-infrared spectroscopy in characterization of a wet granulation process, *J. Pharm. Sci.* 93 (2004) 2232-2243.
- [78] Räsänen E., Rantanen J., Jørgensen A., Karjalainen M., Paakkari T., Yliruusi J., Novel identification of pseudopolymorphic changes of theophylline during wet granulation using near infrared spectroscopy, *J. Pharm. Sci.* 90 (2001) 389-396.
- [79] Davis T. D., Morris K. R., Huang H., Peck G. E., Stowell J. G., Eisenhauer B. J., Hilden J. L., Gibson D., Byrn S. R., In situ monitoring of wet granulation using online X-ray powder diffraction, *Pharm. Res.* 20 (2003) 1851-1857.
- [80] Koradia V., De Lemos A. F. F., Allesø M., De Diego H. L., Ringkjøbing-Elema M., Müllertz A., Rantanen J., Phase transformations of amlodipine besylate solid forms, *J. Pharm. Sci.* 100 (2011) 2896-2910.
- [81] Otsuka M., Kato F., Matsuda Y., Effect of temperature and kneading solution on polymorphic transformation of mefenamic acid during granulation, *Solid State Ionics* 172 (2004) 451-453.
- [82] Otsuka M., Hasegawa H., Matsuda Y., Effect of polymorphic forms of bulk powders on pharmaceutical properties of carbamazepine granules, *Chem. Pharm. Bull.* 47 (1999) 852-856.
- [83] Mirza S., Miroshnyk I., Rantanen J., Aaltonen J., Harjula P., Kiljunen E., Heinämäki J., Yliruusi J., Solid-state properties and relationship between anhydrate and monohydrate of baclofen, *J. Pharm. Sci.* 96 (2007) 2399-2408.
- [84] Herman J., Remon J. P., Visavarungroj N., Schwartz J. B., Klinger G. H., Formation of theophylline monohydrate during the pelletisation of microcrystalline cellulose-anhydrous theophylline blends, *Int. J. Pharm.* 42 (1988) 15-18.
- [85] Airaksinen S., Karjalainen M., Kivikero N., Westermarck S., Shevchenko A., Rantanen J., Yliruusi J., Excipient selection can significantly affect solid-state phase transformation in formulation during wet granulation, *AAPS Pharm. Sci. Tech.* 6 (2005) E311-E322.
- [86] Jørgensen A., Airaksinen S., Karjalainen M., Luukkonen P., Rantanen J., Yliruusi J., Role of excipients in hydrate formation kinetics of theophylline in wet masses studied by near-infrared spectroscopy, *Eur. J. Pharm. Sci.* 23 (2004) 99-104.
- [87] Wikström H., Carroll W. J., Taylor L. S., Manipulating theophylline monohydrate formation during high-shear wet granulation through improved understanding of the role of excipients, *Pharm. Res.* 25 (2008) 923-935.
- [88] Li X., Zhi F., Hu Y., Investigation of excipients and processing on solid phase transformation and dissolution of ciprofloxacin, *Int. J. Pharm.* 328 (2007) 177-182.
- [89] Jayasankar A., Nehm S., Kemper M., Rodriguez-Hornedo N., The use of Raman spectroscopy for real-time monitoring of cocrystal formation during wet granulation, in: Annual Meeting of the American Association of Pharmaceutical Scientists, San Antonio, 2006.

- [90] Viertelhaus M., Hilfiker R., Blatter F., Neuburger M., Piracetam co-crystals with OH-group functionalized carboxylic acids, *Cryst. Growth Des.* 9 (2009) 2220-2228.
- [91] Rehder S., Christensen N. P. A., Rantanen J., Rades T., Leopold C. S., High-shear granulation as a manufacturing method for cocrystal granules, (2013), submitted for publication.
- [92] Bučar D.-K., Henry R. F., Duerst R. W., Lou X., MacGillivray L. R., Zhang G. G. D., A 1:1 cocrystal of caffeine and 2-hydroxy-1-naphthoic acid obtained via slurry screening method, *J. Chem. Crystallogr.* 40 (2010) 933-939.
- [93] Bučar D.-K., Henry R. F., Lou X., Duerst R. W., MacGillivray L. R., Zhang G. G. D., Cocrystals of caffeine and hydroxybenzoic acids composed of multiple supramolecular heterosynthons: screening via a solution-mediated phase transformation and structural characterization, *Cryst. Growth Des.* 9 (2009) 1932-1943.
- [94] Zhang G. G. D., Henry R. F., Borchardt T. B., Lou X., Efficient co-crystal screening using solution-mediated phase transformation, *J. Pharm. Sci.* 96 (2007) 990-995.
- [95] Römer M., Heinämäki J., Miroshnyk I., Sandler N., Rantanen J., Yliruusi J., Phase transformation of erythromycin A dihydrate during pelletisation and drying, *Eur. J. Pharm. Biopharm.* 67 (2007) 246-252.
- [96] Wildfong P. L. D., Samy A. S., Corfa J., Peck G. E., Morris K. R., Accelerated fluid bed drying using NIR monitoring and phenomenological modeling: method assessment and formulation suitability, *J. Pharm. Sci.* 91 (2002) 931-939.
- [97] Airaksinen S., Karjalainen M., Räsänen E., Rantanen J., Yliruusi J., Comparison of the effects of two drying methods on polymorphism of theophylline, *Int. J. Pharm.* 276 (2004) 129-141.
- [98] Byrn S. R., Pfeiffer R. R., Stowell J. G., Solid-state chemistry of drugs, in: SSCI Inc., West Lafayette, 1999.
- [99] Nunes C., Mahendrasingam A., Suryanarayanan R., Investigation of the multi-step dehydration reaction of theophylline monohydrate using 2-dimensional powder X-ray diffractometry, *Pharm. Res.* 23 (2006) 2393-2404.
- [100] Phadnis N. V., Suryanarayanan R., Polymorphism in anhydrous theophylline - implications on the dissolution rate of theophylline tablets, *J. Pharm. Sci.* 86 (1997) 1256-1263.
- [101] Tantry J. S., Tank J., Suryanarayanan R., Processing-induced phase transitions of theophylline - implications on the dissolution of theophylline tablets, *J. Pharm. Sci.* 96 (2007) 1434-1444.
- [102] Stephenson G. A., Groleau E. G., Kleemann R. L., Xu W., Gigsbee D. R., Formation of isomorphic desolvates: creating a molecular vacuum, *J. Pharm. Sci.* 87 (1998) 536-542.
- [103] Stephenson G. A., Stowell J. G., Toma P. H., Pfeiffer R. R., Byrn S. R., Solid state investigations of erythromycin A dihydrate: structure, NMR spectroscopy, and hygroscopicity, *J. Pharm. Sci.* 86 (1997) 1239-1244.
- [104] Bauer J. F., Dziki W., Quick J. E., Role of an isomorphic desolvate in dissolution failures of an erythromycin tablet formulation, *J. Pharm. Sci.* 88 (1999) 1222-1227.
- [105] Zeitler J. A., Kogermann K., Rantanen J., Rades T., Taday P. F., Pepper M., Aaltonen J., Strachan C. J., Drug hydrate systems and dehydration processes studied by terahertz pulsed spectroscopy, *Int. J. Pharm.* 334 (2007) 78-84.
- [106] Kogermann K., Aaltonen J., Strachan C. J., Pöllänen K., Heinämäki J., Yliruusi J., Rantanen J., Establishing quantitative in-line analysis of multiple solid-state transformations during dehydration, *J. Pharm. Sci.* 97 (2008) 4983-4999.
- [107] Aaltonen J., Kogermann K., Strachan C. J., Rantanen J., In-line monitoring of solid-state transitions during fluidisation, *Chem. Eng. Sci.* 62 (2007) 408-415.

- [108] Brittain H. G., Effects of mechanical processing on phase composition *J. Pharm. Sci.* 91 (2002) 1573-1580.
- [109] Otsuka M., Matsuda Y., Effects of environmental temperature and compression energy on the polymorphic transformation during tableting, *Drug Dev. Ind. Pharm.* 19 (1993) 2241-2269.
- [110] Wildfong P. L. D., Morris K. R., Anderson C. A., Short S. M., Demonstration of a shear-based solid-state phase transformation in a small molecular organic system: chlorpropamide, *J. Pharm. Sci.* 96 (2007) 1100-1113.
- [111] Matsumoto T., Kaneniwa N., Higuchi S., Otsuka M., Effects of temperature and pressure during compression on polymorphic transformation and crushing strength of chlorpropamide tablets, *J. Pharm. Pharmacol.* 43 (1991) 74-78.
- [112] Chan H. K., Doelker E., Polymorphic transition of some drugs under compression, *Drug Dev. Ind. Pharm.* 11 (1985) 315-332.
- [113] Schmidt A. G., Wartewig S., Picker K. M., Potential of carrageenans to protect drugs from polymorphic transformation, *Eur. J. Pharm. Biopharm.* 56 (2003) 101-110.
- [114] Ayenew Z., Paudel A., Rombaut P., Van Den Mooter G., Effect of compression on non-isothermal crystallization behaviour of amorphous indomethacin, *Pharm. Res.* 29 (2012) 2489-2498.
- [115] Karmwar P., Boetker J. P., Graeser K., Strachan C. J., Rantanen J., Rades T., Investigations on the effect of different cooling rates on the stability of amorphous indomethacin, *Eur. J. Pharm. Sci.* 44 (2011) 341-350.
- [116] Lefebvre C., Guyot-Hermann A. M., Polymorphic transitions of carbamazepine during grinding and compression, *Drug Dev. Ind. Pharm.* 12 (1986) 1913-1927.
- [117] Picker K. M., "Soft tableting": A new concept to tablet pressure-sensitive materials, *Pharm. Dev. Technol.* 9 (2004) 107-121.
- [118] Schmidt A. G., Wartewig S., Picker K. M., Polyethylen oxides: protection potential against polymorphic transitions of drugs?, *J. Raman. Spectrosc.* 35 (2004) 360-367.
- [119] Savolainen M., Kogermann K., Heinz A., Aaltonen J., Peltonen L., Strachan C., Yliruusi J., Better understanding of dissolution behaviour of amorphous drugs by in situ solid-state analysis using Raman spectroscopy, *Eur. J. Pharm. Biopharm.* 71 (2009) 71-79.
- [120] Huppo P., Grönroos A., Schantz S., Juppo A. M., New processing techniques for viscous amorphous materials and characterisation of their stickiness and deformability, *Eur. J. Pharm. Biopharm.* 72 (2009) 183-188.
- [121] Johari G. P., Kim S., Shanker R. M., Dielectric relaxation and crystallization of ultraviscous melt and glassy states of aspirin, ibuprofen, progesterone, and quinidine, *J. Pharm. Sci.* 96 (2007) 1159-1175.
- [122] Balbach S., Korn C., Pharmaceutical evaluation of early development candidates "the 100 mg-approach", *Int. J. Pharm.* 275 (2004) 1-12.
- [123] Esen C., Šurbek M., Baer S., Ostendorf A., Raman-Spektroskopie an einzelnen levitierten Partikeln, *Chemie Ingenieur Technik* 82 (2010) 2059-2071.
- [124] Santesson S., Andersson M., Degerman E., Johansson T., Nilsson J., Nilsson S., Airborne cell analysis, *Anal. Chem.* 72 (2000) 3412-3418.
- [125] Leiterer J., Delißen F., Emmerling F., Thünemann A. F., Panne U., Structure analysis using acoustically levitated droplets, *Anal. Bioanal. Chem.* 391 (2008) 1221-1228.
- [126] Tuckermann R., Puskar L., Zavabeti M., Sekine R., McNaughton D., Chemical analysis of acoustically levitated drops by Raman spectroscopy, *Anal. Bioanal. Chem.* 394 (2009) 1433-1441.
- [127] Biswas A., Solidification of acoustically levitated o-terphenyl crystals: a Raman study, *J. Cryst. Growth* 147 (1995) 155-164.

- [128] Lierke E.G., Acoustic levitation – a comprehensive survey of principles and applications, *Acta Acust.* 82 (1996) 220-237.
- [129] Xie W. J., Wei B., Parametric study of single-axis acoustic levitation, *Appl. Phys. Lett.* 79 (2001) 881-883.
- [130] Davies A. N., Jacob P., Stockhaus A., Kuckuk R., Hill W., Hergenröder R., Zybin A., Klockow D., Acoustic trap for simplified micro-sample handling in laser spectroscopy, *Appl. Spectrosc.* 54 (2000) 1831-1836.
- [131] Cronin J. T., Brill T. B., Acoustic levitation as an IR spectroscopy sampling technique, *Appl. Spectrosc.* 43 (1989) 253-257.
- [132] Santesson S., Johansson J., Taylor L. S., Levander I., Fox S., Sepaniak M., Nilsson S., Airborne chemistry coupled to Raman spectroscopy, *Anal. Chem.* 75 (2003) 2177-2180.
- [133] Räsänen E., Sandler N., Near infrared spectroscopy in the development of solid dosage forms, *J. Pharm. Pharmacol.* 59 (2007) 147-159.
- [134] Heinz A., Strachan C. J., Gordon K. C., Rades T., Analysis of solid-state transformations of pharmaceutical compounds using vibrational spectroscopy, *J. Pharm. Pharmacol.* 61 (2009) 971-988.
- [135] Wold S., Esbensen K., Geladi P., Principal component analysis, *Chemom. Intell. Lab. Syst.* 2 (1987) 37-52.
- [136] Wold S., Sjöström M., Eriksson L., PLS-regression: a basic tool of chemometrics, *Chemom. Intell. Lab. Syst.* 58 (2001) 109-130.
- [137] De Juan A., Tauler R., Multivariate curve resolution (MCR) from 2000: Progress in concepts and applications, *Crit. Rev. Anal. Chem.* 36 (2006) 163-176.
- [138] Andronis V., Zografu G., Crystal nucleation and growth of indomethacin polymorphs from the amorphous state, *J. Non Cryst. Solids* 271 (2000) 236-248.
- [139] Jaumot J., Gargallo R., De Juan A., Tauler R., A graphical user-friendly interface for MCR-ALS: A new tool for multivariate curve resolution in MATLAB, *Chemom. Intell. Lab. Syst.* 76 (2005) 101-110.
- [140] Rinnan A., v. d. Berg F., Engelsen S. B., Review of the most common pre-processing techniques for near-infrared spectra, *Trends Analyt. Chem.* 28 (2009) 1201-1222.
- [141] Maeder M., Evolving factor analysis for the resolution of overlapping chromatographic peaks, *Anal. Chem.* 59 (1987) 527-530.
- [142] Rodgers J. L., Nicewander W. A., Thirteen ways to look at the correlation coefficient, *Am. Stat.* 42 (1988) 59-66.
- [143] Qu H., Munk T., Cornett C., Wu J. X., Bøtker J. P., Christensen L. P., Rantanen J., Tian F., Influence of temperature on solvent-mediated anhydrate-to-hydrate transformation kinetics, *Pharm. Res.* 28 (2011) 264-273.
- [144] Xia D., Wu J. X., Cui F., Qu H., Rades T., Rantanen J., Yang M., Solvent-mediated amorphous-to-crystalline transformation of nitrendipine in amorphous particle suspensions containing polymers, *Eur. J. Pharm. Sci.* 46 (2012) 446-454.
- [145] Mallick S., Pattnaik S., Swain K., De P. K., Saha A., Ghoshal G., Mondal A., Formation of physically stable amorphous phase of ibuprofen by solid state milling with kaolin, *Eur. J. Pharm. Biopharm.* 68 (2008) 346-351.
- [146] Dreassi E., Ceramelli G., Corti P., Near-infrared reflectance spectrometry in the determination of the physical state of primary materials in pharmaceutical production, *Analyst* 120 (1995) 1005-1008.
- [147] Rucker G., Neugebauer M., Willems S. G., *Instrumentelle Pharmazeutische Analytik*, 3 ed., Wissenschaftliche Verlagsgesellschaft mbH Stuttgart, Stuttgart, 2001.

- [148] Savolainen M., Jouppila K., Pajamo O., Christiansen L., Strachan C., Karjalainen M., Rantanen J., Determination of amorphous content in the pharmaceutical process environment, *J. Pharm. Pharmacol.* 59 (2007) 161-170.
- [149] Seyer J. J., Luner P. E., Kemper M. S., Application of diffuse reflectance near infrared spectroscopy for determination of crystallinity, *J. Pharm. Sci.* 89 (2000) 1305-1316.
- [150] Hédoux A., Guinet Y., Derollez P., Dudognon E., Correia N. T., Raman spectroscopy of racemic ibuprofen: evidence of molecular disorder in phase II, *Int. J. Pharm.* 421 (2011) 45-52.
- [151] Savolainen M., Heinz A., Strachan C., Gordon K. C., Yliruusi J., Rades T., Sandler N., Screening for differences in the amorphous state of indomethacin using multivariate visualization, *Eur. J. Pharm. Sci.* 30 (2007) 113-123.
- [152] Rossi B., Verrocchio P., Viliani G., Mancini I., Guella G., Rigo E., Scarduelli G., Mariotto G., Vibrational properties of ibuprofen-cyclodextrin inclusion complexes investigated by Raman scattering and numerical simulation, *J. Raman Spectrosc.* 40 (2009) 453-458.
- [153] Garetz B. A., Aber J. E., Goddard N. L., Young R. G., Myerson A. S., Nonphotochemical, polarization-dependent, laser-induced nucleation in supersaturated aqueous urea solutions, *Phys. Rev. Lett.* 77 (1996) 3475-3476.
- [154] Kip B. J., Meier R. J., Determination of the local temperature at a sample during Raman experiments using Stokes and Anti-Stokes Raman bands, *Appl. Spectrosc.* 44 (1990) 707-711.
- [155] Delhaye M., Dhamelinourt P., Raman microprobe and microscope with laser excitation, *J. Raman Spectrosc.* 3 (1975) 33-43.
- [156] Lee I. S., Evans J. M. B., Erdemir D., Lee A. Y., Garetz B. A., Myerson A. S., Nonphotochemical laser-induced nucleation of hen egg white lysozyme crystals, *Cryst. Growth Des.* 8 (2008) 4255-4261.
- [157] Zaccaro J., Matic J., Myerson A. S., Garetz B. A., Nonphotochemical, laser-induced nucleation of supersaturated aqueous glycine produces unexpected γ -polymorph, *Cryst. Growth Des.* 1 (2000) 5-8.
- [158] Fleischman S. G., Kuduva S. S., McMahon J. A., Moulton B., Bailey Walsh R. D., Rodriguez-Hornedo N., Zaworotko M. J., Crystal engineering of the composition of pharmaceutical phases: multiple-component crystalline solids involving carbamazepine *Cryst. Growth Des.* 3 (2003) 909-919.
- [159] Trask A. V., Motherwell W. D. S., Jones W., Pharmaceutical cocrystallization: Engineering a remedy for caffeine hydration, *Cryst. Growth Des.* 5 (2005) 1013-1021.
- [160] Vangala V. R., Chow P. S., Tan R. B. H., Characterization, physicochemical and photostability of a co-crystal involving an antibiotic drug, nitrofurantoin, and 4-hydroxybenzoic acid, *Cryst. Eng. Comm.* 13 (2011) 759-762.
- [161] Hickey M. B., Peterson M. L., Scoppettuolo L. A., Morrissette S. L., Vetter A., Guzmán H., Remenar J. F., Zhang Z., Tawa M. D., Haley S., Zaworotko M. J., Almarsson Ö., Performance comparison of a co-crystal of carbamazepine with marketed product, *Eur. J. Pharm. Biopharm.* 67 (2007) 112-119.
- [162] Blagden N., Berry D. J., Parkin A., Javed H., Ibrahim A., Gavan P. T., De Matos L. L., Seaton C. C., Current directions in co-crystal growth, *New J. Chem.* 32 (2008) 1659-1672.
- [163] Fabbiani F. P. A., Allan D. R., David W. I. F., Davidson A. J., Lennie A. R., Parsons S., Pulham C. R., Warren J. E., High-pressure studies of pharmaceuticals: an exploration of the behavior of piracetam, *Cryst. Growth Des.* 7 (2007) 1115-1124.
- [164] Fabbiani F. P. A., Allan D. R., Parsons S., Pulham C. R., An exploration of the polymorphism of piracetam using high pressure, *Cryst. Eng. Comm.* 7 (2005) 179-186.

- [165] Kuhnert-Brandstätter M., Burger A., Völlenklee R., Stability behavior of piracetam polymorphs, *Sci. Pharm.* 62 (1994) 307-316.
- [166] Aakeröy C. B., Crystal engineering: strategies and architectures, *Acta Crystallogr. B* 53 (1997) 569-586.
- [167] Vishweshwar P., McMahon J. A., Peterson M. L., Hickey M. B., Shattock T. R., Zaworotko M. J., Crystal engineering of pharmaceutical co-crystals from polymorphic active pharmaceutical ingredients, *Chem. Commun.* (2005) 4601-4603.
- [168] Liao X., Gautam M., Grill A., Zhu H. J., Effect of position isomerism on the formation and physicochemical properties of pharmaceutical co-crystals, *J. Pharm. Sci.* 99 (2009) 246-254.
- [169] Jayasankar A., Somwangthanaroj A., Shao Z. J., Rodríguez-Hornedo N., Cocrystal formation during cogrinding and storage is mediated by amorphous phase, *Pharm. Res.* 23 (2006) 2381-2392.
- [170] Shan N., Toda F., Jones W., Mechanochemistry and co-crystal formation: effect of solvent on reaction kinetics, *Chem. Comm.* (2002) 2372-2373.
- [171] Friščić T., Childs S. L., Rizvi S. A. A., Jones W., The role of solvent in mechanochemical and sonochemical cocrystal formation: a solubility-based approach for predicting cocrystallization outcome, *Cryst. Eng. Comm.* 11 (2009) 418-426.
- [172] Allesø M., Velaga S., Alhalaweh A., Cornett C., Rasmussen M. A., Van Den Berg F., Lopez De Diego H., Rantanen J., Near-infrared spectroscopy for cocrystal screening. A comparative study with Raman spectroscopy, *Anal. Chem.* 80 (2008) 7755-7764.
- [173] Shattock T. R., Arora K. K., Vishweshwar P., Zaworotko M. J., Hierarchy of supramolecular synthons: persistent carboxylic acid pyridine hydrogen bonds in cocrystals that also contain a hydroxyl moiety, *Cryst. Growth Des.* 8 (2008) 4533-4545.
- [174] Allen F. H., The Cambridge Structural Database: a quarter of a million crystal structures and rising, *Acta Cryst.* 58 (2002) 380-388.
- [175] Bruno I. J., Cole J. C., Edgington P. R., Kessler M., Macrae C. F., McCabe P., Pidcock E., Rodriguez-Monge L., Taylor R., Van De Streek J., Wood P. A., New software for searching the Cambridge Structural Database and visualising crystal structures, *Acta Cryst.* 58 (2002) 389-397.
- [176] Macrae C. F., Bruno I. J., Chisholm J. A., Edgington P. R., McCabe P., Pidcock E., Rodriguez-Monge L., Taylor R., Van De Streek J., Wood P. A., Mercury CSD 2.0 - New features for the visualization and investigation of crystal structures, *J. Appl. Cryst.* 41 (2008) 466-470.
- [177] Maher A., Croker D., Rasmuson A. C., Hodnett B. K., Solubility of form III piracetam in a range of solvents, *J. Chem. Eng. Data* 55 (2010) 5314-5318.
- [178] Chow S. F., Chen M., Shi L., Chow A. H. L., Sun C. C., Simultaneously improving the mechanical properties, dissolution performance, and hygroscopicity of ibuprofen and flurbiprofen by cocrystallization with nicotinamide, *Pharm. Res.* 29 (2012) 1854-1865.
- [179] Sun C. C., Hou H., Improving mechanical properties of caffeine and methyl gallate crystals by cocrystallization, *Cryst. Growth Des.* 8 (2008) 1575-1579.
- [180] Vishweshwar P., McMahon J. A., Bis J. A., Zaworotko M. J., Pharmaceutical co-crystals, *J. Pharm. Sci.* 95 (2006) 499-516.
- [181] Desiraju G. R., Crystal engineering: a holistic view, *Angew. Chem. Int. Ed.* 46 (2007) 8342-8356.
- [182] Childs S. L., Chyall L. J., Dunlup J. T., Smolenskaya V. N., Stahly B. C., Stahly G. P., Crystal engineering approach to forming cocrystals of amine hydrochlorides with organic acids. Molecular complexes of fluoxetine hydrochloride with benzoic, succinic, and fumaric acid, *J. Am. Chem. Soc.* 126 (2004) 13335-13342.

- [183] Takata N., Shiraki K., Takano R., Hayashi Y., Terada K., Cocrystal screening of stanolone and mestanolone using slurry crystallization, *Cryst. Growth Des.* 8 (2008) 3032-3037.
- [184] Frišćić T., Trask A. V., Jones W., Motherwell W. D. S., Screening for inclusion compounds and systematic construction of three-component solids by liquid-assisted grinding, *Angew. Chem. Int. Ed.* 45 (2006) 7546-7550.
- [185] Trask A. V., Motherwell W. D. S., Jones W., Solvent-drop grinding: green polymorph control of cocrystallization, *Chem. Comm.* (2004) 890-891.
- [186] Frišćić T., New opportunities for materials synthesis using mechanochemistry, *J. Mater. Chem.* 20 (2010) 7599-7605.
- [187] Dhumal R. S., Kelly A. L., York P., Coates P. D., Paradkar A., Cocrystallization and simultaneous agglomeration using hot melt extrusion, *Pharm. Res.* 27 (2010) 2725-2733.
- [188] Daurio D., Medina C., Saw R., Nagapudi K., Alvarez-Nunez F., Application of twin screw extrusion in the manufacture of cocrystals, part I: four case studies, *Pharmaceutics* 3 (2011) 582-600.
- [189] Medina C., Daurio D., Nagapudi K., Alvarez-Nunez F., Manufacture of pharmaceutical co-crystals using twin screw extrusion: a solvent-less and scalable process, *J. Pharm. Sci.* 99 (2010) 1693-1696.
- [190] Alhalaweh A., Velaga S. P., Formation of cocrystals from stoichiometric solutions of incongruently saturating systems by spray drying, (2010).
- [191] Fell J. T., Newton J. M., Determination of tablet strength by the diametral-compression test, *J. Pharm. Sci.* 59 (1970) 688-691.
- [192] Sonnergaard J. M., Quantification of the compactibility of pharmaceutical powders, *Eur. J. Pharm. Biopharm.* 63 (2006) 270-277.
- [193] Nørgaard L., Hahn M. T., Knudsen L. B., Farhad I. A., Engelsen S. B., Multivariate near-infrared and Raman spectroscopic quantifications of the crystallinity of lactose in whey permeate, *Int. Dairy J.* 15 (2005) 1261-1270.
- [194] Zografí G., Kontny M. J., The interactions of water with cellulose- and starch-derived pharmaceutical excipients, *Pharm. Res.* 3 (1986) 187-193.
- [195] Arora K. K., Tayade N. G., Suryanarayanan R., Unintended water mediated cocrystal formation in carbamazepine and aspirin tablets, *Mol. Pharm.* 8 (2011) 982-989.
- [196] Jayasankar A., Good D. J., Rodriguez-Hornedo N., Mechanisms by which moisture generates cocrystals, *Mol. Pharm.* 4 (2007) 360-372.
- [197] Wikberg M., Alderberg G., Compression characteristics of granulated materials: V. Mechanical properties of individual granules, assessed by diametral compression, in granulations with different volume reduction behaviour, *Pharm. Sci.* 2 (1992) 313-319.
- [198] Schersch K., Betz O., Garidel P., Muehlau S., Bassarab S., Winter G., Systematic investigation of the effect of lyophilizate collapse on pharmaceutically relevant proteins I: stability after freeze-drying, *J. Pharm. Sci.* 99 (2010) 2256-2278.
- [199] Babu N. J., Nangia A., Solubility advantages of amorphous drugs and pharmaceutical cocrystals, *Cryst. Growth Des.* 11 (2011) 2662-2679.
- [200] Amidon G. L., Lennernäs H., Shah V. P., Crison J. R., A theoretical basis for a biopharmaceutical drug classification: The correlation of in vitro drug product dissolution an in vivo bioavailability, *Pharm. Res.* 12 (1995) 413-420.
- [201] Thayer A. M., Finding solutions, *Chem. Eng. News* 88 (2010) 13-18.
- [202] Hancock B. C., Parks M., What is the true solubility advantage for amorphous pharmaceuticals?, *Pharm. Res.* 17 (2000) 397-404.

- [203] Saidon P. J., Cauchon N. S., Sutton P. A., Chang C. V., Peck G. E., Byrn S. R., Solid-state nuclear magnetic resonance (NMR) spectra of pharmaceutical dosage forms, *Pharm. Res.* 10 (1993) 197-203.
- [204] Taylor L. S., Langkilde F. W., Evaluation of solid-state forms present in tablets by Raman spectroscopy, *J. Pharm. Sci.* 89 (2000) 1342-1353.
- [205] Hassan M. A., Salem M. S., Sallam E., Al-Hindawi M. K., Preparation and characterization of a new polymorphic form and a solvate of glibenclamide, *Acta Pharm. Hung.* 67 (1997) 81-88.
- [206] Hassan M. A., Najib N. M., Suleiman M. S., Characterization of glibenclamide glassy state, *Int. J. Pharm.* 67 (1991) 131-137.
- [207] Rehder S., Sakmann A., Rades T., Leopold C. S., Thermal degradation of amorphous glibenclamide, *Eur. J. Pharm. Biopharm.* 80 (2012) 203-208.
- [208] Suleiman M. S., Najib N. M., Isolation and physicochemical characterization of solid forms of glibenclamide, *Int. J. Pharm.* 50 (1989) 103-109.
- [209] Wojnarowska Z., Grzybowska K., Adrjanowicz K., Kaminski K., Paluch M., Hawelek L., Wrzalik R., Dulski M., Study of the amorphous glibenclamide drug: analysis of the molecular dynamics of quenched and cryomilled material, *Mol. Pharm.* 7 (2010) 1692-1707.
- [210] Hancock B. C., Shamblin S. L., Zografi G., Molecular mobility of amorphous pharmaceutical solids below their glass transition temperatures, *Pharm. Res.* 12 (1995).
- [211] Panagopoulou-Kaplani A., Malamataris S., Preparation and characterisation of a new insoluble polymorphic form of glibenclamide, *Int. J. Pharm.* 195 (2000) 239-246.
- [212] Dressman J., Butler J., Hempenstall J., Reppas C., The BCS: Where do we go from here?, *Pharmaceutical Technology North America* 25 (2001) 68-76.
- [213] Blume H., Ali S. L., Siewert M., Pharmaceutical quality of glibenclamide products: a multinational postmarket comparative study, *Drug Dev. Ind. Pharm.* 19 (1993) 2713-2741.
- [214] Bansal G., Singh M., Jindal K. C., Singh S., Ultraviolet-photodiode array and high-performance liquid chromatographic / mass spectrometric studies on forced degradation behavior of glibenclamide and development of a validated stability-indicating method, *J. AOAC Int.* 91 (2008) 709-719.
- [215] Kurzer F., Sulfonylureas and sulfonylthioureas, in: PhD thesis, Royal Free Hospital School of Medicine, University of London, London, 1951, pp. 46.
- [216] Ulrich H., Sayigh A.A.R., Synthesis of isocyanates and carbodiimides, *Angew. Chem. Int. Ed. Engl.* 5 (1966) 704-712.
- [217] Bottari F., Giannaccini B., Nannipieri E., Saettone M. F., Thermal dissociation of sulfonylureas II: Dissociation of four N- and N'-substituted sulfonylureas in different media, *J. Pharm. Sci.* 61 (1972) 602-606.
- [218] Henck J. O., Griesser U. J., Burger A., Polymorphie von Arzneistoffen - eine wirtschaftliche Herausforderung, *Pharm. Ind.* 59 (1997) 165-169.
- [219] Mura P., Cirri M., Faucci M. T., Ginès-Dorado J. M., Bettinetti G. P., Investigation of the effects of grinding and co-grinding on physicochemical properties of glisentide, *J. Pharm. Biomed. Anal.* 30 (2002) 227-237.
- [220] Hancock B. C., Zografi G., The relationship between the glass transition temperature and the water content of amorphous pharmaceutical solids, *Pharm. Res.* 11 (1994) 471-477.